Estimating ventilation rates and emissions from a naturally ventilated dairy barn: a three-column approach

vorgelegt von
Dipl.-Ing.
David Janke
ORCID: 0000-0002-4211-3404

von der Fakultät V - Verkehrs- und Maschinensysteme
der Technischen Universität Berlin
zur Erlangung des akademischen Grades

Doktor der Ingenieurwissenschaften
- Dr.-Ing. -

genehmigte Dissertation

Promotionsausschuss:
Vorsitzender: Prof. Dr.-Ing. Henning Jürgen Meyer
Gutachterin: Prof. Dr.-Ing. Cornelia Weltzien
Gutachter: Prof. Dr. Thomas Amon

Tag der wissenschaftlichen Aussprache: 10. Februar 2021

Berlin 2021

Zusammenfassung

Die Bestimmung von Luftwechselraten und Emissionen aus frei gelüfteten Tierhaltungssystemen ist mit großen Unsicherheiten behaftet. Das Ziel dieser Dissertation war die Untersuchung des Einflusses von Probenahmepositionen auf die Bestimmung von Luftwechselraten und Emissionen sowie die Optimierung und Weiterentwicklung derzeit angewandter Methoden.

Dazu wurden drei methodische Ansätze in Form eines Drei-Säulen-Modells angewendet: (1) Langzeitmessungen im Experimentalstall - Aufnahme von Gaskonzentrationen zur Ermittlung von Luftwechselraten und Ammoniakemissionen mittels indirekter Massenbilanzmethoden, (2) Versuche im atmosphärischen Grenzschichtwindkanal - Messungen von Geschwindigkeiten und Gaskonzentrationen an einem Modell des Experimentalstalles zur Ermittlung von Luftwechselraten und Emissionen und (3) numerische Untersuchungen des Modells mit zwei quelloffenen transienten Strömungslösern.

Die Ergebnisse zu (1) wiesen, abhängig von der Gasprobenahmestrategie, maximale systematische Unterschiede zwischen den Methoden von bis zu 26 % für die Ammoniakemissionen und 94 % für die Luftwechselraten auf. Basierend auf den Ergebnissen konnten Empfehlungen für Gasprobenahmestrategien in Abhängig der vorherrschenden Strömungsszenarien bei der Anwendung indirekter Massenbilanzmethoden abgeleitet werden. Die Ergebnisse zu (2) zeigten systematische Fehler bei der Ermittlung der Emissionen von bis zu +97 %, wenn Konzentrations- und Geschwindigkeitsmessungen auf einer konstanten Höhe durchgeführt wurden. Dieser Fehler konnte unter 5 % gesenkt werden, wenn die Gaskonzentrationen als vertikale Mischprobe gemessen wurden. Die Ergebnisse zu (3) zeigten eine gute Eignung quelloffener, transienter Strömungslöser für den Anwendungsfall eines durchströmten frei gelüfteten Stalles. Die Luftwechselraten konnten mit einem relativen Fehler <4 % simuliert werden. Die Strömungslöser bieten somit ein großes Potential für detaillierte weiterführende Simulationen des Luftwechsels und der Emission frei gelüfteter Tierhaltungssysteme.

Für jede der drei Methoden konnten ihre jeweiligen Vorteile und Limitierungen aufgezeigt werden, ebenso die Synergieeffekte zwischen den Methoden. Das Drei-Säulen-Modell hat sich daher als vielversprechender Ansatz für die Untersuchung des komplexen Emissionssystems frei gelüfteter Tierställe erwiesen.

Abstract

The determination of air exchange rates and emissions from naturally ventilated livestock systems is subject to great uncertainty. The aim of this thesis was to investigate the influence of the number and positions of gas and velocity samplings on the determination of AER and emissions as well as to optimize and further develop currently applied methods.

For this purpose, three different methods were applied in a three-column approach: (1) on-farm, long-term measurements of gas concentrations in a naturally ventilated dairy barn for the determination of air exchange rates and ammonia emissions by indirect mass balance methods, (2) boundary layer wind tunnel measurements of velocities and gas concentrations on a scaled down model of same the dairy barn for the determination of air exchange rates and emissions by direct measurement and (3) numerical investigations of the scaled down model with two open source transient flow solvers.

The results of (1) showed, depending on the gas sampling strategy, maximum systematic differences between the used strategies of up to 26 % for ammonia emissions and 94 % for air exchange rates. Based on the results, recommendations for gas sampling strategies could be derived depending on the prevailing flow scenarios when using indirect mass balance methods. The results of (2) showed systematic errors in the determination of emissions of up to +97 % when concentration and velocity measurements were performed at a constant height. This error could be reduced below 5 % when gas concentrations were measured as vertical composite sample. The results of (3) showed a good feasibility of open source, transient flow solvers for the application of a cross flow through a naturally ventilated barn. The air exchange rates could be simulated with a relative error < 4 %. The flow solvers thus offer a great potential for detailed further simulations of the air exchange rates and emissions of naturally ventilated animal housing systems.

For each of the three methods their respective advantages and limitations could be shown, as well as the synergy effects between the methods. The three-column approach has therefore proven to be a promising approach for the investigation of the complex emission system of naturally ventilated animal housing systems.

Danksagung

"We demand rigidly defined areas of doubt and uncertainty!"
Douglas Adams, The Hitchhiker's Guide to the Galaxy

Table of Contents

1

General introduction

1.1 Motivation

Agriculture, in particular livestock production, is one of the main contributors of air pollution, causing negative impacts on the environment, animals and humans [1, 2]. Pollutants associated with livestock production are greenhouse gases (GHG) like methane (CH_4), carbon dioxide (CO_2), and nitrous oxide (N_2O), affecting the Earth's radiation budget and causing climate change [3]. Also related is ammonia (NH_3), which causes the formation of particulate matter in the atmosphere and eutrophication as well as soil acidification due to nitrogen deposition [4].

According to the Food and Agriculture Organization of the United Nations (FAO), the sector of agriculture, forestry and other land use (AFOLU) produces 21% of total global GHG emissions. Round 50% of the GHG in the sector AFOLU are contributed by agriculture, with 3.2 Gigatonnes CO_2 equivalent (GtCO2e) of CH_4, 2.3 GtCO2e of N_2O, and 5.2 Gt of CO_2, resulting in an overall of 10.6 GtCO2e [2]. The largest share of agricultural emissions in CO_2 equivalent at global level can be related to livestock, namely by enteric fermentation, mainly by ruminants like cattle (40%), and manure of livestock (27%) [2, 5].

According to the latest emission inventory report of the European Environment Agency (EEA), agriculture contributes up to 93% of the European ammonia emissions, where 11% are related to the manure management of dairy cattle [6].

The numbers clearly indicate, that a huge mitigation potential for pollutants from livestock husbandry exists. Correspondingly, several mitigation enactments on international, European, national and local level exist. For the implementation of the legally binding Paris Agreement [7], the necessary nationally determined contributions for Germany were defined in the Climate Action Plan 2050 [8], where the goal is to reduce the GHG emissions from agriculture until 2030 up to 56%, compared to the level of 1990. The mitigation of ammonia was resolved in the international enactment of the Gothenburg Protocol [9] and the European directive of national emission ceilings (NEC-directive) [10]. Accordingly, Germany has committed itself to a reduction of ammonia of 29% for 2030, compared to the level of 2005.

In order to reduce emissions related to livestock husbandry, appropriate mitigation strategies have to be developed and applied. The performance of the applied mitigation strategy needs to be assessable, and therefore measurable. No matter, how effective a mitigation strategy might be, if the method to measure it is not accurate enough, no conclusion can be drawn. Therefore, accurate measurements of emissions are a prerequisite for a successful mitigation strategy. Of the same importance is the reliable quantification of the status quo of livestock-related emissions, which is reflected in the emission factors. These emission factors are not only used to calculate the mandatory national inventories, but are also the basis of far-reaching political decisions. Consequentially, the accurate measurement of emissions, and at least the precise determination of the associated uncertainty of the measurement, is of great importance.

In the following, the challenges associated with the measurements of emissions from livestock housing systems are discussed in detail.

1.2 Measuring emissions from naturally ventilated barns

The emission of a pollutant can be defined as mass flow rate $\dot{m}$, which is the mass of the pollutant leaving a system per time. With the area A, which is the boundary of the system, the velocity vector $\vec{v}$ of the pollutant, which is normal to A and pointing out of the system, and the density ρ of the pollutant, $\dot{m}$ can be expressed as:

$$\dot{m} = \vec{v} \cdot A \cdot \rho \tag{1.1}$$

The product $\vec{v} \cdot A$ can be expressed as volume flow rate Q. If the density ρ of a gaseous pollutant is displayed as the mass concentration c_p of the pollutant in the flow, the emission E_p of the pollutant can be expressed as:

$$E_p = Q \cdot c_P \tag{1.2}$$

Hence, in order to estimate the emission of a pollutant from an animal housing system, both the volume flow rate of the system and the concentration of the pollutant in the volume flow (i.e. the gas concentration) have to be measured.

For housing systems with a mechanical ventilation, this task is usually not a particular challenge. Here, the volume flow rate Q is externally predefined and the the gas concentration measurements can be carried out easily at the small, well defined area of the exhaust.

The economically highly relevant dairy cows sector typically uses naturally ventilated barns (NVB) across Europe – a housing system which is partly also used for poultry or pigs [11]. The main advantage of these buildings is their energy saving property since in general natural ventilation does not require electrical energy to operate fans or a furnace. Usually, the dimensions of the opening areas of these naturally ventilated buildings exceed several hundred square metres, see figure 1.1. These large openings are the interface between the barn and the environment, resulting in a more or less direct coupling of ambient turbulent weather conditions with the inside air flow pattern and barn climate [12, 13, 14]. Accordingly, the normal velocity vector $\vec{v}$ changes rapidly, both in time and space, and a classical inlet or outlet of the system NVB is hard to define [15, 16]. This makes the estimation of Q

challenging for both, measurement technology and methodology [17, 18]. The same applies
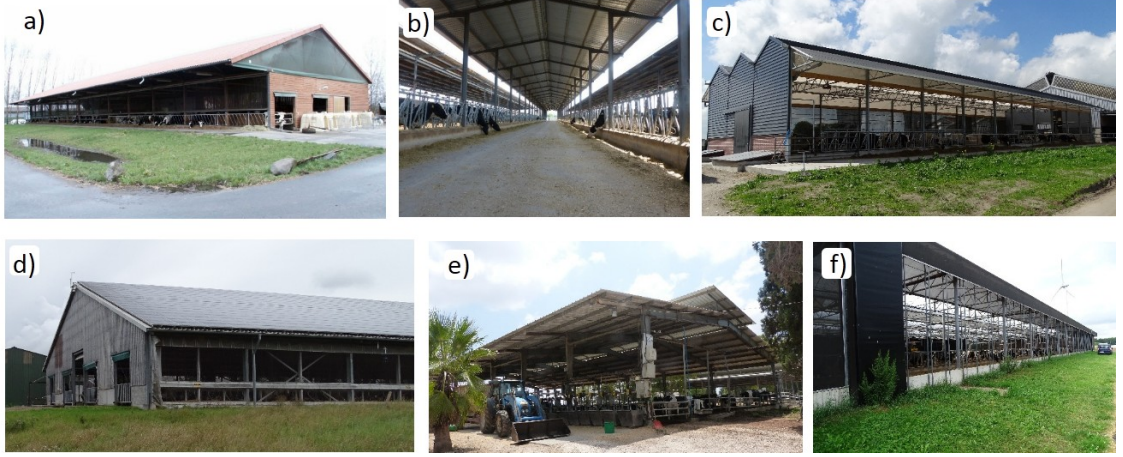
Figure 1.1: Examples of different opening geometries of naturally ventilated dairy barns in Europe. a) Groß Kreutz, Germany b) Valencia, Spain c) Leeuwarden, Netherlands d) Dummerstorf, Germany e) Betera, Israel and f) Heibloem, Netherlands. All photos by U. Stollberg (ATB).

to the measurement of the gas concentration c_p. In order to estimate emissions according to equation 1.2, c_p has to be measured as a representative concentration of the barn leaving exhaust air. Similar to the velocity vectors, the gas concentrations inside an NVB are subject to large variations, both in space and time, making a representative measurement challenging [19, 20, 21].

1.3 Measuring emissions using gas balancing methods

To overcome the issues with the measurement of the volume flow rate Q in NVBs, indirect gas balancing methods are usually applied to estimate emissions [22, 23]. Here, the dilution of a tracer gas with a known release rate is measured. Equation 1.2 can be transposed to

$$Q = \frac{E_T}{c_T} \tag{1.3}$$

with E_T as the release rate of the tracer gas and c_T as the tracer gas concentration in the exhaust air. The volume flow rate derived in this way is then further used in equation 1.2, so the problem of estimating the pollutant emissions E_P is reduced to measuring the concentrations of tracer gas c_T and pollutant gas c_P. In most cases, both the tracer gas and the pollutant gas are contained in the atmosphere and so in the barn entering inflow. The concentrations of these ambient, barn entering gas concentrations need to be measured and subtracted from the measured gas concentrations of the exhaust air, so that equations 1.2 and 1.3 are formulated as:

$$Q = \frac{E_T}{c_{T_{inside}} - c_{T_{outside}}} \tag{1.4}$$

with $c_{T_{inside}}$ as the inside measured tracer gas concentration of the exhaust air and $c_{T_{outside}}$ as the outside measured ambient tracer gas concentration entering the barn, and as:

$$E_p = Q \cdot (c_{P_{inside}} - c_{P_{outside}}) \tag{1.5}$$

with $c_{P_{inside}}$ as the inside measured pollutant gas concentration of the exhaust air and $c_{P_{outside}}$ as the outside measured ambient pollutant gas concentration entering the barn.

The tracer gas can be either artificial or natural. Artificial tracer gases like sulphur hexafluoride (SF_6) or trifluoromethylsulphur pentafluoride (SF_5CF_3) have the advantage of practically not being present in the atmosphere, hence the measurement of $c_{T_{outside}}$ is not needed. However, these gases have the disadvantages of being very harmful greenhouse gases [24], and they have to be injected into to barn with an elaborate tubing system [25, 26]. A review of different further used tracer gases is given in [23].

Instead of using an artificially injected gas, the metabolically produced and released CO_2 of the cows can be used as a natural tracer. This method is called the CO_2 mass balance method. The source strength of CO_2 (corresponding to E_T in equation 1.4) can be estimated by empirically derived production models [27, 28]. This is also the main disadvantage of the CO_2 mass balance method, because the estimated CO_2 production term contains a number of uncertainties, since it depends on weight, activity, productivity and pregnancy, and usually does not take into account animal individual variations [29]. On the other hand, however, the CO_2 mass balance method holds big advantages. Because the tracer gas is naturally produced and released, no additional effort like tubing systems or mass flow controller is needed for it's injection. Also, because CO_2 is constantly produced by the (in most cases) moving cows, a better mixing of the tracer in the air is expected than with injection systems for artificial tracer gases [23]. Further, the constant production of CO_2 as tracer enables the application of long term measurements.

Due to these advantages, the CO_2 mass balance method is widely used in the context of volume flow rate and emission measurements in NVBs, e.g. [21, 18, 30, 19], and will also be the chosen method for on-Farm measurements in this study.

In the literature, regardless of the used tracer, the position of the gas sampling is reported as a main influencing factor for the estimation of volume flow rates and emissions [23, 29]. Various studies have investigated the influence of point measurements on the estimation of volume flow rates and emissions. König et al. [19] and Ngwabie et al. [31] investigated gas concentrations with point wise measurements inside a naturally ventilated barn. They found variations for the volume flow rates up to 46% [19] and variations for ammonia concentrations up to 35% [31], when only individual sampling points were taken into account. A more elaborate variant of single sampling point measurements is the use of sampling lines. Here, the sampling air is sucked through tubes with many orifices over their length, that allow a high spatial resolution of sampling locations. Edouard et al. [32] used both, individual sampling points and sampling lines to investigate the influence of different spatial sampling strategies on the estimation of the volume flow rates. They found that using only a single point instead of five points in a line could lead to a deviation of 35% in the calculation of the volume flow rates.

However, the mentioned studies investigated the influence of the sampling position on the emission estimates only based on short-term measurements, where the lengths of the measurement campaigns varied between 7 days [31] and 47 days [32]. The exception is the study of König et al. [19], who measured over a period of one year with 8 sampling points inside the barn, but only investigated the volume flow rates, not emissions.

In the further text of this thesis, the term *sampling strategy* will be used in the context of indirect measurement as the method to measure with sampling lines the inside gas concentrations, outside gas concentrations, and their respective combination to form the difference terms shown in equation 1.4 and 1.5.

So far, no attempt was made to investigate the influence of different sampling strategies on the estimation of volume flow rates and emissions of gaseous pollutants based on long-term measurements. To overcome this gap of knowledge, the first part of the dissertation deals with this systematic investigation.

1.4   Measuring emissions using direct methods

A more straightforward approach than the before described indirect methods to estimate volume flow and emissions is the direct method. As the name suggests, in this approach, the normal velocity vectors $\vec{v}$ of the airflow entering and leaving the NVB are directly measured and used to calculate the volume flow rate Q. Additionally to $\vec{v}$, the associated concentrations of pollutant gas c_P in incoming and in the exhaust air need to be measured. According to equation 1.2, the emission of the barn can then be computed as the product of directly measured volume flow rate and the concentration c_P.

In comparison to indirect methods, only few scientific reports can be found in the literature that investigate the application of direct methods to estimate volume flow rates and emissions from NVB. This is probably due to the before mentioned difficulties in estimating the volume flow in the context of the large openings and turbulent flow conditions. Theoretically, the velocities and gas concentrations have to be measured at each opening of the NVB in the highest possible spatial resolution to gain the most accurate results [22]. In practice, the limits of what is practically and economically feasible are quickly reached.

Joo et al. [15] measured the volume flow rate and the emissions of two NVB with a direct method. They sampled the velocity and gas concentrations at 16 locations at each barn, where 12 ultrasonic anemometers (USA) and gas sampling points where evenly distributed along the side openings at a constant height, and 4 additional sampling points were sampled at the ridge opening of the barn. They reported a discrepancy between measured inflow and outflow with 19% lower outflow rates than the inflow rates, which is an indication for an insufficient resolution of sampling positions.

Van Overbeke et al. [33] measured the velocity at two opposite, small openings at a test barn, each equipped with a mobile ultrasonic anemometer on a traverse system, and concluded that the validity of the estimated volume flow rates depends on the sampling rate and sensor positions. De Vogeleer et al. [34] adopted this conclusion and investigated at the same test barn the effect of the velocity sampling density on the estimation of volume flow rates. They found that the distribution of the sampling locations at openings to be as important as the number of sampling locations used. Even if the number of sensors was constant, not representatively selected sampling locations could lead to systematic over- or underestimation of the volume flow rates, resulting in deviances up to 23%.

Wang et al. [16] used the same measurement set up as Joo et al. [15] and measured the volume flow rates both with the CO_2 mass balance method and the direct method, and used

the direct method to assess the CO_2 mass balance method. They could demonstrate the superiority of the direct method over the CO_2 mass balance method in situations, where the modeled CO_2 production term causes systematic errors (e.g. related to the animal activity correction term for the diurnal production pattern given in [27] or within milking periods, where not all animals were present), or when the difference of inside-outside concentrations of CO_2 (the denominator of equation 1.4) is so low that non-physical values for the volume flow rates are computed.

Despite these difficulties in finding representative sensor positions, direct methods provide a high potential in measuring volume flow rates and emissions from naturally ventilated barns, or in more general, from any arbitrary housing system. The prerequisite for this is a sufficiently dense spatial sensor resolution. Since the costs for sensors are high, usually the aim is to have a most efficient measurement design, meaning a lowest possible number of sensors with a maximum possible accuracy.

Concerning the investigations to quantify the uncertainty or at least the precision of applied direct methods in dependence of the sensor density, the focus was on the estimation of the volume flow rates, and these studies were conducted on rather small housing systems for pigs, with substantially smaller dimensions than housing systems for dairy cows. What is missing is a systematic investigation of the influence of sensor density, both for velocity and gas concentrations, on the accuracy of directly estimating the emissions of a real scale naturally ventilated dairy barn. This is probably due to the large dimensions, making it hard to install a real dense sensor network under real conditions. A promising alternative for overcoming this challenge is the use of modeling, which will be described in the following section.

1.5 Modeling emissions

All the emissions from NVB have in common that they are transported with the airflow, and in many cases, like e.g. NH_3 or particulate matter, the airflow is not only responsible for their transport, but also plays a significant role in their formation [35, 36]. Hence, a profound understanding of the airflow and the processes of gas dispersion is necessary to measure and mitigate emissions from NVBs. The modeling of the airflow and dispersion of gas concentrations can help to understand the driving mechanisms in great detail, whereby recommendations for real scale on-farm measurements can be derived.

This can be done either in the physical, real world by using laboratory conditions, or with the help of numerical simulations, using computational methods.

1.5.1 Physical modeling in an atmospheric boundary layer wind tunnel

1.5.1.1 Theory

The flow field in and around naturally ventilated barns is mainly dominated by the flow processes in the atmospheric boundary layer (ABL). The idea of physical modeling with atmospheric boundary layer wind tunnels (ABLWT) is therefore, to scale down the model of investigation in company with the physical properties of the corresponding ABL. For such purpose, certain similarity criteria have to be met, which will partly be discussed in the following.

The vertical velocity profile of the ABL has a shape that can be described by a power law:

$$u = u_r \left(\frac{z}{z_r} \right)^{\alpha} \tag{1.6}$$

where u is the wind speed in m·s^{-1} at height z in m, u_r is the reference wind speed in m·s^{-1} at a reference height z_r in m, and α is a profile exponent. In the atmosphere near ground (100 m and less above ground), the logarithmic wind profile is recommended to describe the vertical velocity profile [37]:

$$u_z = \frac{u_*}{\kappa} \left[\ln \left(\frac{z}{z_0} \right) \right] \tag{1.7}$$

with u_* as the friction velocity in m·s^{-1}, κ as the von Kármán constant (≈ 0.4), and z_0 as the roughness length in m. The atmospheric boundary layer near ground develops a logarithmic shape, because the wind is slowed down towards the ground. This is due to the friction at the rough ground, which induces turbulent vortices into the flow and decelerates it. Different roughnesses induce different portions of turbulence, resulting in different deceleration rates. This is described by the the roughness length z_0, which is a measure for the roughness of the investigated terrain. In an ABLWT, this is imitated with the help of roughness elements and other flow obstacles, as depicted in figure 1.3b). Figure 1.2a) sketches the influence of the roughness length on the shape of the velocity profile. When investigating a scaled down model in the ABLWT, the roughness length according to the scale of the experiment must be the same or similar to the roughness length, which characterizes the terrain in the real scale.

The roughness-induced turbulence can be measured by the turbulence intensity, which is defined as the standard deviation of the velocity component divided by the mean velocity of the component. Since different roughness levels introduce different levels of turbulence intensity, the vertical profile of turbulence intensity in the ABLWT must be within the boundaries of the respective roughness level to obtain a similar flow to the real scale, depicted in figure 1.2b).

The Reynolds number describes the ratio of inertial forces to viscous forces and is defined as

$$Re = \frac{uL}{\nu} \tag{1.8}$$

with u as the velocity in m·s^{-1}, L as a characteristic length of the flow problem in m, and ν as the kinematic viscosity of the fluid in m^2·s^{-1}. For similarity, the Reynolds number in the ABLWT experiments must be equal to the Reynolds number in the real scale. In most cases, due to the large scaling factors, this is not possible. Instead, a certain threshold Reynolds number needs to be exceeded, with a threshold dependent on the application [37, 38, 39].

Provided that the above discussed similarity criteria are met, the investigated flow and dispersion processes from the ABLWT measurements with scaled-down models can be scaled up to the real world. The boundary conditions for the experiments can be fully controlled, and velocities and gas concentrations can be measured under representative and reproducible conditions. This makes ABLWT modeling an attractive tool for the investigation of volume flow rates and emissions from naturally ventilated barns.
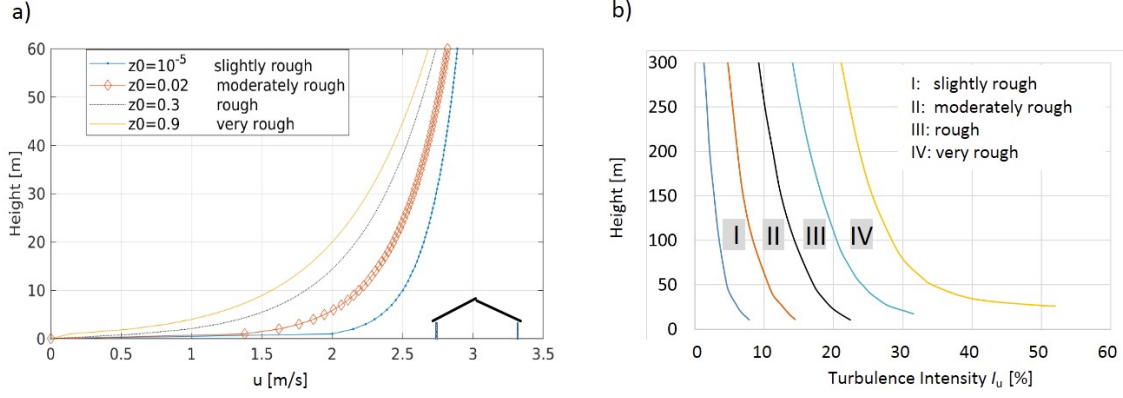
Figure 1.2: a): Influence of the roughness class on the vertical velocity profile in main flow direction of the boundary layer. b): Boundaries for the turbulence intensity for the velocity component in flow direction. To achieve a flow similar to the real scale, the modeled vertical turbulence intensity must be within the boundaries of the real scale roughness class. Examples for roughness classes are I: water surface, II: grass- and farmland, III: suburban area, and IV: inner-city area.

1.5.1.2 Application of ABLWT modeling for naturally ventilated buildings

In the context of naturally ventilated barns, several previous studies were done using ABLWTs to investigate inside airflow characteristics. The flow pattern studies were used to estimate the well-being of the animals and also for investigations of the volume flow rate. Yi et al. [40] studied the velocity distribution in a dairy barn model and could prove a significant impact of the opening geometry on the airflow pattern, especially in the animal occupied zones. The opening geometries of naturally ventilated barns were also studied by Shen et al. [41], De Paepe et al. [42], and Yi et al. [43], who all concluded a crucial impact of the opening size and position on the volume flow rates. However, none of these studies investigated the influence of the number and position of velocity sensors on the measurement of volume flow rates.

Several studies can be found that study the emission characteristics of naturally ventilated buildings by investigating the transport and dispersion of tracer gases. The near-field immission potential of a naturally ventilated pig barn was investigated by Yi et al. [44]. Although no concentrations of a pollutant were measured, the characteristics of the downstream airflow patterns were used to assess the immission potential related to the opening geometry.

A recent study of Nosek et al. [45] investigated the influence of the atmospheric boundary layer, opening configuration and animal presence on the flow field and the dilution of a uniformly injected tracer gas in a naturally ventilated dairy barn. They found that the tracer gas for all studied cases was not well mixed within the barn, which could lead to high errors (factor 3) when applying indirect tracer gas methods to determine the volume flow rate.

So far, no attempt was made to use the advantages of an atmospheric boundary layer wind tunnel to systematically investigate the accuracy of direct emission measurements in dependence of the sensor density.

The second part of the thesis aims therefore to close this gap and investigates a model of a naturally ventilated dairy barn, where emissions are directly measured as the product of the normal velocity vector $\vec{n}$ and the pollutant gas concentration c_P. The influence of the

sampling strategy on the accuracy of volume flow rate and emission estimation is investigated by a systematic variation of the sampling point distribution.

1.5.2   Numerical modeling

1.5.2.1   Theory

A Newtonian fluid can be fully described by the Navier-Stokes equations, which express the conservation of mass, momentum, and Energy. For an incompressible Newtonian fluid of constant temperature, the Navier-Stokes equations can be formulated in Cartesian coordinates and partial differential form as:

$$\frac{\partial u_i}{\partial x_i} = 0 \tag{1.9}$$

$$\frac{\partial u_i}{\partial t} + \frac{\partial}{\partial x_j}(u_i u_j) = -\frac{1}{\rho}\frac{\partial p}{\partial x_i} + \frac{\partial}{\partial x_j}(2\nu s_{ij}) \tag{1.10}$$

with u_i as the velocity, x_i the position, p the pressure, t the time, ρ the density, ν the kinematic viscosity, and s_{ij} the strain-rate tensor:

$$s_{ij} = \frac{1}{2}\left(\frac{\partial u_i}{\partial x_j} + \frac{\partial u_j}{\partial x_i}\right) \tag{1.11}$$

Computational Fluid Dynamics (CFD) is the discipline of numerically solving the Navier-Stokes equations. For that, the equation system is discretized by transferring it to an algebraic equation system, which is then solved by iterative methods. Usually, more or less simplifying assumptions are made, especially regarding the turbulence, which is discussed in the following section

DNS

All flows of technical interest are of turbulent nature, hence the treatment of turbulence is of particular relevance. In principle, all turbulent scales in a flow could be resolved and the Navier Stokes equations could be solved without any approximation of the turbulence. This approach is called direct numerical simulations (DNS). Due to the immense computational effort, DNS is only used in fundamental investigations of basic flow problems [46].

RANS

Reynolds-averaged Navier-Stokes (RANS) models provide a good cost-benefit ratio and are used in scientific and industrial applications since more than 40 years. With the RANS equations, only the mean flow is solved, while all scales of the turbulence are parametrized. This results in comparatively little computational costs and a good cost-benefit ratio. For the turbulence parametrization, a turbulence model is applied. The choice of the turbulence model has a huge impact on the accuracy of the results [47]. The disadvantage of these models is that time-varying processes, that are inherent to atmospheric flows, are not resolved. In addition, certain flow problems can hardly be simulated with sufficient accuracy using the RANS equations. Three-dimensional separating and reattaching flows for example, as often occur on downwind sided barn roofs or behind blunt flow obstacles inside the barn, can not be simulated accurately with the vast majority of turbulence models, due to their limitations like e.g. the assumption of isotropic turbulence.

An excellent overview on turbulence models within the RANS approach is given in [48], a more specific discussion on the feasibility of RANS for the discipline of building simulations (to which studies of naturally ventilated barns can be assigned) can be found in [49].

LES

In Large Eddy Simulations (LES), the assumption is made, that in the larger scales of turbulence, the most energy is transported, and in an energy cascade transported down to the smaller scales, where it dissipates. Hence, the large vortex structures are calculated directly, as with DNS, and only the small vortices are mapped using a turbulence model. Thus, LES models have the potential to predict transient processes with comparatively less computational effort.

Filtering the Navier-Stokes equations results in Eq.(1.12) where $\tau_{ij}^{SGS} = \widetilde{u_i u_j} - \tilde{u}_i \tilde{u}_j$ is the sub grid stress(SGS) which considers the effect of small vortices.

$$\rho \frac{\partial \tilde{u}_i}{\partial t} + \rho \frac{\partial \tilde{u}_i \tilde{u}_j}{\partial x_j} = \rho \frac{\partial}{\partial x_j} \left[\nu \frac{\partial \tilde{u}_i}{\partial x_j} - \tau_{ij}^{SGS} \right] - \frac{\partial \tilde{p}}{\partial x_i} + \rho g_i \tag{1.12}$$

The sub grid stresses are calculated using turbulence models. One of the most used is the Smagorinsky-Lilly turbulence model, which uses the idea of Prandtl mixing theory and calculates the stress as

$$\tau_{ij}^{SGS} \approx -2\nu_{SGS}\tilde{s}_{ij} + \frac{1}{3}\tau_{kk}^{SGS} \tag{1.13}$$

According to Smagorinsky, the subgrid viscosity is calculated as

$$\nu_{SGS} = (C_s \Delta)^2 \sqrt{2\tilde{s}_{ij}\tilde{s}_{ij}}, \qquad \tilde{s}_{ij} = \frac{1}{2}\left(\frac{\partial \tilde{u}_i}{\partial x_j} + \frac{\partial \tilde{u}_j}{\partial x_i} \right) \tag{1.14}$$

where $\tilde{s}_{ij}$ is the strain rate tensor and C_s is the constant of Smagorinsky. The constant of Smagorinsky was estimated by Lilly theoretically in the range of 0.17 - 0.21.

Because LES are transient by nature, they have the clear advantage that the influence of time dependent, dynamic processes can be investigated [50, 47]. Hence, in the prediction of transport and dilution of gas concentrations, they can be considered superior to RANS models in terms of accuracy [51]. Also, since they solve the biggest portion of anisotropic turbulent processes and only model the small scale, isotropic turbulence portions of the flow, their prediction of turbulence, shear flows and the flow separation and reattachment is more accurate than steady state RANS simulations [47, 52, 53].

However, the mentioned advantages go along with an immense increase of needed computational effort. This is due to higher requirements on the mesh density and most importantly due to the small time steps along with a required duration of simulation time, until the results statistically converge [54]. Typically, higher computation times of the factor 40-100 are reported [47, 51, 49], when LES are compared to RANS.

1.5.2.2 Application of CFD in livestock housing

CFD is a useful tool for acquiring detailed insight into the complex flow fields encountered in naturally ventilated barns. In particular, CFD allows to predict the main features of the flow fields also at locations where measurements are practically infeasible, or to perform virtual

assessment studies with the help of computational models. The use of CFD has an increasing focus in agricultural applications since the past 30 years [55, 56].

Related to the livestock sector, CFD is used with a wide variety of applications. It ranges from the modeling of heat transfer from animals (e.g. [57, 58, 59]), the formation of pollutants (in particular ammonia), [60, 61, 62], the distribution of heat and vapour inside the housing systems [63, 64, 65], and also the transport and dispersion of gaseous and particulate pollutants in and around housing systems [66, 67].

Since the airflow pattern and the volume flow rate play an important role in the estimation of emissions in naturally ventilated barns, a large number of studies can be found investigating this topic, as reviewed by Norton et al. [56] and [60]. The volume flow rates are either computed directly as the surface integral of the normal velocity vectors over the model openings, or by indirect computation with a simulated tracer gas [68, 69, 70].

In agricultural applications, numerical flow simulations typically rely on the RANS (Reynolds averaged Navier-Stokes) approach [55, 71]. Studies with LES simulations, or transient simulations at all are the exception. Only few papers can be found, e.g. Villagran, Romero, and Bojaca [72], where 2D transient simulations with Ansys Fluent were carried out with the focus on greenhouses.

In order to benefit from the above mentioned advantages of computationally cost intensive transient LES, the use of high performance computing (HPC) with parallel computing CPUs is required. It is not uncommon, that commercial software license policy fees are increasing with the number of CPU, so that additionally to the increased computational effort, higher financial costs arise.

Also, many of the computer clusters freely accessible to research institutes do not even offer the use of proprietary software. Moreover, commercial tools do not give access to the source code, thus making it difficult to understand the details of numerical methods used within the solver. Open source solvers can represent here an appealing alternative. Besides being free of charge, they provide complete control over the numerical methods and give also the possibility of customizing the code and implementing tailored methods.

In the literature, only few studies can be found using non-commercial solvers to investigate the flow inside or around agricultural buildings. A research group around Lee used OpenFOAM with a steady-state RANS approach [73, 74, 75], and a research group around Kateris used finite-element-methods with an in-house code written in FORTRAN [76].

The third part of the thesis therefore aims to fill this gap and to investigate the feasibility of transient open source solvers for turbulent flow simulations inside and around an agricultural building.

1.6 Three-column approach

The estimation of emissions from large naturally ventilated barns is highly complex. The dominating processes are most of the time of turbulent and transient nature. Most likely, there is no 'one perfect' solution to the challenge of accurate, precise estimates. However, each of the methical approaches *on-farm measurement*, *ABLWT modeling*, and *numerical modeling*, has its own specific strengths and benefits, and limitations. Wind tunnel modeling for example has

the benefit of controllable and statistically stable boundary conditions, leading to reproducible results. On the other hand, wind tunnel modeling has certain limitations, like the restriction to iso-thermal flows or to a stable wind incident angle per experiment (see for that also section 5.1.4). These phenomena can better be investigated by on-farm measurements, which don't lack such limitations. However, the limitation in on-farm measurements is often the insufficient resolution of sensors for a representative sampling of gas concentrations. This can be overcome by the use of numerical modeling, where gas concentrations and air flow patterns can be determined in detail, and recommendations for the on-farm measurement setup can be derived.

For the reasons mentioned above, in this thesis, the use of three different approaches for the same problem is made, under the assumption that the benefits of each method can overcome the limitations of the respective other methods, and synergy effects arise. This methodology will be called 'three-column approach' in the further text.
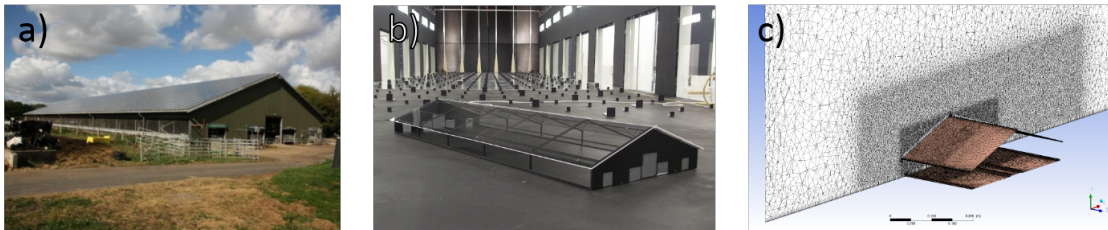
Figure 1.3: The investigated barn with the three column approach. a) in real scale b) as model in the wind tunnel with roughness elements c) as CFD model.

1.7 Objectives and hypotheses of the thesis

The main objectives of the thesis are (O.1) the systematic quantification of induced errors due to the measuring method, both for direct and indirect measurements. (O.2) Based on this, recommendations for the measurements of volume flow rates and emissions under the studied conditions shall be derived, both for direct and indirect methods. (O.3) Furthermore, a simulation tool for the investigations of volume flow rates and emissions of arbitrary flow situations and building geometries shall be applied and assessed.

Following hypotheses have been formulated, that will be tested:

H1 The sampling strategy has a significant influence on the estimation of ventilation flow rates and emissions, which is mainly dependent on the position of the sampling points.

H2 Different sampling strategies and sensor locations lead to systematic over- or underestimations of volume flow rates and emissions of pollutants. Hence, systematic errors can be reduced with a deeper insight of the flow and recommendations for a reduced bias can be formulated.

H3 The application of different methodologies permits a deeper understanding of the driving mechanisms of the complex emission system NVB, and the benefits of each method can help to overcome the limitations of the respective other methods.

To reach the main objectives and test the hypotheses, following specific objectives have been formulated:

O.1.1 Long-term measurements for the estimation of volume flow rates and emissions of a naturally ventilated dairy barn shall be applied. A sufficiently large dataset shall be produced, that enables the investigation of the influence of the sampling strategy on the estimation of volume flow rates and emissions, using the CO_2 mass balance method.

O.1.2 Based on the dataset, the influence of the sampling strategy on the estimation of volume flow rates and emissions using the indirect CO_2 mass balance method shall be quantified

O.1.3 Recommendations shall be derived for the application of a respective sampling strategy under respective flow conditions and building specifications.

O.2.1 An experimental setup that enables to investigate direct measurements of a large naturally ventilated dairy barn under stable conditions shall be designed

O.2.2 The impact of number and position of anemometers and gas sensors on the estimation of volume flow and emissions shall be quantified

O.2.3 Practical suggestions for measurement setups in terms of number and positioning of anemometers and gas sensors shall be derived

O.3.1 Wind tunnel measurements of the turbulent characteristics and the air flow pattern in and around a naturally ventilated dairy barn shall be conducted to generate a benchmark database.

O.3.2 The database shall be used to investigate the feasibility of transient open source solvers for turbulent flow simulations inside and around the naturally ventilated dairy barn.

1.8 Outline of the dissertation

This thesis is structured as follows:

Chapter 1 presents an overview of the current state of research and theory formation in the field of emission measurements and modeling from naturally ventilated barns, followed by the formulation of research questions and objectives of the thesis.

Chapter 2 presents the study of long term measurements of volume flow rates and ammonia emissions of a naturally ventilated dairy barn, using the CO_2 mass balance method. It is devoted to reach the specific objectives O.1.1 - O.1.3.

Chapter 3 presents a study in an ABLWT on the accuracy of direct methods, based on high resolution measurements of velocities and concentrations. It is devoted to reach the specific objectives O.2.1 - O.2.3.

Chapter 4 presents the measurements of airflow patterns inside a naturally ventilated dairy barn in an ABLWT. Two transient open source solver were used to simulate the measured airflow pattern using LES. It is devoted to reach the specific objectives O.3.1 - O.3.2.

Chapter 5 summarizes and discusses the main findings of the individual studies, provides general conclusions and proposes directions for future research.
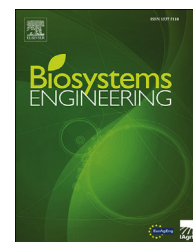
2

Calculation of Ventilation Rates and Ammonia Emissions: Comparison of Sampling Strategies for a Naturally Ventilated Dairy Barn

Available online at www.sciencedirect.com

ScienceDirect

Research Paper

Calculation of ventilation rates and ammonia emissions: Comparison of sampling strategies for a naturally ventilated dairy barn

David Janke [a],[*], Dylia Willink [a], Christian Ammon [a], Sabrina Hempel [a], Sabine Schrade [c], Peter Demeyer [d], Eberhard Hartung [f], Barbara Amon [a],[g], Nico Ogink [e], Thomas Amon [a],[b]

[a] Leibniz Institute for Agricultural Engineering and Bioeconomy(ATB), Max-Eyth-Allee 100, 14469 Potsdam, Germany
[b] Institute of Animal Hygiene and Environmental Health, Department of Veterinary Medicine, Free University of Berlin, Robert-von-Ostertag-Str. 7-13, 14163 Berlin, Germany
[c] Agroscope, Ruminant Research Unit, Taenikon, 8356 Ettenhausen, Switzerland
[d] Flanders Research Institute for Agriculture, Fisheries and Food (ILVO), Technology and Food Science Unit, Belgium
[e] Wageningen UR Livestock Research, Wageningen, the Netherlands
[f] University of Kiel, Institute of Agricultural Engineering, Kiel, Germany
[g] University of Zielona Góra, Faculty of Civil Engineering, Architecture and Environmental Engineering, Poland

Emissions and ventilation rates (VRs) in naturally ventilated dairy barns (NVDBs) are usually measured using indirect methods, where the choice of inside and outside sampling locations (i.e. sampling strategy) is crucial. The goal of this study was to quantify the influence of the sampling strategy on the estimation of emissions and VRs. We equipped a NVDB in northern Germany with an extensive measuring setup capable of measuring emissions under all wind conditions. Ammonia (NH$_3$) and carbon dioxide (CO$_2$) concentrations were measured with two Fourier-transform infrared spectrometers. Hourly values for ventilation rates and emissions for ammonia over a period of nearly a year were derived using the CO$_2$ balance method and five different sampling strategies for the acquisition of indoor and outdoor concentrations were applied. When comparing the strategy estimating the highest emission level to the strategy estimating the lowest, the differences in NH$_3$ emissions in winter, transition, and summer season were +26%, +19% and +11%, respectively. For the ventilation rates, the differences were +80%, +94%, and 63% for the winter, transition and summer season, respectively. By accommodating inside/outside concentration measurements around the entire perimeter of the barn instead of a reduced part of the perimeter (aligned to a presumed main wind direction), the amount of available data substantially increased for around 210% for the same monitoring period.

* Corresponding author.
E-mail address: djanke@atb-potsdam.de (D. Janke).

1.   Introduction

Agriculture contributes up to 92% of the European ammonia emissions, where 11% are related to the manure management of dairy cattle (EEA, 2016). Accurate measurements are a basis for efficient emission mitigation measures. Dairy cows are mainly housed in naturally ventilated barns (NVB). In NVBs, air exchange rates and gaseous emissions are usually measured by indirect gas balancing methods, where the air exchange rates can be derived from measuring the dilution of a tracer gas with a known release rate. The emission rate of the target gas can then be derived as the product of the air exchange rate and the target gas concentration. A common approach is to use CO_2 (which is produced by the animals with a known release rate) as a tracer gas to estimate the air exchange rate (Ogink et al., 2013). Due to their large openings, NVBs are directly influenced by outside climatic conditions. This results in complex flow fields inside and around the building, where the concentrations of gases like CO_2 and NH_3 are distributed highly heterogeneously, both in time and space. Since the estimation of ventilation rates (VR) and ammonia emissions (E_{NH3}) relies on indirect balancing methods, the differences of measured outdoor and indoor concentrations of CO_2 (for the VR) and NH_3 (for the E_{NH3}) have a major influence on the accuracy of the results. The magnitude of the difference is directly dependent on the choice of sampling location for the outdoor and indoor concentration measurements (Edouard et al., 2016; König et al., 2018).

When using indirect CO_2 balancing methods, measurements of the NH_3 and CO_2 concentrations are required which are representative for the exhaust, barn leaving gas concentrations. The same applies to the measurements of NH_3 and CO_2 concentrations that are entering the barn. The challenge is to identify the position(s), where a representative measurement of exhaust and entering concentrations is possible. In the following, the exhaust gas concentrations will be called *inside gas concentrations* and the barn entering concentrations will be called *outside gas concentrations*.

Another important aspect is the time resolution and duration of the measurements. It needs to be chosen in a way, that representative results can be expected. Although important, this aspect will not be investigated in this study. This study considered hourly wind and concentration conditions.

1.1.   Measuring inside gas concentrations

Van Buggenhout et al. (2009) conducted experiments in a laboratory test room with mechanical ventilation to investigate the influence of the sampling location on the accuracy of the estimation of VRs with a tracer gas technique. They found that the positioning of sampling points had a significant influence on the result of the ventilation rate estimation, and can cause errors up to 86%, due to heterogeneously distributed gas concentrations inside the building. The best results were derived when the sampling was done directly at the outlet, where the error was always lower than 10%.

König et al. (2018) and Ngwabie et al. (2009) investigated gas concentrations with point wise measurements inside a NVB.

They found variations for the VRs up to 46% (König et al., 2018) and variations for NH_3 concentrations up to 35% (Ngwabie et al., 2009), when only individual sampling points were taken into account. Both authors suggest therefore the use of multipoint measurements to measure the gas concentrations inside the barn.

An intensive variant of these multipoint measurements is the use of so-called sampling lines. Here, the sampling air is sucked through tubes with many orifices over their length, that allow a high spatial resolution of sampling locations. Their use is published e.g. by Wu et al. (2012), where sampling lines were positioned at the two side openings and the ridge opening of a NVB. They chose these positions following the studies of Demmers et al. (2001) and Demmers et al. (1998), who concluded that due to no identifiable representative zone inside the building, the best location to measure the concentrations was at the outlets.

Edouard et al. (2016) used both, individual sampling points and sampling lines to investigate the influence of different spatial sampling strategies on the estimation of the VR. The sampling points and sampling lines under investigation were all positioned at the central axis in the middle of the barn, based on previous studies by Shen et al. (2012) optimization and Mendes et al. (2015) and on the assumption, that in NVBs the outlets can also act as inlets, which would bias the results.

Mohn et al. (2018) measured NH_3 of a compartment in a NVB and used a net of sampling lines, that were connected with each other, so that physically mixed sample was generated and measured as inside gas concentration.

Schrade et al. (2012) measured NH_3 in several different NVB, where they installed sampling lines either at every opening (ridge, gate, windows), or net-like over the animal occupied zones. In contrast to Mohn et al. (2018), the mean value of all sampling lines was not formed directly by physically mixing the concentrations of all lines, but sequentially measuring line after line and then forming the mean value afterwards. Both Schrade et al. (2012) and Mohn et al. (2018) used the artificial tracer gases SF_6 and SF_5Cf_3 instead of the naturally produced CO_2.

The VERA test protocol (VERA, 2018) gives a guideline on the measurement strategy for naturally ventilated buildings. For measuring the inside concentrations, it recommends either to place a sampling line in the middle of the building (for symmetrical houses), or for more open barns towards the side walls (that are described here as outlet openings), with a minimum distance of 2 m to the walls.

Concerning the measurement of gas concentrations within the barn, it can be summarised that multi-point sampling is preferable to single-point sampling. Sampling lines with many orifices provide a good opportunity to sample gas concentrations in a high spatial resolution over a long distance. No clear trend in the literature is recognisable whether these sampling lines should (i) cover only the outlets, (ii) be placed in the middle of the barn or (iii) cover as many regions inside the barn as possible.

1.2.   Measuring outside gas concentrations

The measurement of the outside concentrations can be categorised in three approaches. In the first approach, the mean

value of several point measurements positioned outside the barn is used. It is based on the idea that the more sampling points, the more representative the result will be. Examples can be found e.g. in Saha et al. (2013), Saha, Fiedler, et al. (2014) and Ngwabie et al. (2011). In the second approach, a sampling point is located at the approaching wind direction and measures the concentrations transported with the actual wind direction. This can be done either for only one main wind direction where situations with deviating wind directions are not taken into account (Schmithausen et al., 2018) or with several sampling points, taking into account variations of the approaching wind direction (König et al., 2018). The third approach takes into account several measurement points around the barn (e.g. one at each side opening) and uses the point with the lowest concentration for the outside gas concentration. The assumption behind this approach is that the sampling point positioned at the respective inlet opening must be the one with the lowest concentration. This strategy was used by e.g. by Ngwabie et al. (2009) and Wu et al. (2012), and is also recommended in the VERA test protocol (VERA, 2018). The only study we found that investigated the influence of different outside sampling locations was done by König et al. (2018). Four outside concentration sampling points were positioned at each side opening of a NVB. The VR was estimated based on each single point and based on the point at the respective approaching flow direction, defined by wind direction measurements. Compared to the wind direction strategy, the median values for VRs estimated by the fixed single points differed between −15% and +4%.

1.3. Combination of measuring outside and inside gas concentrations

We define the *sampling strategy* as the combination of outside and inside sampling locations that are used to calculate the difference of gas concentrations. With many sampling locations (or sampling lines) inside and outside the barn, many sampling strategies are possible to quantify the concentration differences. All sampling strategies found in the literature rely on comprehensible assumptions regarding the flow behavior and the transport of gas concentrations, and they combine different degrees of information to estimate VRs and E_{NH3}. In summary, an increase in accuracy is expected by increasing the quantity (more sampling locations) and/or quality of information (additional sources of information such as wind measurements or previous smoke tests) to reduce the risk of systematic errors. So far, the influence of different sampling strategies on the estimation of VR and E_{NH3} is insufficiently understood.

Our hypotheses are (1) The sampling strategy has a significant influence on the estimation of VR and E_{NH3}; and (2) Different sampling strategies lead to systematic deviations (over- or underestimation of VR and E_{NH3}) due to their design. The corresponding objectives of this study are to test these hypotheses and to quantify the influence of the sampling strategy on VR and E_{NH3} estimates.

To achieve the objectives, a set of five sampling strategies was considered and applied to a dataset of measurement values generated from long term measurements in a NVB, which will be described in the following in chapter 2.4.

2. Material and methods

2.1. Barn and site description

Measurements were carried out in an experimental dairy barn located in Dummerstorf in the northeast of Germany (54°1′ 0″ N, 12° 13′ 60″ E, altitude 43 m) near the city of Rostock. The barn's dimensions are 96.15 m length and 34.2 m width; its metal roof has a triangular shape, with the gable top reaching a maximum height of 10.7 m, decreasing to 4.2 m at the lowest point (on the sides). The total volume of the barn is 25,499 m^3. The floor is made of solid concrete and is cleaned every 90 min by automatic scrapers that push the slurry into four manure pits outside the barn. The barn is naturally ventilated, with open side walls and a ridge opening with a width of around 0.5 m. Only at very cold winter nights the side walls are closed using a polyethylene film. For air movements inside the barn, four additional ceiling fans (Powerfoil X2.0, Big Ass Fans HQ, Lexington, KY, USA) are installed on a height of 5.6 m above the floor over the feeding alley. They have a diameter of 7.34 m and operate temperature controlled under partial load for 10 °C > T > 5 °C, and under full load for T > 10 °C. The barn capacity was 375 dairy cows, which are free to move inside the barn. In north eastern direction, the barn is partly surrounded by other buildings, including a milking parlour, storage tanks, a young stock house and another NVB. In south western direction, the barn is surrounded by open field.

2.2. Instrument setup and data collection

2.2.1. Measuring instruments description
For the current work, more than 900 m of sampling lines made of PTFE with an inner diameter of 6 mm were installed inside and around the barn. Figure 1 presents a detailed plan of the distribution of the sampling lines. Table 1 lists the distances of the lines to the respective walls. Every 8–10 m, the lines were equipped with critical orifices, which ensured a constant volume flow over the length of each line. Carbon dioxide and ammonia concentrations were measured every hour from four sample lines representing outdoor concentrations, and from six sample lines for indoor concentrations. Two high-resolution Fourier-transform infrared (FTIR) spectrometers (Gasmet CX4000, Gasmet Technologies Oy) were used for measurements, each equipped with a multichannel to switch between the lines. The FTIR spectrometer had a standard uncertainty of 5–8% and worked in parallel, each connected to six sampling lines. The lines were measured one after another. In total, each line was measured 10 min. Seven minutes were used to flush the line and the measuring cell and 3 min were used for concentration measurements. By this, all 12 lines were measured within one hour, and hourly values for VR and emissions could be derived. Table 2 shows one example measurement cycle. It has to be mentioned that, due to wind variation within the period of the 1-h measurement cycle, this procedure might also involve an additional uncertainty in the measurements, which will not be investigated in this study. Before the measurements, additionally to the in-built libraries, both FTIR were calibrated for CO_2 with calibrating gas containing a concentration of 500 ppm for CO_2 and
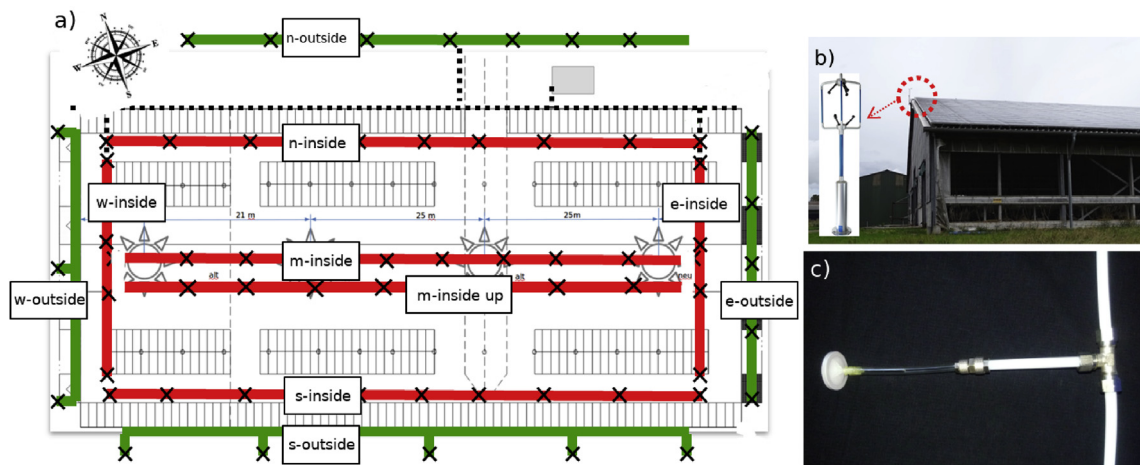
Fig. 1 — a) Plan of the location of measurement sample lines inside (red line) and outside (green lines) the barn. The first letters in the captions refer to north, east, south, west and middle, the second for inside and outside the barn. All lines were positioned at a height of 3.2 m, except line 'm-inside up', which was positioned at a height of 6.8 m. Every x represents a critical orifice. **b)** Position and detailed view of the outside positioned ultrasonic anemometer. **c)** detailed view on the critical orifice.

Table 1 — Positions of the sampling lines. Distances are defined as distance from a line to it's corresponding building wall. The names of the sample lines indicate the cardinal directions with which they are aligned (n - north, e - east, s - south and w - west) as well as whether the lines are outside or inside the building.

Line	Distance (m)	Height (m)
n-outside	6	3.2
e-outside	4	3.2
s-outside	3	3.2
w-outside	3	3.2
n-inside	4	3.2
e-inside	8	3.2
s-inside	4	3.2
w-inside	8	3.2
m-inside	17	3.2
m-inside-up	17	6.8

Table 2 — One example measurement cycle of one hour with the two measurement devices FTIR1 and FTIR2. The lines 'extra 1' and 'extra 2' were additional lines, that were not taken into account for this study.

Time (min)	FTIR 1	FTIR 2
	Line	Line
10	n-outside	e-outside
20	s-inside	w-inside
30	m-inside	extra 1
40	s-outside	w-outside
50	n-inside	e-inside
60	m-inside-up	extra 2

calibrating gases containing concentrations of 0.5 ppm, 3 ppm and 5 ppm for NH_3. An ultrasonic anemometer (USA, Windmaster Pro ultrasonic anemometer, Gill Instruments Limited, Lymington, Hampshire, UK) was installed on the roof of the barn to measure the approaching wind velocity and direction. Inside the barn, temperature and relative humidity was measured with four EasyLog USB 2+ sensors (Lascar Electronics Inc., USA).

2.2.2. Animal data

CO_2 balance method calculations require information on the animals, including number of cows in the barn, their live weight (kg), average pregnancy length (days) and average milk production (kg day^{-1}). This data was collected by the administration of the Dummerstorf barn who kindly provided it to us for the current study. The cows had an average mass of 682 kg, the mean herd milk yield was 39.2 kg d^{-1} per animal. On average, 355 lactating Holstein-Friesian cows were in the barn and no dry cows were present. The cows were fed on totally mixed ration (TMR), consisting of corn and maize silage. For the computation of the CO_2 production term, the respective daily herd mean values were taken.

2.3. Air exchange rate and emissions calculations via indirect method

The ventilation rate was estimated from calculations of the mass balance of CO_2:

$$Q_t = \frac{C_{prod}}{(CO2_{inside} - CO2_{outside})} \cdot N_{animals}, \tag{1}$$

where Q_t is the total ventilation rate (m^3 h^{-1}), $CO2_{inside}$ and $CO2_{outside}$ are the concentrations of CO_2 inside and outside the barn respectively, C_{prod} is the estimated CO_2 production rate per animal and provided in g h^{-1}, and $N_{animals}$ is the number of animals inside the barn. The sources of CO_2 inside the barn were divided into two types: gas produced by animals and gas emitted from manure and bedding material. The gas produced by animals was considered to make up 95%, and the manure together with the bedding straw was considered to produce 5%, following the approach of Wang et al. (2016).

The CO_2 mass balancing method has been previously described in detail (Bjerg et al., 2012; Estellés et al., 2011; Pedersen, 2002, pp. 1–46; Pedersen et al., 1998; Samer & Abuarab, 2014; Wang et al., 2016), and is based on the estimation of animal heat production. Heat production varies due to animal physiology, different actions (milking, feeding, rumination), and animals' physical activity (Calvet et al., 2013). Those parameters must also be considered during calculations with the CO_2 balance method. The formula for calculating CO_2 production rate is presented as Equation (2). Heat production per cow (W) is multiplied by a factor of 0.185 and by an animal activity factor which varies depending on time of the day and type of animal, and can be identified as shown in Equation 6 (Pedersen, 2002).

$$C_{prod} = \frac{0.185 \cdot Heat_{prod} \cdot A}{1000} \tag{2}$$

$$Heat_{prod} = \Phi_{tot} \cdot t_{factor} \tag{3}$$

$$\Phi_{tot} = \Phi_{LM} + \Phi_{MY} + \Phi_p = 5.6m^{0.75} + 22Y_1 + 1.6 \cdot 10^{-5}p^3 \tag{4}$$

$$t_{factor} = 1000\left(1 + 4 \times 10^{-5}(20 - t)^3\right) \tag{5}$$

$$A = 1 - a \cdot (\sin(2 \cdot \pi / 24) \cdot (h + 6 - h_{min})) \tag{6}$$

where A is the relative animal activity; a is a constant expressing the amplitude with respect to the constant 1; h_{min} is the time of the day with minimum activity (hours after midnight); Φ_{LM} is heat dissipation due to maintenance of essential function (W); Φ_{MY} is heat dissipation due to milk yield (W); m is body mass of the cow (kg); Y_1 = milk production, (kg day^{-1}); t is the temperature inside the barn (°C), and p is days of pregnancy. Y_1 and p were provided by the barn operators, t was measured with the TH-logger inside the barn (see section 2.2.1).

Formula 3 provides the corrected total heat production $Heat_{prod}$ (W), calculated per cow at a temperature of 20 °C.

The total emission rate E_t (g h^{-1}) can be defined using the following equation:

$$E_t = Q_t \cdot (NH3_{inside} - NH3_{outside}) \tag{7}$$

where Q_t is the total ventilation rate (Eq. 1) and $NH3_{inside}$ and $NH3_{outside}$ are the NH_3 concentrations inside and outside the barn, respectively, in g m^{-3}. In order to make the results comparable to other studies, the measured NH_3 emissions will be provided as the emissions per livestock unit LU in g h^{-1} LU^{-1}, where 1 LU is the body mass equivalent of 500 kg, N is the number of animals and m is the average mass of one animal:

$$E = \frac{E_t \cdot LU}{N \cdot m}. \tag{8}$$

2.4. Sampling strategies

The approaching flow was divided into four sectors, each with an angle of 90°. The angles were adjusted to the orientation of the barn (+17° spin to the north–south axis), thus, each sector's symmetry line was perpendicular either to the longitudinal or the lateral openings. In the following text, flow entering the barn at the longitudinal side openings will be called north or south, and flow entering at the lateral openings at the gable walls will be called west or east. Consequently, in the following text flows from east or west will be called lateral flows, flows from south or north will be called cross flows.

Figure 1 shows the location of the sample lines, four on the outside and five inside the barn. Theoretically, there are 26 possible combinations to represent the value for the inside concentration (e.g. only the middle line or the mean value of all lines) and 15 possible combinations to represent the value for the outside concentration. This leads to 26 · 15 = 390 possible combinations for creating the inside - outside concentration difference. Based on the literature survey summarised in chapter 1 and additional assumptions regarding the flow characteristics inside the barn, we reduced this multitude of combinations to five different sampling strategies, that are summarised in Table 3 and further explained in the following subsections.

2.4.1. Strategy 1 - based on wind direction
Sampling strategy 1 was based on observed hourly wind directions. A visual description of this strategy is presented in Fig. 2 (M1). According to the wind direction, we defined every hour an actual inlet (green line) and outlet (red line) of the barn. The outside concentrations were then taken from the inlet sample line, the inside concentration from the outlet sample line.

2.4.2. Strategy 2 — based on combined wind directions and spatial averaging
Like strategy 1, sampling strategy 2 used hourly observed wind directions to determine the sample line for outside concentrations. In contrast to strategy 1, the inside concentrations were estimated for each hour as an average of all sample lines inside the barn, independent of the wind direction.

2.4.3. Strategy 3 — based on spatial average of sampling lines
This approach did not use any information about the wind direction. Instead, the mean values from all inside sampling lines were averaged to characterise the inside concentration, and the mean values from all outside sampling lines were averaged to characterise the outside concentrations.

2.4.4. Strategy 4 — based on spatial average for inside, lowest concentration for outside concentrations
In this strategy, the inside concentrations were estimated as an average of all sample lines inside the barn. For the outside concentration, the sample line with the respective hourly minimum concentration value was chosen.

2.4.5. Strategy 5 — based on spatial average for inside without the middle sampling line, lowest concentration for outside
This approach is a modified version of strategy 4, without taking into account the middle sample line $m - inside$ for inside concentrations. It was done because during the warm period in the middle of the barn, 4 huge cooling fans were constantly switched on. Those fans are installed in the middle of the barn (see Fig. 1 under line $m - inside$). We assume a high dilution of the concentrations at the position of sampling line $m - inside$, which may result in an underestimation of actual

Table 3 – Description of the applied sampling strategies.

Strategy	Inside sampling	Outside sampling	Assumption	Used by
M1	line in downwind direction	line in wind direction	The incoming flow pushes the gas concentrations in wind direction through the barn.	Schmithausen et al. (2018)
M2	mean value of all lines[a]	wind ward line	Using more sampling lines inside makes M2 more error-resistant than choosing only one line at the suspected outlet	König et al. (2018)
M3	mean value of all lines[a]	mean value all lines[a]	Robust strategy through smoothing out high concentration gradients	Saha et al. (2013), Saha et al. (2014b), Ngwabie et al. (2011)
M4	mean value of all lines[a]	line with minimum CO_2 concentration	The incoming flow must consist the lowest CO_2 concentrations, hence the outside line with lowest CO_2 concentrations must be at the inlet.	Ngwabie et al. (2009), Wu et al. (2012)
M5	mean value of lines positioned at openings[a]	line with minimum CO_2 concentration	Measuring concentrations at the openings is sufficient, no sampling in the middle is needed.	VERA (2018)

[a] The mean concentration values were computed every hour by forming the mean value of the individual sampling lines concentrations.

gas concentrations; thus, the central concentration line was skipped in this strategy.

2.5. Climate conditions

Weather in Germany is more or less stable with strongly-pronounced seasons and moderate climate, with deviation from North to South and from West to East due to geographical unevenness, surrounding by Baltic and Northern seas and the Alps located in the south of the country. The experimental barn is in the north-east, 20 km southern-east from a relatively big port city named Rostock and around 30 km away from Baltic sea. That makes the experimental place subjected to northern climate processes.

In order to investigate the role of wind direction on the estimation of VR and NH_3 emissions, wind vectors were measured with the anemometer described in chapter 2.2.1. They are presented as wind roses in Fig. 3. Wind roses are presented in several ways: for the whole researched year (Fig. 3 a); for November (Fig. 3 b) and by season (Fig. 3 c-e). The wind situation changes with the seasons; for example, in winter, winds are observed with near-equal frequencies from a spectrum of directions between east-south-east and north-north-west. In spring, more north-westerly winds were observed, while in summer, winds observed to blow primarily in western and south-eastern directions. A total of 6093 hourly values (described below as *events*) were taken into consideration. The wind data obtained during the measurement period were distributed as follows: 737 events from the north, 1862 from the south, 2004 events from the west, and 1490 events from the east. Thus, we can conclude that western and southern winds were the most frequently observed.

2.6. Data treatment and overview

Measurements took place throughout the period from November 2016 until September 2017 and hence covered all seasons. An overall amount of 5604 hourly data sets for gas concentrations in each sampling line was collected. In accordance to the recording date, the data was divided into the seasons winter (Dec−Feb), summer (Jun−Aug) and transition (Mar−May & Sep−Nov). Corresponding to the alignment of the barn, these data sets were further divided into northern, eastern, southern and western sectors, as depicted in Fig. 3. Table 4 shows the number of measurement values divided in seasons and wind directions.

The whole dataset with hourly measured gas concentrations in the sampling lines and additional ambient and animal parameters can be found in Janke et al. (2020).

2.7. Statistics

For statistical analysis the software packages SAS 9.4 (SAS Institute Inc., Cary, NC, USA) and Matlab were used. The derived results both for VR and E_{NH3} followed a skewed, non-Gaussian distribution. As a consequence, they were harmonised using a natural logarithmic transformation (Wilks, 2011). Repeated measures covariance analysis models were used to estimate the VR and E_{NH3} by strategy as well as to test differences between the five strategies while taking into account
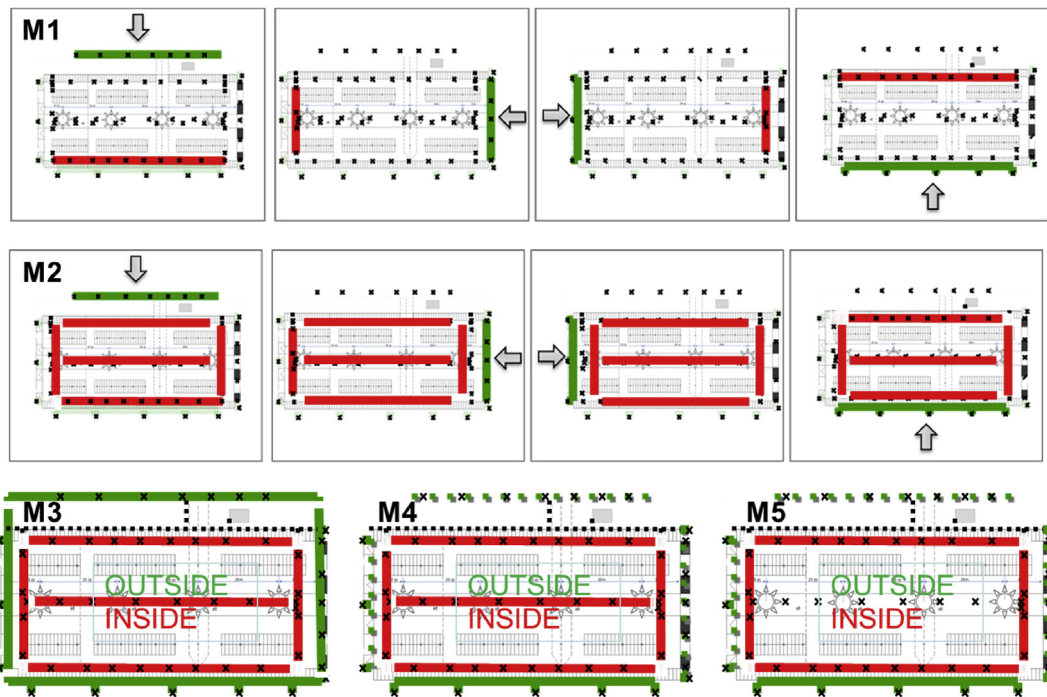
Fig. 2 – Schematic view of the sampling strategies M1, M2, M3, M4 and M5. Green lines correspond to outside measurements, red lines to inside measurements. The grey arrow marks the respective wind direction. Dashed colored lines for strategies M4 and M5 represent possible outside sampling lines, dependent on the concentration minimum.
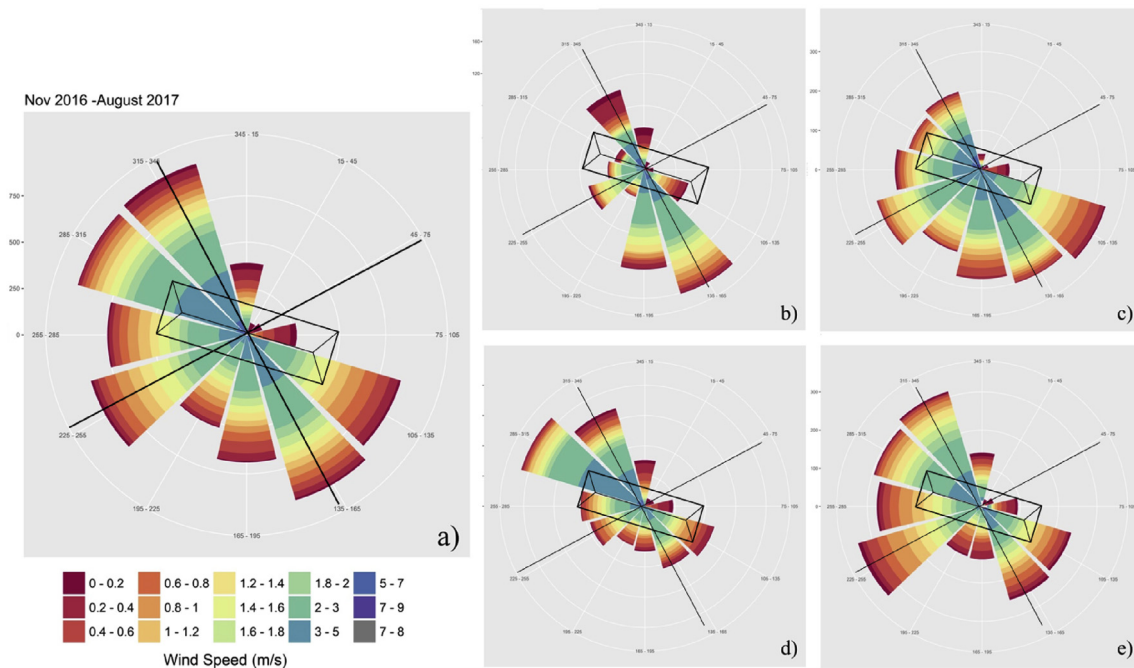
Fig. 3 – Wind roses obtained from the ultrasonic anemometer placed over the barns roof for a) November 2016–August 2017; b) November 2016; c) Winter 2016–2017; d) Spring 2017; e) Summer 2017. According to the alignment of the barn, the data sets were divided into four 90°-sectors, that were rotated 17° from the normal north, east, south and west sectors.

wind direction, wind speed and temperature, separately for each season. Fixed effects were strategy, wind direction and the interaction between strategy and wind direction. Wind speed and temperature were included as linear regression

covariables. The repeated hourly measures within each strategy were considered with a spatial power covariance structure of the R matrix (variance-covariance matrix of the residuals). Hypotheses were tested at a significance level of

Table 4 – Number of hourly gas concentration measurements, sorted for wind direction and season. The second column shows the average temperatures and standard deviation.

	T (°C)	N	E	S	W	Overall
Winter	1.8±3.8	163	571	790	617	2141
Transition	10.3±5.9	404	574	650	717	2345
Summer	19.1±4.3	71	233	320	494	1118
Overall	638	1378	1760	1828	5604	

5%. After analysis, the results were transformed back into normal space and are presented here as mean values with the upper and lower limits of their respective 95% confidence intervals (CI).

3. Results and discussion

The five strategies introduced in section 2.4 were used to calculate VRs and E_{NH3} for the whole dataset. In the following, the results will be presented and discussed.

3.1. Ventilation rates

3.1.1. Comparison with the literature

Figure 4 shows the mean ventilation rates in m^3 per hour and livestock unit estimated by the five strategies, sorted by seasons and wind directions. For all seasons and strategies, a wide spread of estimated values for VRs is visible, from 1190 m^3 h^{-1} LU^{-1} (lowest CI-limit of strategy 1 in winter season from northern wind directions) to 4267 m^3 h^{-1} LU^{-1} (highest CI-limit of strategy 3 in transition season with northern wind directions). In Saha et al. (2013) and König et al. (2018), the same barn as in this study was measured, but with a different instrumental setting and in different time periods. König et al. (2018) used a sampling strategy equal to our strategy 2 and published a total yearly mean value for the VR in the range between 1811 and 2012 m^3 h^{-1} LU^{-1}. This corresponds well with our measurements with a yearly mean value computed with strategy 2 in the range between 1576 and 2127 m^3 h^{-1} LU^{-1}.

In Saha et al. (2013), a sampling strategy equal to our strategy 5 was used. Their published results for VRs in a summer season were sorted after wind direction. Following values were estimated: 1122–1500 m^3 h^{-1} LU^{-1} for northern winds, 1112–1301 m^3 h^{-1} LU^{-1} for eastern winds, 2109–2922 m^3 h^{-1} LU^{-1} for southern winds, and 1433–1920 m^3 h^{-1} LU^{-1} for western winds. The results for VRs from our study agree well with the results from Saha et al. (2013) for wind directions from south and west (no significant differences). Slightly higher VRs are estimated in our study for wind directions from east, and significantly higher VRs (appr. +60%) are estimated for northern winds. A reason for the high deviation for northern winds could be the relatively low number of data samples for the summer period with northern winds (71 in our study, 62 in the study of Saha et al. (2013)), that can lead to over- or underestimation of gusts or calms or simply different weather conditions in the different years of the studies (2012 and 2017).

3.1.2. Intercomparison of the strategies

According to Fig. 4b), significant differences can be identified between the results of strategy 1, strategy 3, and the group of strategies 2, 4 and 5. For all wind directions and seasons, strategy 3 estimates the highest values for VRs, strategy 1 the lowest. When comparing strategy 3 to strategy 1, differences between the mean values of +80% in the winter, +94% in the transition, and +63% in the summer period are estimated, respectively.

The high VR values estimated with strategy 3 can be explained by the sampling of outside concentrations with this strategy. By forming the mean value of all outside lines, the outside concentration value for CO_2 is artificially increased, which leads to smaller inside-outside differences, resulting in very high VR values. It can be concluded, that using strategy 3 results in an immense overestimation of the VR, independently of season and wind direction.

The low results for VRs estimated with strategy 1 can be explained by the assumption of a flow pushing the gas through the barn, where the CO_2 concentrations are accumulated with the flow direction. Strategy 1 uses for outside concentrations the line, where the flow enters the barn and as inside concentration the line, where the flow leaves the barn. Hence, the inside-outside concentration differences must be maximum, which results in minimum estimated VRs.

No significant differences exist between the estimated VRs of strategies 2, 4 and 5. This allows two conclusions to be drawn. Firstly, since strategy 4 and strategy 5 only differ by the use of the sampling line in the middle of the barn, it can be concluded that this line does not provide any extra information and could be skipped when measuring the ventilation rate. Secondly, since strategy 2 and strategy 4 only differ in the strategy for estimating the outside concentration - strategy 2 uses the line towards the wind direction, strategy 4 uses the line with the minimum CO_2 concentration - it can be concluded that the extra information about the wind direction for outside sampling does not change the estimation of ventilation rates and choosing the line with the minimum concentration is sufficient.

In all cases, strategy 2 estimates higher VRs than strategy 1. This is because strategy 2 is forming the value for the inside concentration as a mean value from all inside sampling lines. By this, upwind positioned sample lines inside the barn with lower concentrations are also taken into account and will dilute the average value. This lower inside concentration value leads to lower inside-outside concentration differences, which result in higher VRs.

3.2. Emissions

3.2.1. Comparison with the literature

Figure 5a) shows the mean NH_3 emissions estimated by the five strategies in grams per hour and livestock unit, sorted by seasons and wind directions. The numerical values from the figures can be found in Tables A.7, A.8 and A.9 in Appendix A. For the winter season, the estimated emissions throughout all five strategies are in a range between 0.67 g h^{-1} LU^{-1} (strategy 4 for eastern winds) and 1.10 g h^{-1} LU^{-1} (strategy 1 for western winds). These values agree with the results published by Saha,
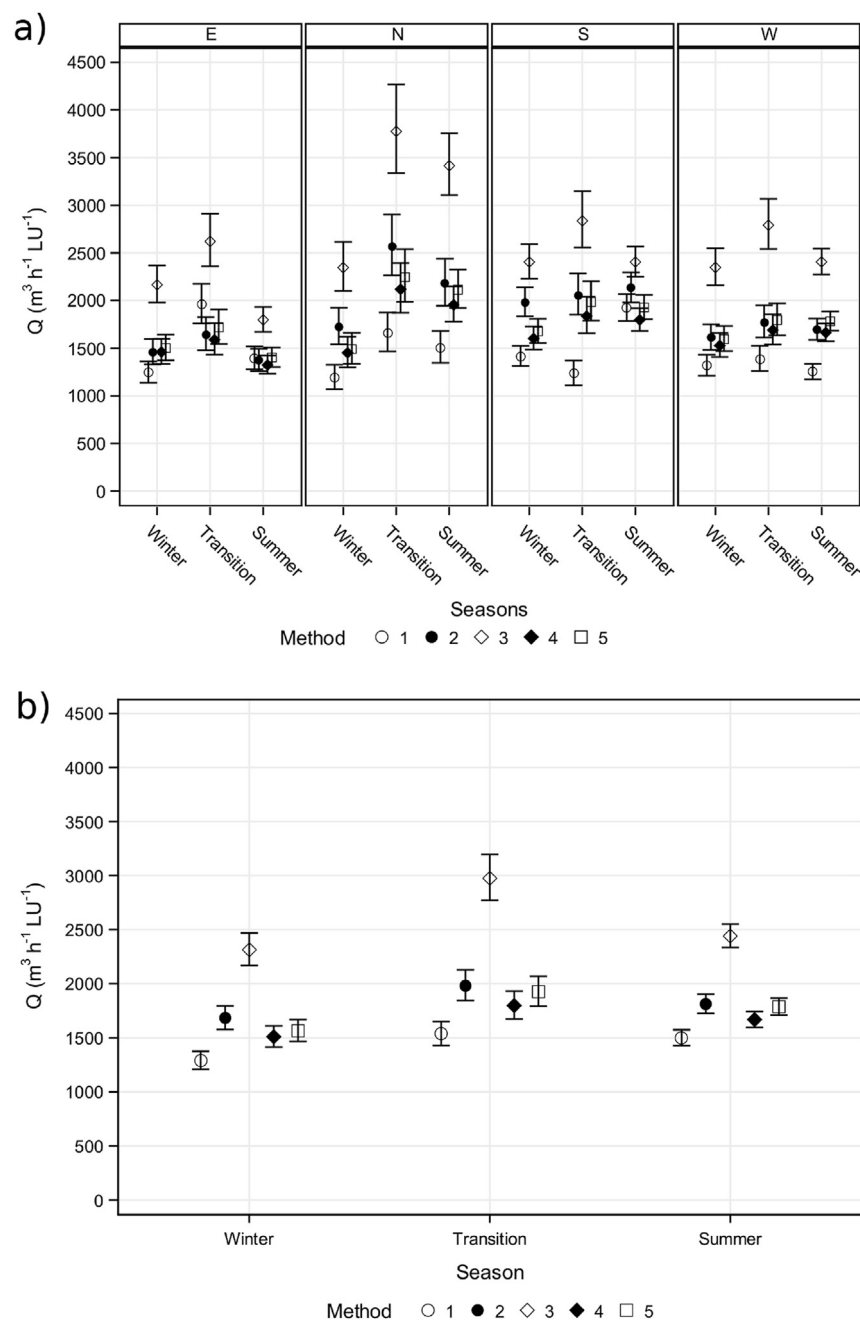
Fig. 4 – Ventilation rates per hour and livestock unit, computed by the five strategies. Symbols mark the mean values, error bars the upper and lower border of the 95% confidence interval. a) sorted by wind direction and seasons. b) sorted only by seasons and aggregated wind directions.

Ammon, et al. (2014), who measured the same barn that was the object of this study. For the winter period, their measured NH_3 emissions were in a range from 0.33 to 1.47 g h^{-1} LU^{-1}. The emissions for a NVB with a solid floor in the winter season were also measured by Schrade et al. (2012) and are in the range from 0.25 to 0.96 g h^{-1} LU^{-1}, which is slightly lower but still in agreement with this study. Winter measurements in a NVB with solid floor were published by Zhang et al. (2005) with emissions in a range from 0.51 to 0.64 g h^{-1} LU^{-1}, which is lower than our results, probably due to the colder climate conditions in Denmark.

For the transition season, the estimated emissions are in a range from 1.07 g h^{-1} LU^{-1} (strategy 4 for northern winds) and 1.73 g h^{-1} LU^{-1} (strategy 3 for eastern winds). This range is completely covered by the results for transitional period measurements in the before mentioned studies of Schrade et al. (2012) (0.67–1.83 g h^{-1} LU^{-1}) and Saha, Ammon, et al. (2014) (0.23–3.89 g h^{-1} LU^{-1}) and partially covered by the results of Zhang et al. (2005), which are slightly lower with ranges between 0.50 and 1.45 g h^{-1} LU^{-1}.

For the summer season, the estimated emissions are in a range from 1.77 g h^{-1} LU^{-1} (strategy 4 for northern winds) and
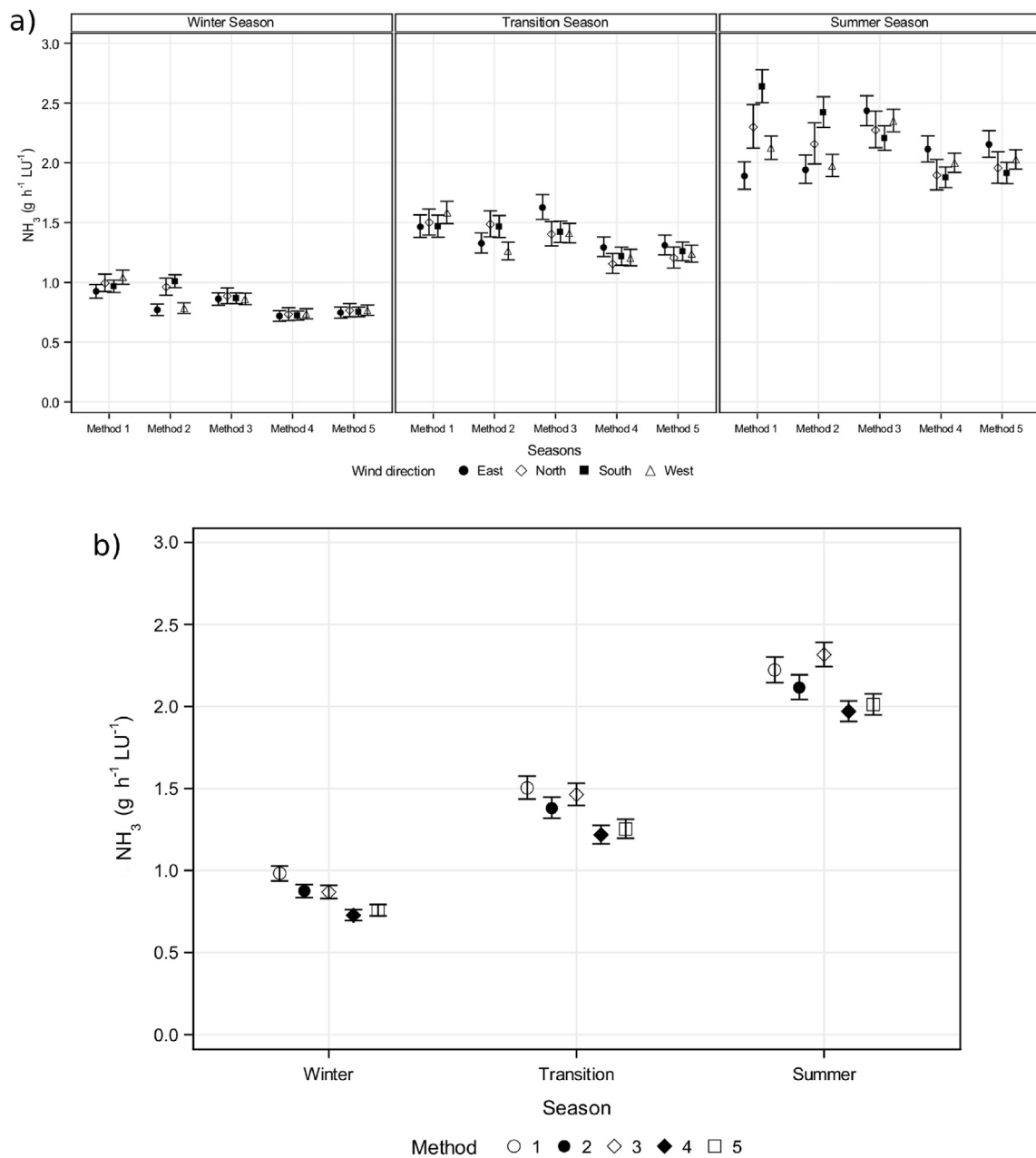
Fig. 5 – Ammonia emissions computed by the five strategies, a) sorted by wind direction and method for every season and b) sorted for season with aggregated wind directions. Symbols mark the mean values, error bars the upper and lower border of the 95% confidence interval.

2.78 g h⁻¹ LU⁻¹ (strategy 1 for southern winds). These values are completely covered by the results for summer period measurements in the before mentioned studies of Schrade et al. (2012) (1.29–2.79 g h⁻¹ LU⁻¹), Saha, Ammon, et al. (2014) (0.367–4.41 g h⁻¹ LU⁻¹), and Zhang et al. (2005) (1.12–4.21 g h⁻¹ LU⁻¹).

Regardless of the wind direction and strategy, ammonia emissions were highest in the summer and lowest in the winter. The reason for that is the temperature-dependent production of ammonia and the higher temperatures in the transition- and summer season. Similar to this, the variances in the estimated values increases from the winter season over

the transition season to the summer season. The reason for that is the higher temperature fluctuations in the transition- and summer season. Both, the seasonal increase in emissions and in variance (high in summer, low in winter) were also reported in Saha, Ammon, et al. (2014), Schrade et al. (2012), and Zhang et al. (2005).

3.3. Intercomparison of the strategies

Referring to Fig. 5a), in none of the 12 cases (four wind directions with three seasons), a significant difference between the estimated values from strategy 4 and strategy 5 is

visible.The only difference between these two strategies was the sample line in the middle (*m-in* in Fig. 1), which was taken into account for strategy 4 and not taken into account for strategy 5. Hence, it can be concluded that when deriving the inside concentration as a mean value of all sampling lines inside (strategy "the-more-the-better"), the use of the middle sampling line does not deliver any extra information and is therefore not needed.

Regarding the results sorted for seasons shown in Fig. 5b), strategies 4 and 5 show the lowest values for NH$_3$ emissions for all seasons. The highest values are estimated by strategy 1 for the winter and transition season, and by strategy 1 and 3 (no significant difference) for the summer season. If strategy 1 (highest) is directly compared to strategy 4 (lowest, reference), the resulting differences of the mean values are +26% for the winter, +19% for the transition, and +11% for the summer season. Table 5 shows the p-values for the differences between the estimated mean values of each method, sorted for winter, transition and summer season, corresponding to Fig. 5b).

When deriving a whole-year emission value from the actual dataset, strictly using strategy 1 would result in a value of 13.74 kg y^{-1} LU^{-1}, while strictly using strategy 4 would result in 11.43 kg y^{-1} LU^{-1}. As a consequence, the predicted emissions per year per LU would be +20% higher when using strategy 1 instead of strategy 4. We can therefore conclude that hypotheses 1 and 2 have proven to be correct: the sampling strategy has a significant influence on the estimation of NH$_3$ emissions (hypothesis 1) and the different sampling strategies lead to systematic errors (hypothesis 2).

When comparing strategy 2 with strategy 4, the influence of the outside sampling strategy can be investigated: both strategies use the same strategy for sampling the inside concentrations (mean value of all inside sampling lines). Hence, any differences between their estimated emissions must be caused by the choice of the outside concentration line. In strategy 2, this choice is wind-driven, in strategy 4, the line with the minimum CO$_2$ level is chosen. The results for NH$_3$ emissions shown in Fig. 5a) show a behavior dependent on the wind direction, or more precisely, dependent on whether the flow is entering the barn cross-wise (north/south) or lateral-wise (east/west). For the lateral cases, no difference between strategy 2 and 4 can be seen. For the cross-wise cases, significant differences with a clear trend towards higher values for strategy 2 are present for all seasons except northern winds in the summer (same trend, but no significance). Expressed as relative differences, with strategy 4 as reference, strategy 2 delivers for southern winds +40%, +20% and +29% higher values for the winter, transitional and summer season, respectively. For northern winds, the differences are +31% for

the winter and +28% for the transitional season (no significant difference for the summer season). This leads to overall differences of +20% for the winter, +14% for the transition, and +7% for the summer season, to be seen in Fig. 5b). For the whole dataset, strictly using wind direction information for the choice of the outside sampling line as in strategy 2, would result in an emission factor of 12.77 kg y^{-1} LU^{-1}, which corresponds to a difference of +12%. These differences did not show up when the ventilation rates were estimated with strategies 2 and 4 and only the concentration of CO$_2$ was considered.

It was concluded in the previous chapter, that both, choosing the sampling line with the minimum concentration or choosing the sampling line based on wind direction, deliver the same estimates of ventilation rates. Consequently, for CO$_2$, the outside sampling line towards the approaching flow was always the one with the CO$_2$ minimum. For NH$_3$, this appears not to be the case, otherwise strategy 2 would not estimate different NH$_3$ emissions than strategy 4. A possible reason for that might be wind directions in between two sectors or rapidly changing wind directions, combined with outside positioned additional sources of NH$_3$, like manure pits. The differences are only visible for cross-wise directions; for strategy 4 this would e.g. mean, that a wind from south-east shows minimum CO$_2$ values in the eastern line, which is then consequently chosen, while strategy 1 would choose the southern outside line. The western outside line, positioned over the manure pits, could show in this case higher NH$_3$ concentrations, which would decrease the inside-outside difference and lead to lower E$_{NH3}$ levels. It can be concluded, that in the case of existing outside sources of NH$_3$, and unstable, rapidly changing wind conditions, the outside sampling line should rather be determined by the wind direction than by the concentration minimum.

Strategy 3 was, when estimating the ventilation rates, the strategy with the by far highest values. This behavior can not be noticed when strategy 3 is used to estimate the NH$_3$ emissions. According to equations 1 and 7, a decrease of inside-outside concentrations leads to an increase of ventilation rates and a decrease of NH$_3$ emissions. This means, that the increase of VRs due to the artificial increase of outside CO$_2$ concentrations in strategy 3 is compensated by the same artificial increase of NH$_3$ concentrations.

3.4. Discussion and assessment of the different strategies

The strategy-induced differences in estimated VRs and NH$_3$ emissions have been quantitatively determined. In the following, the applicability for each strategy under given

Table 5 — p-values for the differences of the mean values estimated by the five strategies, shown in Fig. 5b).

	Winter Season				Transition Season				Summer Season			
	M2	M3	M4	M5	M2	M3	M4	M5	M2	M3	M4	M5
M1	0.0053	0.0018	<.0001	<.0001	0.0834	0.9175	<.0001	<.0001	0.3090	0.4253	<.0001	0.0006
M2	–	0.9998	<.0001	0.0002	–	0.4252	0.0011	0.0256	–	0.0027	0.0259	0.2229
M3	–	–	<.0001	0.0004	–	–	<.0001	<.0001	–	–	<.0001	<.0001
M4	–	–	–	0.7187	–	–	–	0.9115	–	–	–	0.8913

circumstances will be assessed. The assessment of the strategies will be based on the following assumptions.

The first is the assumption of an accumulation of gas concentrations aligned with the flow direction inside the barn. That means the lowest gas concentrations can be measured directly at the inlet of the barn, the highest at the outlet. This assumption is especially related to strategy 1, since this strategy presupposes the existence of a defined outlet. At this outlet, the inside gas concentrations are measured with only one sampling line. If the assumption is not fulfilled, it means that the flow inside the barn is not straightly following the direction of the incoming wind direction. This might happen when the flow is drifted laterally due to complex flow pattern or obstacles inside the barn. In these cases, strategy 1 would be a weak choice, because the "wrong" outlet sampling line would be considered.

The second assumption is that the release rate of NH_3 is independent of the wind direction. Apart from shifts in local flow velocities over emission-active surfaces that slightly shift the chemical equilibrium, the direction of the flow should have no influence on the level of NH_3 emissions. This was already published by Saha et al. (2013), who investigated the same barn as in this study and found no significant influence of the wind direction on the NH_3 emissions. As a consequence, the NH_3

estimates of a strategy should not vary significantly within the four wind directions. This assumption is related to all strategies.

Figure 6 shows the gradients of the CO_2 and NH_3 concentrations in the lines over the whole measurement period, sorted by the four approaching wind directions. In the left (blue) box of each figure, the concentration levels of the lines aligned in the main flow direction are shown, e.g. for a flow from south, first the outside southern line is shown, followed by southern inside, middle, northern inside and northern outside line. In the right (white) box, the concentrations of the lines aligned to the left and right of the flow direction are shown, meaning that e.g. for southern flow direction, the inside east, then outside east, inside west and last the outside west line concentrations.

For winds from the south, north, and west, the concentrations both for NH_3 and CO_2 show increasing values along the flow direction, which confirms assumption 1. For eastern winds, the concentrations show higher values at the middle line which then stagnate or even decrease towards the outlet. The reason for that might be the formation of more complex flow structures for lateral flows from east, that accumulate the gas concentrations at the middle line location. Another explanation could be the distribution of wind directions for the eastern sector, shown in Fig. 3a). The incoming flow direction in
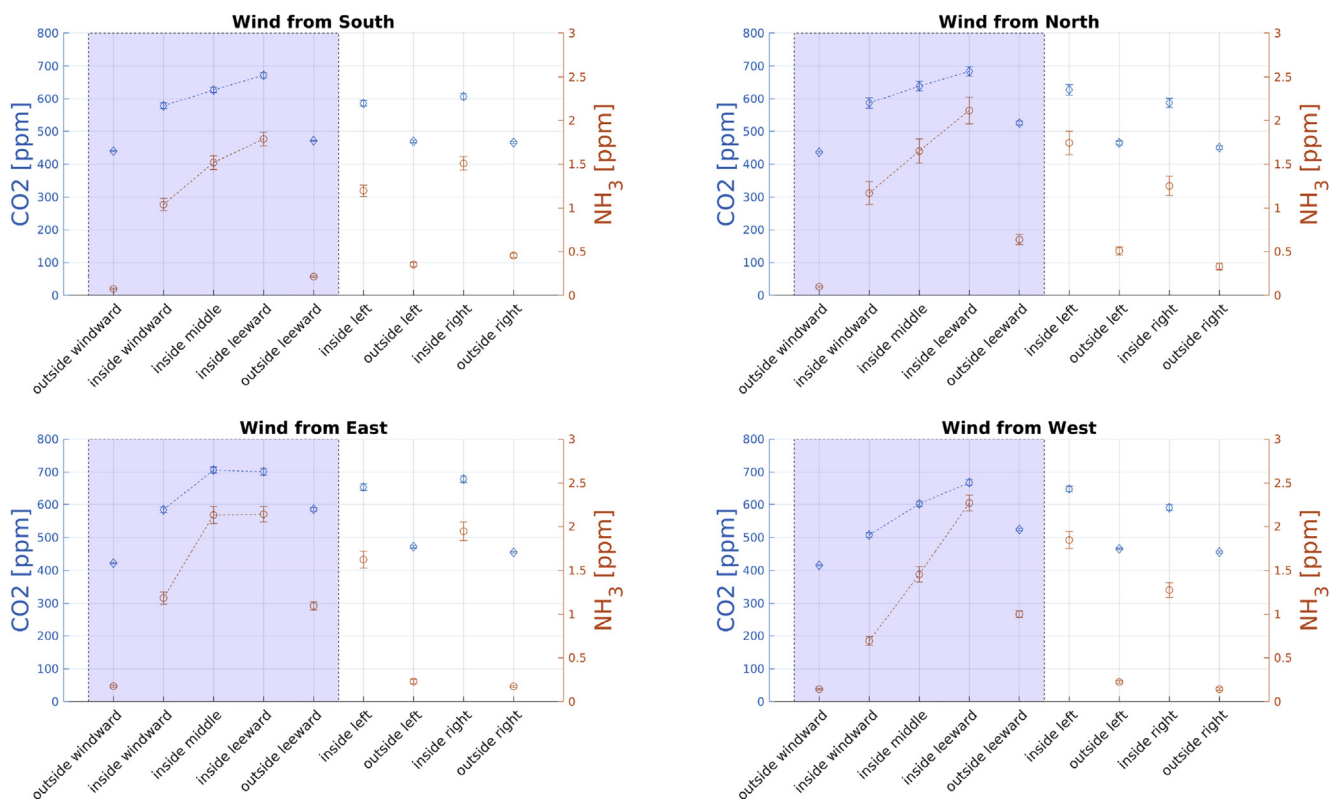
Fig. 6 — Accumulation of the gas concentrations along the flow direction. The dataset was sorted by the wind directions south, north, east and west. For each wind direction, the mean values of the gas concentrations in each sample line were computed. Blue dots and bars show the mean concentrations and confidence intervals of CO_2, red dots present the values for NH_3. The respective sample lines are ordered for each wind direction and renamed after their position relative to the flow direction, e.g. *inside windward* is the sample line positioned at the inlet inside the barn, *outside right* is the sample line outside the barn on the right side when facing in direction of the flow (starboard side). The blue area marks values from sample lines positioned along the flow, where an accumulation of concentrations is expected. (For interpretation of the references to color in this figure legend, the reader is referred to the Web version of this article.)

Table 6 – Suitability of the different strategies for certain wind- and site conditions and general tendencies of the strategies for the estimation of ventilation rates and ammonia emissions. $CO2_{in}$ and $NH3_{in}$ are carbon dioxide and ammonia concentrations for the inside concentration values, $CO2_{out}$ and $NH3_{out}$ for the outside concentration values. Scenario Sc1: straight and stable flow through the barn, either cross or lateral. Sc2: unstable and weak wind conditions and ambiguous wind directions. Sc3: building and wind combination leading to flow deflection or complex flow pattern (e.g. long barns with mainly lateral flow, large flow obstacles inside the barn). Sc4: incoming flow is contaminated with gas concentrations from different outside sources. Sc5: measurement campaigns with multiple barns with different geometries and wind conditions.

Strategy	Sc1	Sc2	Sc3	Sc4	Sc5	tendency VR (explanation)	tendency E_{NH3} (explanation)
M1	+	−	−	o	o	lowest (estimates maximum $CO2_{inside}$ - $CO2_{outside}$)	highest (uses maximum $NH3_{inside}$)
M2	−	−	+	+	o	moderate	moderate
M3	−	+	o	o	o	highest[!] (artificial maximum of $CO2_{outside}$)	moderate
M4	−	+	+	−	+	moderate	lowest (uses low $NH3_{inside}-NH3_{outside}$)
M5	−	+	+	−	+	moderate	lowest (uses low $NH3_{inside}-NH3_{outside}$)

[+]Recommended for the scenario [−]Not recommended for the scenario [o]No general recommendation possible [!]Strong overestimation, not recommended for estimation of VR.

this sector is not equally distributed around the barns eastern opening, but has a trend to south-east directions. This could lead to less definite flow regimes. Instead of a clear lateral flow, a mix of cross flow and lateral flow would be the result. Based on these observations, it can be concluded that strategy 1 should be applied under clear wind conditions (either cross- or lateral flow). Here, the chance of a well defined outlet is high, and the sampling line would measure the indeed leaving concentrations, giving the most accurate results. For rather unclear wind conditions, another strategy should be considered. Imaging wind conditions with very low incoming speeds, or even a lull, strategy 1 should be avoided. In these cases, a more robust strategy like strategy 3, which does not consider inlets or outlets at all, should be the first choice.

To use the second assumption as an evaluation of the strategies, the strategy-wise results for NH_3 emissions are shown in Fig. 5, sorted after season and wind direction. If we assume the emission rates are independent of the wind direction, then a strategy performs well when the estimated emission rates show no dependency on the wind directions. For the winter season, the results estimated with strategies 1, 3, 4 and 5 do not show any significant differences within the wind directions. Strategy 2 estimates significantly higher values for cross-wind directions. In the transition season, strategies 1, 4 and 5 do not show significant differences within the wind directions. Strategy 2 shows the same behavior as in the winter season with higher values for cross-winds and lower values for lateral winds. In the summer season, the only strategy estimating values independently of the wind direction is strategy 3. Strategy 1 and 2 show the highest variations with significantly higher values for southern winds and lowest values for lateral wind directions. The higher variation for strategy 1 and 2 can be explained by the summer weather, where less stable wind conditions with generally lower wind speed and more changing wind directions are present. This affects the strategies that use information about the wind direction most, while strategies using only information about the gas concentrations (strategy 4 and 5) or no information at all (strategy 3) seem to be more robust. Hence, under unstable, weak wind conditions, strategies relying on information about the wind direction (for inside or outside concentrations) should be avoided.

In case of designing several measurement campaigns with different barns, e.g. for the collection of data for national inventories, a strategy should be considered, which delivers as many useable samples as possible in a given time frame. For example, Schmithausen et al. (2018) used a setup similar to strategy 1, with the constraint of a given main wind direction. This led, depending on the wind conditions, to a rejection of data in the amount of around 80%. With the actually installed setup for this study, every wind direction could be taken into account, which means a gain of data of around 210%, if beforehand conditions with only straight southern wind directions were considered (see Table 4). This could be even enhanced, if an adaption of strategy 2 would be applied, where all sampling lines inside the barn would be physically connected, and the mean value for inside concentration would be determined by physically mixing the single line concentrations. By that, the needed time for a whole measurement circle with all lines could be reduced by the factor 2, because only one value for inside concentrations would be measured. The suitability of each strategy for certain wind and site conditions is summarised in Table 6.

Finally, no influence of the surroundings on the estimation of the emissions can be found. In the north, the barn is surrounded by several other barns and buildings, in the south, it is surrounded by free field. However, the different roughness is not noticeable, since no strategy (except strategy 1 in the summer season) estimates differences between the values from north and south.

4. Conclusions

The sampling strategy has a significant influence on the estimation of ventilation rates and ammonia emissions, which leads to systematic errors, depending on the applied strategy.

The choice for the outside sampling (either wind-dependent or choosing the minimum CO_2 level) influences the estimation of ammonia emissions up to 20%, but does not affect the estimation of ventilation rates, probably as a consequence of outside NH_3 sources combined with unstable inflow conditions.

The strictly wind-dependent strategy 1 estimates the highest values for ammonia emissions, the concentration

(outside), and mean value (inside) based strategies 4 and 5 estimate the lowest values.

Using the mean value of all outside lines for the outside concentration value (strategy 3), leads to unrealistically high ventilation rates. However, the estimation of ammonia emissions is not affected by this strategy, probably because the artificial decrease of CO_2 concentration difference induced by this strategy is compensated by inducing an artificial decrease of NH_3 concentration difference in the same relative magnitude.

Neither for the estimation of VRs nor the estimation of ammonia emissions, the use of a sampling line in the middle of the barn delivers any extra information and can therefore be skipped.

No influence of the surrounding of the barn in terms of flow obstacles (buildings or free field) could be found.

All investigated strategies followed reasonable assumptions, so none can be considered superior to the other. The main problem when trying to assess the strategies is the lack of a highly accurate reference dataset to compare against and validate the investigated strategies. Hence, the interpretation of the results and the assessment of the strategies had to be done based on some basic assumptions concerning the flow and the transport of gas.Following conclusions could be drawn: The wind-dependent strategy 1 should be used for stable wind conditions, either clear cross or lateral flow. Under these conditions, this strategy quantifies the barn-leaving emissions most accurately. Under unstable or indifferent wind conditions strategy 1 should be avoided.

Strategies 3, 4 and 5 show a robust behavior towards unstable wind conditions. In cases of lateral flow, where a more complex flow pattern inside the barn is expected, the inside sampling should not rely on only one line at the expected outlet, but on more lines like in strategies 3, 4, and 5. Therefore, for these cases, either strategy 3 or strategy 4 is recommended.

This study focused on the spatial distribution of sampling locations. The important aspect of the distribution in time was not considered. The frequency of sampling, the duration of measurement periods and the number of repetition of measurements will have a major influence on the estimation of VRs and E_{NH3}. Further investigations should therefore be done regarding these aspects.

The systematic investigation of different sampling strategies under different influencing factors will help to set up a robust measurement design with an optimised sampling strategy, adjustable to the respective conditions. By this, the outcomes of this study will help to improve the CO_2 balancing method, which is widely used to estimate ventilation rates and emissions from naturally ventilated barns.

Declaration of competing interest

The authors declare that they have no known competing financial interests or personal relationships that could have appeared to influence the work reported in this paper.

Acknowledgements

Appendix A. Tables Emission Factors and ventilation rates

Table A.7 – Winter Season: ammonia emissions and ventilation rates. "up" and "low" mark the upper and lower limit of the 95% confidence interval.

		NH_3 (g h^{-1} LU^{-1})					Q (m^3 h^{-1} LU^{-1})				
		M1	M2	M3	M4	M5	M1	M2	M3	M4	M5
East	Up	0.98	0.82	0.91	0.76	0.79	1363	1595	2370	1598	1644
	Mean	0.92	0.77	0.86	0.72	0.75	1245	1456	2165	1460	1502
	Low	0.87	0.72	0.81	0.67	0.70	1138	1329	1979	1334	1372
North	Up	1.07	1.04	0.95	0.79	0.82	1327	1926	2617	1619	1662
	Mean	1.00	0.96	0.89	0.73	0.77	1190	1723	2346	1452	1490
	Low	0.92	0.89	0.82	0.68	0.71	1067	1542	2102	1302	1336
South	Up	1.02	1.06	0.91	0.76	0.79	1526	2138	2593	1728	1808
	Mean	0.97	1.01	0.87	0.72	0.75	1415	1981	2404	1602	1677
	Low	0.92	0.96	0.82	0.69	0.71	1312	1835	2229	1486	1555
West	Up	1.10	0.83	0.91	0.78	0.81	1429	1750	2549	1660	1733
	Mean	1.04	0.78	0.86	0.74	0.77	1316	1611	2347	1529	1596
	Low	0.99	0.74	0.81	0.70	0.72	1211	1482	2162	1408	1469
Overall	Up	1.03	0.92	0.91	0.76	0.79	1375	1795	2468	1610	1669
	Mean	0.98	0.87	0.87	0.73	0.76	1289	1682	2312	1509	1564
	Low	0.94	0.84	0.83	0.69	0.72	1208	1577	2169	1415	1466

Table A.8 – Transition Season: ammonia emissions and ventilation rates. "up" and "low" mark the upper and lower limit of the 95% confidence interval.

		NH$_3$ (g h^{-1} LU^{-1})					Q (m^3 h^{-1} LU^{-1})				
		M1	M2	M3	M4	M5	M1	M2	M3	M4	M5
East	Up	1.57	1.42	1.74	1.38	1.40	2175	1826	2911	1764	1909
	Mean	1.47	1.33	1.63	1.30	1.31	1957	1644	2621	1588	1718
	Low	1.38	1.25	1.53	1.22	1.23	1761	1479	2359	1430	1547
North	Up	1.62	1.60	1.51	1.24	1.30	1875	2904	4268	2394	2539
	Mean	1.50	1.49	1.40	1.16	1.21	1658	2564	3775	2118	2247
	Low	1.40	1.38	1.31	1.08	1.12	1466	2264	3340	1874	1988
South	Up	1.56	1.56	1.51	1.30	1.34	1370	2284	3148	2038	2202
	Mean	1.47	1.47	1.42	1.22	1.26	1234	2058	2837	1837	1985
	Low	1.38	1.38	1.34	1.14	1.18	1111	1853	2557	1656	1789
West	Up	1.68	1.34	1.49	1.278	1.31	1527	1951	3066	1856	1972
	Mean	1.58	1.26	1.41	1.21	1.24	1388	1774	2791	1690	1796
	Low	1.49	1.19	1.33	1.14	1.17	1261	1612	2541	1539	1635
Overall	Up	1.44	1.32	1.40	1.16	1.20	1649	2128	3196	1931	2069
	Mean	1.50	1.38	1.46	1.22	1.25	1535	1980	2975	1798	1926
	Low	1.58	1.45	1.53	1.28	1.31	1429	1843	2770	1674	1793

Table A.9 – Summer Season: ammonia emissions and ventilation rates. "up" and "low" mark the upper and lower limit of the 95% confidence interval.

		NH$_3$ (g h^{-1} LU^{-1})					Q (m^3 h^{-1} LU^{-1})				
		M1	M2	M3	M4	M5	M1	M2	M3	M4	M5
East	Up	2.01	2.07	2.56	2.23	2.27	1519	1495	1933	1425	1508
	Mean	1.90	1.94	2.43	2.11	2.16	1394	1372	1798	1325	1402
	Low	1.78	1.83	2.31	2.01	2.05	1280	1259	1672	1232	1304
North	Up	2.49	2.34	2.43	2.02	2.09	1683	2439	3756	2149	2323
	Mean	2.30	2.16	2.28	1.90	1.96	1505	2178	3415	1955	2113
	Low	2.13	1.99	2.13	1.78	1.83	1347	1946	3105	1778	1922
South	Up	2.78	2.55	2.31	1.97	2.00	2069	2297	2567	1919	2059
	Mean	2.64	2.42	2.21	1.88	1.91	1922	2132	2404	1797	1928
	Low	2.50	2.30	2.11	1.79	1.83	1786	1979	2252	1683	1806
West	Up	2.22	2.07	2.45	2.08	2.11	1336	1810	2545	1760	1886
	Mean	2.12	1.98	2.35	2.00	2.03	1252	1695	2406	1664	1783
	Low	2.03	1.89	2.26	1.92	1.95	1174	1588	2275	1573	1686
Overall	Up	2.30	2.19	2.39	2.03	2.08	1574	1904	2551	1743	1867
	Mean	2.22	2.12	2.32	1.97	2.01	1499	1812	2441	1668	1787
	Low	2.15	2.04	2.24	1.91	1.95	1428	1726	2336	1596	1710

REFERENCES

Bjerg, B., Zhang, G., Madsen, J., & Rom, H. B. (2012). Methane emission from naturally ventilated livestock buildings can be determined from gas concentration measurements. *Environmental Monitoring and Assessment, 184*, 5989–6000.

Calvet, S., Gates, R. S., Zhang, G., Estelles, F., Ogink, N. W., Pedersen, S., & Berckmans, D. (2013). Measuring gas emissions from livestock buildings: A review on uncertainty analysis and error sources. *Biosystems Engineering, 116*, 221–231.

Demmers, T., Burgess, L., Short, J., Phillips, V., Clark, J., & Wathes, C. (1998). First experiences with methods to measure ammonia emissions from naturally ventilated cattle buildings in the UK. *Atmospheric Environment, 32*, 285–293.

Demmers, T., Phillips, V., Short, L., Burgess, L., Hoxey, R., & Wathes, C. (2001). Se—structure and environment: Validation of ventilation rate measurement methods and the ammonia emission from naturally ventilated dairy and beef buildings in the United Kingdom. *Journal of Agricultural Engineering Research, 79*, 107–116.

Edouard, N., Mosquera, J., van Dooren, H. J., Mendes, L. B., & Ogink, N. W. (2016). Comparison of CO^2-and SF^6-based tracer gas methods for the estimation of ventilation rates in a naturally ventilated dairy barn. *Biosystems Engineering, 149*, 11–23.

EEA, E. E. A. (2016). *European Union emission inventory report 1990-2016 — European Environment Agency* (vol. 6). https://www.eea.europa.eu/publications/european-union-emission-inventory-report-1.

Estellés, F., Fernandez, N., Torres, A., & Calvet, S. (2011). Use of CO^2 balances to determine ventilation rates in a fattening rabbit house. *Spanish Journal of Agricultural Research, 9*, 713–720.

Janke, D., Dilya, W., Hempel, S., Amon, B., Römer, A., & Amon, T. (2020). High resolution long-term measurements af carbon dioxide and ammonia concentrations in a naturally ventilated dairy barn. *PUBLISSO Repository for Life Sciences.* https://doi.org/10.4126/FRL01-006420709

König, M., Hempel, S., Janke, D., Amon, B., & Amon, T. (2018). Variabilities in determining air exchange rates in naturally ventilated dairy buildings using the CO^2 production model. *Biosystems Engineering, 174*, 249–259.

Mendes, L., Ogink, N., Edouard, N., van Dooren, H., Tinôco, I., & Mosquera, J. (2015). Ndir gas sensor for spatial monitoring of carbon dioxide concentrations in naturally ventilated livestock buildings. *Sensors, 15*, 11239—11257.

Mohn, J., Zeyer, K., Keck, M., Keller, M., Zähner, M., Poteko, J., Emmenegger, L., & Schrade, S. (2018). A dual tracer ratio method for comparative emission measurements in an experimental dairy housing. *Atmospheric Environment, 179*, 12—22.

Ngwabie, N., Jeppsson, K.-H., Gustafsson, G., & Nimmermark, S. (2011). Effects of animal activity and air temperature on methane and ammonia emissions from a naturally ventilated building for dairy cows. *Atmospheric Environment, 45*, 6760—6768.

Ngwabie, N., Jeppsson, K.-H., Nimmermark, S., Swensson, C., & Gustafsson, G. (2009). Multi-location measurements of greenhouse gases and emission rates of methane and ammonia from a naturally-ventilated barn for dairy cows. *Biosystems Engineering, 103*, 68—77.

Ogink, N. W., Mosquera, J., Calvet, S., & Zhang, G. (2013). Methods for measuring gas emissions from naturally ventilated livestock buildings: Developments over the last decade and perspectives for improvement. *Biosystems Engineering, 116*, 297—308.

Pedersen, S. S. K. (2002). *Climatization of animal houses. heat and moisture production at animal and house levels*. Horsens, Denmark: Danish Inst of Agric Sci.

Pedersen, S., Takai, H., Johnsen, J. O., Metz, J., Koerkamp, P. G., Uenk, G., Phillips, V., Holden, M., Sneath, R., Short, J., et al. (1998). A comparison of three balance methods for calculating ventilation rates in livestock buildings. *Journal of Agricultural Engineering Research, 70*, 25—37.

Saha, C., Ammon, C., Berg, W., Fiedler, M., Loebsin, C., Sanftleben, P., Brunsch, R., & Amon, T. (2014a). Seasonal and diel variations of ammonia and methane emissions from a naturally ventilated dairy building and the associated factors influencing emissions. *Science of the Total Environment, 468*, 53—62.

Saha, C. K., Ammon, C., Berg, W., Loebsin, C., Fiedler, M., Brunsch, R., & von Bobrutzki, K. (2013). The effect of external wind speed and direction on sampling point concentrations, air change rate and emissions from a naturally ventilated dairy building. *Biosystems Engineering, 114*, 267—278.

Saha, C. K., Fiedler, M., Ammon, C., Berg, W., Loebsin, C., Amon, B., & Amon, T. (2014b). Uncertainty in calculating air exchange rate of naturally ventilated dairy building based on point concentrations. *Environmental Engineering and Management Journal (EEMJ), 13*.

Samer, M., & Abuarab, M. E. (2014). Development of CO^2 balance for estimation of ventilation rate in naturally cross-ventilated dairy barns. *Transactions of the ASABE, 57*, 1255—1264.

Schmithausen, A., Schiefler, I., Trimborn, M., Gerlach, K., Südekum, K.-H., Pries, M., & Büscher, W. (2018). Quantification of methane and ammonia emissions in a naturally ventilated barn by using defined criteria to calculate emission rates. *Animals, 8*, 75.

Schrade, S., Zeyer, K., Gygax, L., Emmenegger, L., Hartung, E., & Keck, M. (2012). Ammonia emissions and emission factors of naturally ventilated dairy housing with solid floors and an outdoor exercise area in Switzerland. *Atmospheric Environment, 47*, 183—194. https://doi.org/10.1016/j.atmosenv.2011.11.015

Shen, X., Zong, C., & Zhang, G. (2012). Optimization of sampling positions for measuring ventilation rates in naturally ventilated buildings using tracer gas. *Sensors, 12*, 11966—11988.

Van Buggenhout, S., Van Brecht, A., Özcan, S. E., Vranken, E., Van Malcot, W., & Berckmans, D. (2009). Influence of sampling positions on accuracy of tracer gas measurements in ventilated spaces. *Biosystems Engineering, 104*, 216—223.

VERA. (2018). *Vera test protocol: For livestock housing and management systems*.

Wang, X., Ndegwa, P. M., Joo, H., Neerackal, G. M., Stöckle, C. O., Liu, H., & Harrison, J. H. (2016). Indirect method versus direct method for measuring ventilation rates in naturally ventilated dairy houses. *Biosystems Engineering, 144*, 13—25.

Wilks, D. S. (2011). *Statistical methods in the atmospheric sciences* (3rd ed.). Oxford: Academic Press.

Wu, W., Zhang, G., & Kai, P. (2012). Ammonia and methane emissions from two naturally ventilated dairy cattle buildings and the influence of climatic factors on ammonia emissions. *Atmospheric Environment, 61*, 232—243.

Zhang, G., Strøm, J. S., Li, B., Rom, H. B., Morsing, S., Dahl, P., & Wang, C. (2005). Emission of ammonia and other contaminant gases from naturally ventilated dairy cattle buildings. *Biosystems Engineering, 92*, 355—364.

3

Direct Measurements of the Volume Flow Rates and Emissions in a large Naturally Ventilated Building

Direct Measurements of the Volume Flow Rate and Emissions in a Large Naturally Ventilated Building

David Janke [1,*], Qianying Yi [1], Lars Thormann [1], Sabrina Hempel [1], Barbara Amon[2,3], Štěpán Nosek [4], Philippe van Overbeke [5] and Thomas Amon[1,6]

[1] Department Engineering for Livestock Management, Leibniz Institute for Agricultural Engineering and Bioeconomy (ATB), Max-Eyth-Allee 100, 14469 Potsdam, Germany; QYi@atb-potsdam.de (Q.Y.); lthormann@atb-potsdam.de (L.T.); shempel@atb-potsdam.de (S.H.); tamon@atb-potsdam.de (T.A.)

[2] Department Technology Assessment and Substance Cycles, Leibniz Institute for Agricultural Engineering and Bioeconomy (ATB), Max-Eyth-Allee 100, 14469 Potsdam, Germany; bamon@atb-potsdam.de

[3] Faculty of Civil Engineering, Architecture and Environmental Engineering, University of Zielona Góra, Licealna 9/9, 65-417 Zielona Góra, Poland

[4] Institute of Thermomechanics, The Czech Academy of Sciences, v.v.i., Dolejškova 1402/5, 18200 Prague, Czech Republic; nosek@it.cas.cz

[5] Flanders Research Institute for Agriculture, Fisheries and Food (ILVO),Technology and Food Science Unit, 9090 Melle, Belgium; philippe.vanoverbeke@ilvo.vlaanderen.be

[6] Free University Berlin (FUB), Department of Veterinary Medicine, Institute of Animal Hygiene and Environmental Health, Robert-von-Ostertag-Str. 7-13, 14163 Berlin, Germany

* Correspondence: djanke@atb-potsdam.de

Abstract: The direct measurement of emissions from naturally ventilated dairy barns is challenging due to their large openings and the turbulent and unsteady airflow at the inlets and outlets. The aim of this study was to quantify the impacts of the number and positions of sensors on the estimation of volume flow rate and emissions. High resolution measurements of a naturally ventilated scaled building model in an atmospheric boundary layer wind tunnel were done. Tracer gas was released inside the model and measured at the outlet area, using a fast flame ionization detector (FFID). Additionally, the normal velocity on the area was measured using laser Doppler anemometry (LDA). In total, for a matrix of 65×4 sensor positions, the mean normal velocities and the mean concentrations were measured and used to calculate the volume flow rate and the emissions. This dataset was used as a reference to assess the accuracy while systematically reducing the number of sensors and varying the positions of them. The results showed systematic errors in the emission estimation up to +97%, when measurements of concentration and velocity were done at one constant height. This error could be lowered under 5%, when the concentrations were measured as a vertical composite sample.

Keywords: boundary layer wind tunnel; air exchange; laser Doppler anemometer; flame ionization detector; dairy barn

1. Introduction

Agriculture is a main contributor to the European ammonia and greenhouse gas (GHG) emissions—around 11% for ammonia [1] and 37% for GHG can be related to the livestock management of cattle [2]. Accurate measurements are the basis for efficient emission mitigation measures. Dairy cows are mainly housed in naturally ventilated dairy barns (NVDBs) with large openings, connected directly to the ambient, turbulent weather conditions. This makes the measurements of volume flow rate and gaseous emissions from these buildings challenging. In NVDBs, volume flow rate and gaseous emissions are usually measured by indirect mass balancing methods, wherein the

air exchange rates can be derived from measuring the dilution of a tracer gas with a known release rate. The emission rate of the target gas can then be derived as the product of the air exchange rate and the target gas concentration. Further detailed information on mass balancing methods can be found, e.g., in Eren Ozcan et al. [3] and Ogink et al. [4]. Indirect methods are based on the assumption of the perfect mixing of tracer gas and target gas. Since in reality, this assumption can not be fulfilled, high uncertainties in the estimation of emissions can occur [5,6]. If the carbon dioxide (CO_2) produced by the animals is used as tracer gas, which is the most common approach, additional error sources can occur in the estimation of the CO_2 source term, which directly biases the estimation of the air exchange rates [7]. These additional error sources can be related to animal parameters, such as weight, activity, productivity and pregnancy, and also additional CO_2 sources, such as manure [6].

A more straightforward approach to estimate volume flow rate and emissions is the direct method. As the name suggests, in this approach, the velocity vectors of the airflow entering or leaving the NVDB are directly measured and used to calculate the volume flow rate and air exchange rate (a measure of how many times per hour the air within a room is replaced). Additional to the velocity, the associated concentration of target gas in the leaving airflow needs to be measured. The emission rate of the barn can then be computed as the product of directly measured volume flow rate and the simultaneously measured gas concentration.

The challenge in applying direct methods for NVDB is to find representative sensor positions for the measurement of both velocity and concentration. Due to the direct coupling of the large openings with unsteady weather regimes, it is impossible to define constant inlets or outlets [8,9]. Hence, under real conditions, an increasing number of sensors for velocity and gas concentration can be expected to increase the accuracy of the results. Since the costs for sensors are high, usually the aim is to have a most efficient measurement design, meaning the lowest possible number of sensors with the maximum possible accuracy.

De Vogeleer et al. [10] systematically investigated the influence of the density of sampling positions for estimating the volume flow rate in a mock-up test building of a pig barn, with side openings of 0.5 m × 3 m. They also measured the concentrations of a tracer gas at varying positions, but did not use the results for the direct estimation of emissions, but to compute the volume flow rate with an indirect method and compare the results with the direct method. Generally, it was found that better accuracy was obtained with a higher number of sampling locations, and unrepresentative selected sampling locations could lead to systematic overestimation or underestimation of the airflow rates.

So far, no systematic investigation of the influences of the number and positions of sensors on the direct estimation of both air exchange and emissions on a real scale NVDB has been done. This is most likely due to the immense effort needed: in order to measure most accurate results that could act as reference data for large NVDBs, a very high number of sensors for both velocity and concentrations would be needed. Under real conditions, installing these would be highly impractical and expensive.

Wind tunnel measurements can be a promising alternative. Provided that similarity laws are obeyed, arbitrary constant boundary conditions can be applied to scaled down models, and the gained results can be transferred back to the natural scale [11]. For agricultural applications, several studies in recent years have been conducted to investigate animal husbandry systems. Zhang et al. [12] investigated the influences of obstacles upstream of a fully opened pig barn on the transport and dilution of a pollutant gas on the downwind side of the barn. They found that the presence of obstacles could reduce the pollution in the area downstream the barn. Aubrun and Leitl [13] investigated the dispersion of odor around a pig barn in a 1:400 scaled model. By properly modeling the unsteady behavior of the flow, they could identify the plume characteristics as the main effect for dispersion of odor. Several studies investigated the ventilation performances of naturally ventilated barns [14–20]. Shen et al. [20] investigated a 1:25 scaled model of a NVDB and found that the positions of the openings had no influence on the total air change rates, but the size of the opening did. Yi et al. [16] also investigated the influences of the positions of the openings of a 1:40 scaled model of a NVDB. They found that the opening position had a major impact on the inside flow pattern and on the internal

air changes in the animal occupied zones. Nosek et al. [21] investigated the airflow patterns and the dispersion of a tracer gas inside a 1:50 scaled model of a NVDB. They found that the size of the openings and the roughness of the terrain had a significant effect on the airflow pattern and also the dispersion of the tracer gas. De Paepe et al. [18] and De Paepe et al. [17] investigated a 1:60 scaled model of a NVDB. They found that with a fully open outlet, the inside velocities were up to four times higher [18], and that the total air change rates were affected by the inflow angle [17].

These studies illustrate the benefits of the method wind tunnel modeling, which allows measurements in high detail, both for velocities and gas concentrations, and under reproducible and stable boundary conditions. However, until now, the direct measurement of emissions from a NVDB (by measuring both the gas concentrations and velocity vectors at the openings of the NVDB) was not yet investigated with this method.

In this study, we applied high resolution wind tunnel measurements to derive a reference dataset for both volume flow rate and emissions of a NVDB. Based on this dataset, variations of sampling configurations with a systematic reduction of the number of sensors were investigated and assessed regarding the resulting accuracy. We hypothesized that: (1) The positioning of the sensors introduces a systematic bias to the results, which is caused by an in-homogeneous velocity distribution and an imperfect mixing of the gas concentrations. (2) The spatial variation of the gas concentrations introduces a larger systematic error due to sensor positioning than the spatial variation of velocity. The aims of this study were to (1) quantify the impacts of number and position of sensors on the estimations of volume flow rate and emissions and (2) to derive practical advice for measurement setups in terms of number and positioning of these sensors.

This study investigated the most basic scenario of flow through a NVDB and is considered as the prelude for following campaigns with incrementally increased complexity of flow and building geometry. Hence, following simplifications in the modeling and measurement setup were made:

(a) The barn was investigated under straight cross-flow, isothermal conditions and no variation in the inflow direction. (b) The side-openings were fully open and did not change size or position. (c) The presence of animals inside the barn was not modeled. (d) Only the advective pollution flux was measured, not the turbulent pollution flux. The potential implications of the respective simplifications (a)–(d) are discussed in the Results and Discussion sections.

2. Materials and Methods

2.1. Wind Tunnel

The experiments were conducted in an atmospheric boundary layer wind tunnel (ABLWT) at ATB Potsdam; see Figure 1.
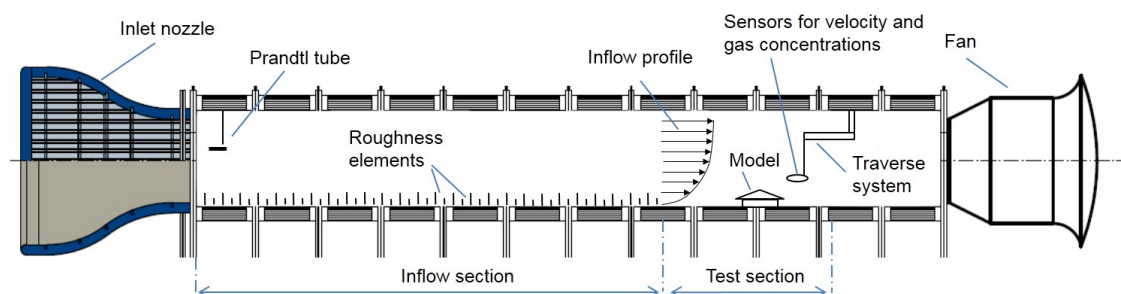
Figure 1. Sketch of the atmospheric boundary layer wind tunnel at ATB.

The ABLWT was specially designed to investigate ventilation and dispersion processes in agricultural buildings [15,16,22]. It is 28.5 m long, consisting of an air inlet fitted of honey combs, an air outlet equipped with an axial fan and a 19.5 m long inflow section to develop the atmospheric boundary layer. The cross-sectional area of the test section had a width of 3 m and a height of 2.3 m.

2.2. Studied Building and Gas Release

The studied building is a naturally ventilated dairy barn located in Northern Germany, with a building envelope typical for that region. The barn has a length of 96 m and a width of 34 m, and the roof height varies from 4.2 m at the side walls up to 11.4 m at the gable top. The barn has the capacity for 375 dairy cows, with completely open side walls and a ridge opening with a width of around 0.5 m. During frost periods, the opening of the side walls is reduced or completely closed with wind screens. Further detailed information about the barn can be found in Konig et al. [7].

A 1:100 scaled model of this building was made of 2 mm thick acrylic glass and a supporting structure, shown in Figure 2.
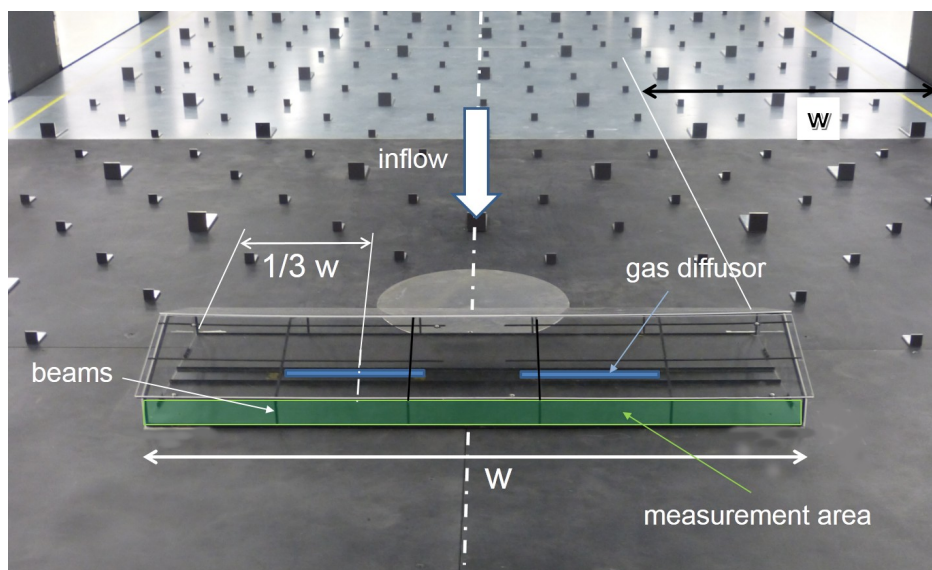
Figure 2. Scaled model positioned inside the wind tunnel. Gas was released with two gas diffusion stones, marked blue. Normal velocities and gas concentrations were measured at the green marked outlet plane.

The model was built with closed gable walls and a closed ridge opening, but completely opened side walls. The floor geometry with an elevated feeding alley and entrance edges was modeled, but the presence of animals was not modeled, since a previous study indicated that their effect was insignificant to the flow pattern and pollutant transport under cross-flow conditions [21]. The model was investigated in Janke et al. [23], where more detailed information about the geometry can be found.

The model was placed at the symmetry line of the wind tunnel, oriented with sidewall openings perpendicular to the approaching flow and the measurement area at the downwind side. The blockage ratio of the scaled model to the cross-section of the wind tunnel was 1.6%, which is less than the recommended maximum value of 5% for wind tunnel tests in VDI-guideline 3783/12 [11], and thus tunnel effect can be neglected. Figure 2 shows the wind tunnel with the scaled model placed inside.

Along the longitudinal symmetry line of the model, two gas diffusers were mounted on the floor. They consisted of porous stone material (Marina Extendable Airstone, HAGEN GROUP, Holm, Germany). They had a height of 13 mm, a width of 23 mm (shown in Figure 3) and a length of 260 mm and were symmetrically positioned with their middle point at 1/3 w and 2/3 w, according to Figure 2.

The height of the gas release would be 1.3 m in real scale and was chosen to mimic the animals' mouths heights, where most of the CO_2 and also methane is released. The diffusors were positioned along the feeding alley of the real scale barn, so the scenery of eating cows was simulated. The positioning of the source is further discussed in the discussion part. The gas used in this study was ethane. A controlled flow rate of 120 std l h^{-1} (standard liters per hour) of a gas mixture consisting of 50% ethane and 50% synthetic air was realized with mass flow controllers (red-y smart controller GSC,

Vögtlin Instruments AG, Switzerland). The gas mixture was injected into the two gas diffusers with a symmetric tube system. Preliminary studies were done to ensure uniform gas release along the length of each diffuser. With the overall surface area of the diffusers of 0.01196 m^2, the given volume flow of 120 std l h^{-1} under ambient conditions with 20 °C resulted in an average vertical exhaust tracer velocity w$_t$ of 0.003 m/s, so that the flow field was not disturbed by the momentum of the injected tracer gas. The gas mixture was chosen after preliminary tests in the outlet area, in order to gain a sufficient signal-to-noise ratio with the fast flame ionization detector (FFID).
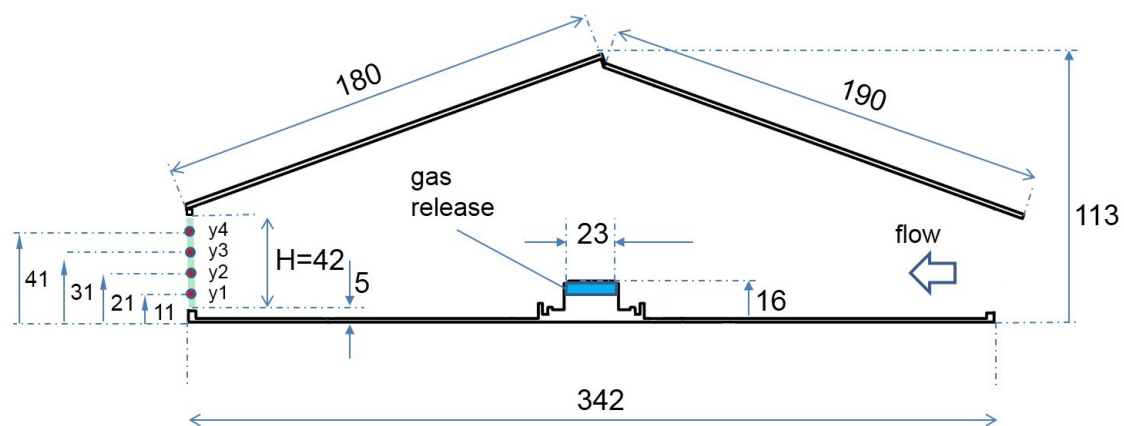
Figure 3. Sectional view of the scaled model. Dimensions are in mm. The green line at the outlet opening marks the measurement area.

2.3. Sensors and Additional Equipment

Air velocities at the measurement area were measured using a 2D fibre-optic laser doppler anemometer (LDA) (Dantec Dynamics, Skovlunde, Denmark) combined with the BSA Flow Software package (Dantec Dynamics, Skovlunde, Denmark). The LDA probe head was 0.06 m in diameter and 0.45 m in length and provided a focal length of 0.25 m. The precision of the LDA measurements for the velocities in flow direction was determined with repeated measurements of a vertical velocity profile and found to be <1%.

Gas concentrations were measured using a fast-flame-ionization-detector (FFID) (HFR400 Fast Response FID, Cambustion, Cambridge, England). The gas was sampled with a sampling needle 200 mm long with a diameter of 0.24 mm. Before the measurements, the FFID was calibrated with calibration gas (ethane) of three different concentrations (300 ppm, 1000 ppm, 5000 ppm). The measured mean concentrations at the outlet area were in a range of 5 ppm and 850 ppm. The test gas was also used to derive the uncertainty of the FFID, which was found to be below 1%.

Both the LDA probe and the FFID probe were mounted one after another on a three-dimensional computer-controlled traverse system that allowed automated and precise probe positioning with an uncertainty of <0.1 mm. A fog generator Tour Hazer II (Smoke Factory, Burgwedel, Germany) was placed at the wind tunnel inlet to produce seeding particles for LDA measurements.

The free stream wind speed at the wind tunnel inlet was measured using a Prandtl tube, connected to a pressure transducer MKS Baratron® Type 120A (MKS Instruments, Andover, MA, USA). The Prandtl tube was located at the center of the entrance of the test section at a height of 1.3 m from the wind tunnel floor.

2.4. Measurement Procedure

Measurements were done at the outlet area of the model shown in Figure 2. A matrix of 65 sampling points (SPs) in x-direction times 4 SPs in y-direction was measured, resulting in 260 SPs overall, sketched in Figure 4.
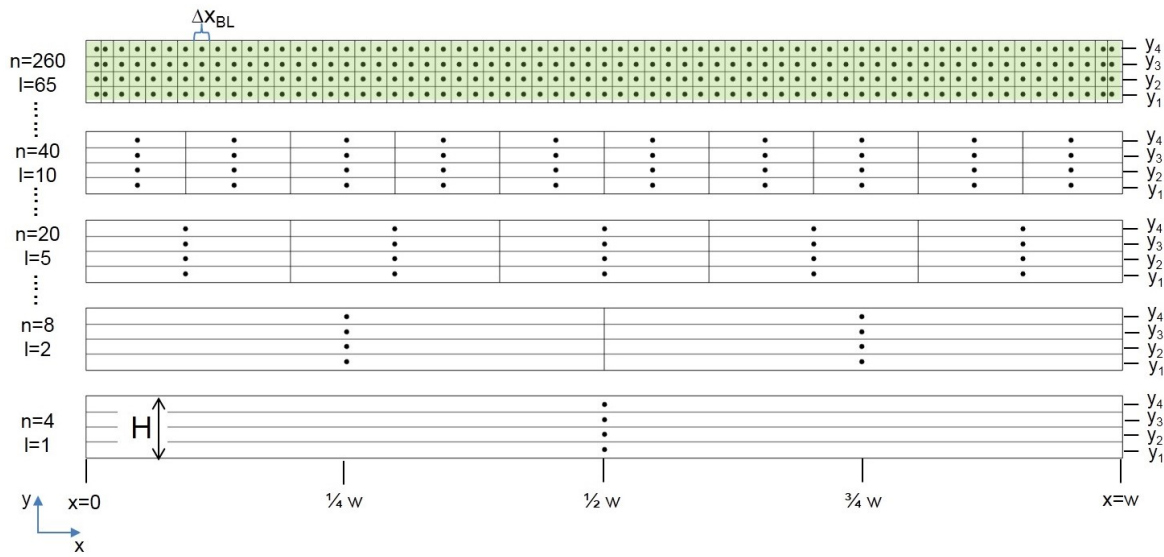
Figure 4. Lateral (x-direction) and vertical (y-direction) division of sampling positions. l is the number of vertical divisions and is increased incrementally from 1 to 65. n is the resulting total number of sampling points. The green marked area is the baseline configuration with the maximum amount of sampling points, with Δx_{BL} being the width of the area around each sampling point.

In the following, this set of SPs will be called *baseline*. The width of the area around each sampling point for the baseline was $\Delta x_{BL} = 15\,\text{mm}$, which corresponds to 1.5 m in the real scale. The four vertical SP positions were at heights of 11 mm for y1, 21 mm for y2, 31 mm for y3 and 41 mm for y4, shown in Figure 3. This resulted in a height of the area around each sampling point (marked as Δy in Figure 5) of 11 mm for SPs on y1 and y4 (1.1 m in real scale), and 10 mm for SPs on y2 and y3 (1.0 m in real scale).
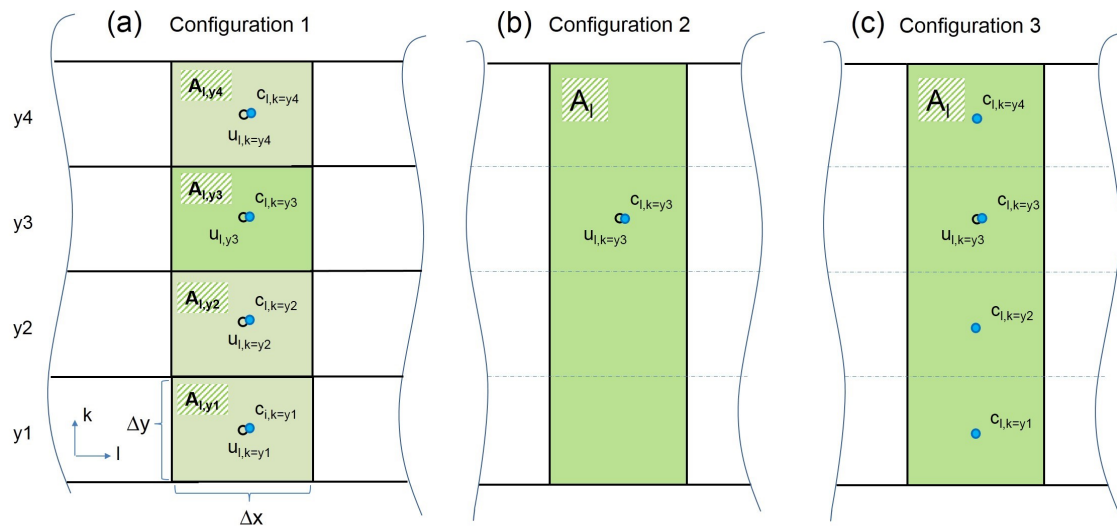
Figure 5. Construction of the area for each sampling point and the calculation of volume flow rates and emissions with the three configurations. The index *l* is for the lateral division of the measurement area in x-direction ([1...65]), the index *k* is the vertical position ([y1, y2, y3, y4]). Black dots and blue dots symbolize measurements of the velocity *u* and gas concentration *c*, respectively. Subfigures (**a**), (**b**), and (**c**) show configurations 1, 2, and 3, respectively. For configuration 1, the emission rate for a lateral division *l* is computed as $E_l = \sum_{k=1}^{4} A_{l,k} \cdot u_{l,k} \cdot c_{l,k}$. For configuration 2, the emission rate for a lateral distribution *l* and a vertical position k (in this example, k = y3) is computed as $E_{l,y3} = A_l \cdot u_{l,y3} \cdot c_{l,y3}$. For configuration 3, the emission rate for a lateral distribution *l* and a vertical position k (in this example, k = y3) is computed as $E_{l,y3} = A_l \cdot u_{l,y3} \cdot \frac{1}{4}(c_{l,y1} + c_{l,y2} + c_{l,y3} + c_{l,y4})$.

2.5. Boundary Layer

The total height H of the outlet area was 42 mm; the total width W was 966 mm.

First, the LDA probe was mounted on the traverse system and velocities were measured. A sample number of 60,000 at the outlet was found to reach statistically converged results. Hence, every sample location was measured until this sample number was reached. The sampling rate varied between approximately 90 and 500 Hz, depending on the sampling position and concentration of seeding particles.

After velocity measurements were completed, the FFID probe was mounted on the traverse system and the same measurement positions as with the LDA were measured. Measurements of the gas concentrations at each point were done with a sampling frequency of 500 Hz. After preliminary tests at three different sampling heights on the outlet area, a sample number of 20,000 was found to deliver statistically converged results of the mean concentration values; hence, each sampling point was measured until this sample number was reached.

2.6. Investigated Configurations

Variations of three different configurations were investigated. Configuration 1 took into account all vertical sampling positions y1, y2, y3 and y4 at each lateral sampling division, sketched in Figure 5a).

For real scale measurements, sensors are usually not positioned on top of each other at several heights, but distributed along one constant height [8,9]. This is reflected in configuration 2, where only one sampling point at the height of y1, y2, y3 or y4 was chosen for each lateral division. The respective area for the sampling point was computed as related width of the sampling point (same as in the first variation) multiplied by the height H of the measurement area; see Figure 5b).

Configuration 3 combines configurations 1 and 2. Volume flow rates were computed the same way as in configuration 2 with only one constant height. However, for real scale measurements, gas concentrations are often not measured with single sampling points but as spatial composite samples; sampling tubes with several openings are used. Usually, the spatial composite sampling is done inside the barn at a constant height in lateral directions. This idea was adapted for the vertical direction in configuration 3, where the concentration value was computed as the mean value of the concentrations measured at y1, y2, y3 and y4 at each lateral position, sketched in Figure 5.

All three configurations were varied by incrementally decreasing the number of lateral sampling positions; Figure 4 gives an example for configuration 1.

Within the wind tunnel, a fully developed turbulent flow with a logarithmic vertical velocity profile was generated though the presence of roughness elements at the inflow section. The vertical velocity profile of the generated boundary layer is shown in Figure 6.

The vertical velocity profile was measured without the presence of the model at the symmetry line of the wind tunnel (dashed white line in Figure 2 at the position, where the inflow opening of the model would be). Reynolds number independence was tested for the undisturbed inflow profile upstream in the model and at the outlet section of the model. The velocity profile was found to be independent of the Reynolds number, when the undisturbed inlet velocity was ≥ 8 m s^{-1}, which is a basic prerequisite for transferring the wind tunnel results of the boundary layer to natural conditions. The inflow profile fulfilled the criteria for a boundary layer over a moderately rough terrain according to VDI [11].

Choosing as characteristic length scale $L = 0.11$ m (approximate height of the barn) and as characteristic velocity scale $u = 5$ m s^{-1} (velocity at the opening of the barn model with an undisturbed wind tunnel inlet velocity of $u = 8$ m s^{-1}), and with $\nu = 1.48 \times 10^{-5}$ m s^{-1} as the kinematic viscosity of air at 15 °C, the internal Reynolds number of the flow is given by

$$\mathrm{Re} = \frac{Lu}{\nu} \approx 37,200$$

This number fulfills the criterion for an internal independence of the Reynolds number which must be greater than 2×10^4, as stated in Cermak et al. [24]; hence, the inside flow pattern is considered as fully turbulent and transferable to the real scale.

2.7. Computation of Volume Flow Rate and Emissions

Gas emissions E were computed following this equation:

$$E = \sum_{i=1}^{N_{SP}} Q_i \cdot c_i \qquad (1)$$

where N_{SP} is the number of sampling points used, Q is the volume flow rate and c is the gas concentration in the respective sampling point. Q and c are the mean values of the consecutively measured volume flow and gas concentrations; hence the emissions estimated and presented in this study are the advective mean emission fluxes, but the instantaneous, turbulent emission fluxes were not recorded due to limitations in the setup of the measurement devices. The volume flow rate at each sampling point was computed as the product of the area around the point and the normal velocity vector u pointing out of that area:

$$Q_i = A_i \cdot u_i \qquad (2)$$

where A_i was constructed dependent on the respective configurations of investigated sampling points, sketched in Figure 5.
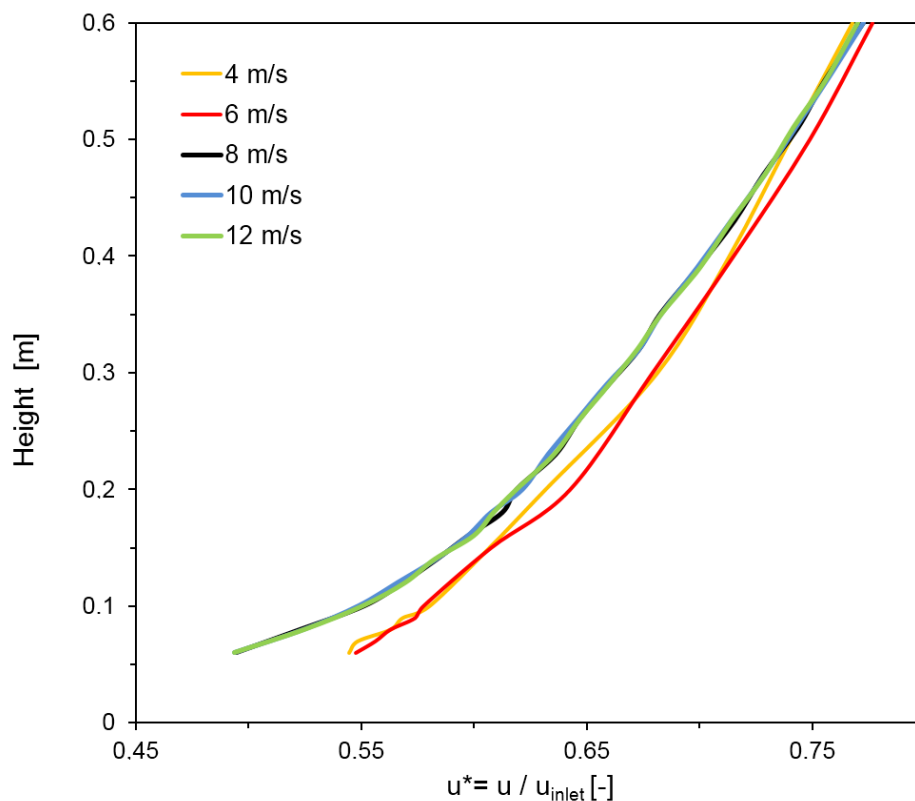
Figure 6. Vertical velocity profiles of the atmospheric boundary layer, with measured velocities u in position on the model. The undisturbed inlet velocity u_{inlet} at the inlet of the wind tunnel was gradually increased from 4 to 12 m s^{-1}. The dimensionless velocity u* was normalized with u_{inlet}. For velocities $u_{inlet} \geq 8$ m s^{-1}, u* is constant, meaning that a fully turbulent, and hence Reynolds number-independent boundary layer, is achieved.

2.8. Calculation of the Deviations

　　　The results of the measurements for the different configurations are shown in the following section. Deviations are presented as relative errors compared to the baseline dataset with the highest number of measurement points:

$$\Delta_P = \frac{P_{CFG} - P_{BL}}{P_{BL}} \cdot 100 \tag{3}$$

where the *P* is a placeholder for the considered property (velocity *u* and gas concentration *c*), the subscript *CFG* stands for the investigated sampling configuration and *BL* stands for baseline configuration.

3. Results

3.1. Baseline Configuration

　　　Figure 7 shows the results for the normal velocity *u* and the gas concentrations measured at the outlet of the baseline configuration.
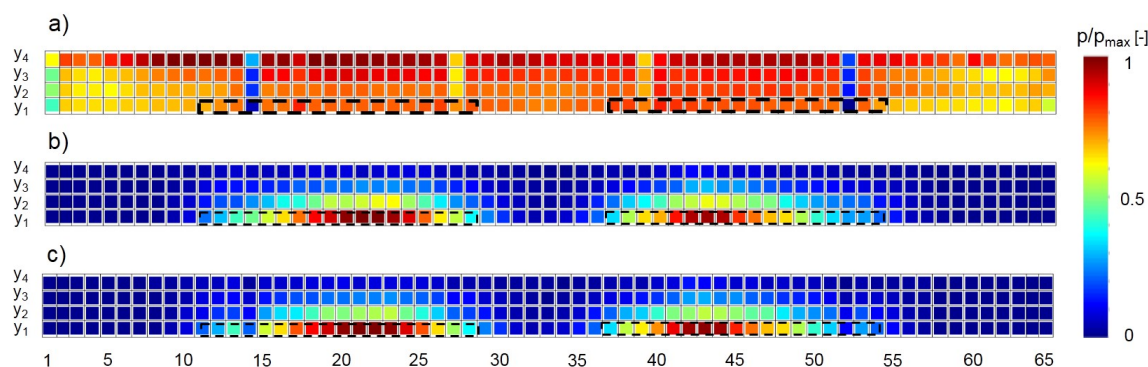
Figure 7. Measured concentrations, normal velocities and calculated emissions of the baseline configuration. Upper (**a**) shows the mean velocity u in normal direction for each sampling point; (**b**) shows the mean concentration c for each sampling point. (**c**) The computed emissions E = Q·c, where Q was calculated as the product of u and the area A that surrounded each sampling point. The results are normalized with the respective maximum values of u, c and E. "p" at the colorbar is a placeholder for the property shown—concentration, velocity or emissions. Numbers on the x-axis index the lateral sampling position. The black dotted lines sketch the positions of the gas diffusers inside the barn.

　　　The values for *u* are spatially dependent. In vertical direction, a trend is visible with higher velocities towards the roof, meaning that the highest velocities were measured at line y4.

　　　In lateral directions, the velocity is accelerated towards the symmetry line of the measurement area, with respective lower velocities in the sampling positions between 1–14 and 52–65. This is probably due to the frictional resistance of the closed sidewalls of the model. A region with lower velocities can be seen at the symmetry line at positions 32 and 33, especially in the lower region. The cause for this is probably the formation of interacting vortex systems of the both gas diffusers, resulting in a deceleration of the flow.

　　　Reduced velocities at sampling positions 14 and 52, and also at positions 27 and 39, can be seen. In the vicinity of these positions, vertical beams of the model's supporting structure were present; see Figure 2. Although the beams were very thin (2 mm), and measurements were not conducted directly behind them, but with a distance of approximately 1 mm, their influence is still clearly visible.

　　　The values for the gas concentrations c show a heterogeneous distribution of gas concentration at the outlet with a clear accumulation of concentration downstream the two gas diffusers inside the barn. The highest concentrations can be seen on the height of y1 around the symmetry axis of each diffuser. In this area, the highest vertical gradients of concentrations can be noticed, which are at lateral

sampling position 21, with 14 times higher concentrations at y1 than at y4. On average, sampling height y1 had seven times higher concentrations than y4. This clearly indicates that the assumption of a well mixed gas is not fulfilled and most of the gas released at the surface of the diffuser was transported towards the ground in the downwind direction.

3.2. Volume Flow Rates Estimated with Configurations 1 and 2

In this section, the results for the volume flow rates estimated with configurations 1 and 2 are presented. As configuration 3 computes the volume flow rate the same way as configuration 2, it is not shown here. For configuration 1, Figure 8 shows the progress of the error for the total volume flow rate estimation with an increasing number of lateral sampling positions.
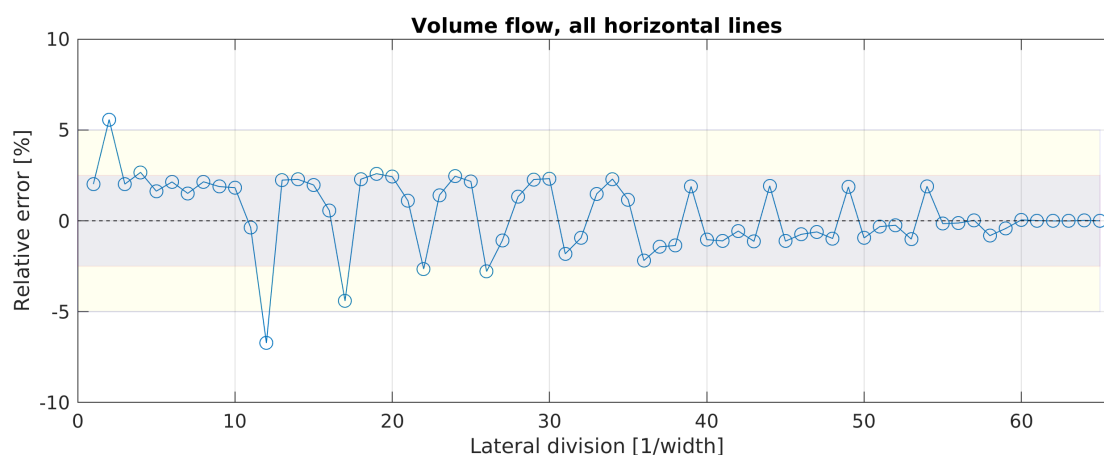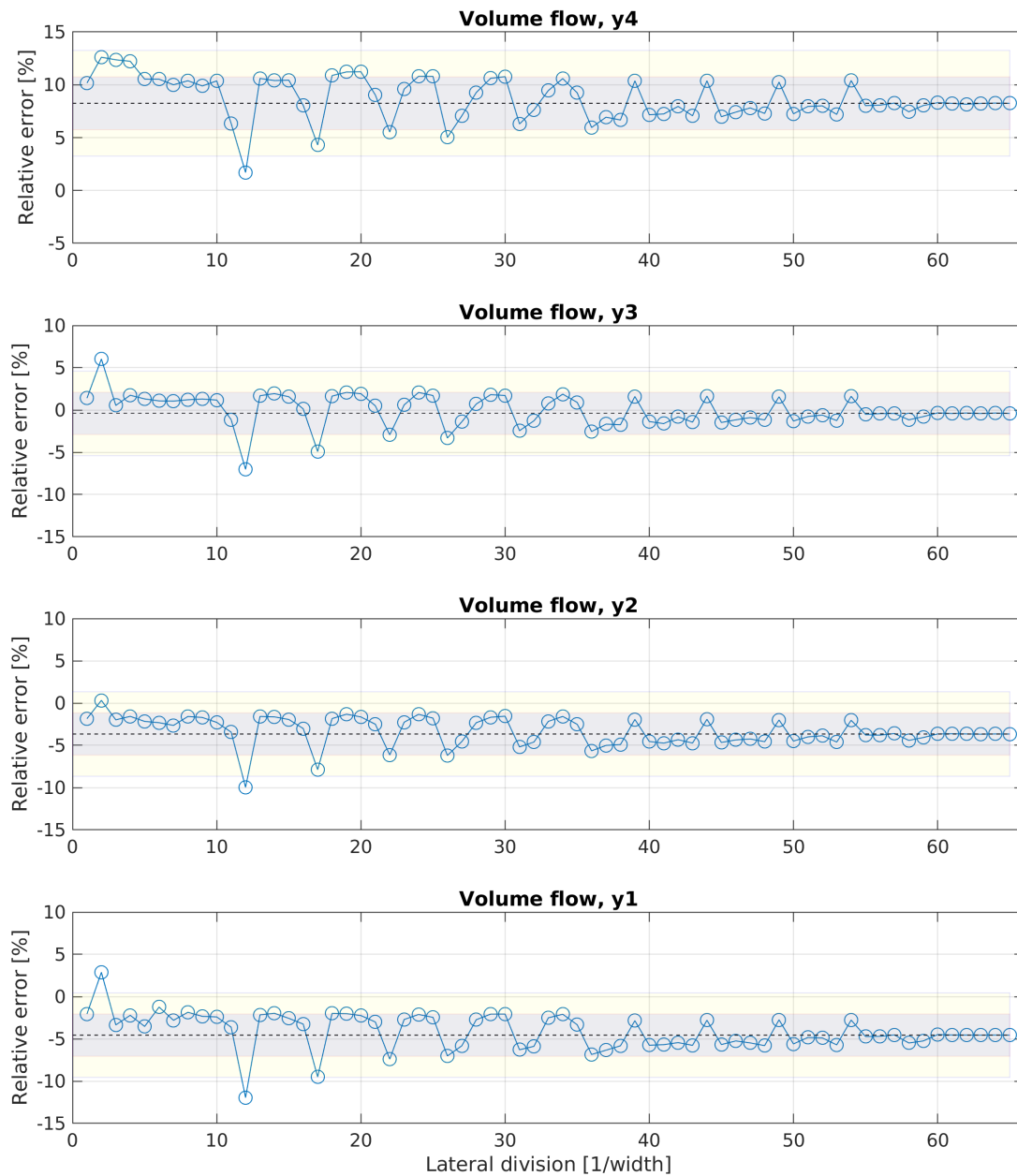

Figure 8. Evolution of the error for estimating the volume flow rate with a growing number of lateral sampling positions, using configuration 1. The dotted line represents the converged mean value (CMV) of the estimated volume flow rate with the maximum number of lateral divisions. The gray and yellow areas mark the error spans of $\pm 2.5\%$ and $\pm 5\%$ around the CMV, respectively.

The magnitude of the error exceeds 5% only for a lateral division of $l = 2$ and $l = 12$; for all other divisions, it is less than 5%, where the majority (five exceptions) has an error even less than 2.5%. It should be mentioned that the accurate results with an error <2.5% for only one vertical set of sensors ($l = 1$) were achieved rather by coincidence. The position of the sensor set $l = 1$ is on the vertical symmetry line. At this position, the volume flow of the $l = 1$ set is very close to the average volume flow of all sampling points (baseline configuration). If $l = 1$ would have been positioned elsewhere, e.g., behind one of the diffusors or near the construction beams, the error would have been greater.

The negative outlier for $l = 12$ can be explained by the geometrical division. With the configuration $l = 12$, the lateral sampling positions 14 and 52 were taken into account. As described before and seen in Figure 7, these are the two positions with the lowest velocities in all four vertical sampling points due to the presence of the construction beams. These values decrease the mean value for the estimated total volume flow rate. This behavior can also be noticed for configurations where either lateral sampling positions 14 and 52 or (less effective) 27 and 39 were used, e.g., for $l = 17$, $l = 22$ or $l = 25$. The positive outlier for $l = 2$ can be explained by the positioning of the two lateral divisions at the symmetry line of each gas diffuser, where the highest velocities occurred, as described in the previous section.

For configuration 2, Figure 9 shows the progress of the error independently of the lateral division, when sensors would be positioned only on one height.

Figure 9. Evolution of the error for estimating the volume flow rate with a growing number of lateral sampling positions and only one constant height of the sampling points. The dotted line represents the value of the estimated volume flow rate with the maximum number of lateral divisions at the respective height.

For all four heights, the error scatters around the converged mean value (CMV), which is estimated with the maximum number of lateral divisions, in a range of $\pm 5\%$. At each height, the positive outlier at $l = 2$ and the negative outlier at $l = 12$ can be observed, similarly to the characteristic in configuration 1. For all heights except y4, an error span around the CMV less than $\pm 2.5\%$ was reached with $l = 3$. However, the values of the CMV can be interpreted as the induced bias of the configuration. The CMV showed a trend towards higher volume flow rates with a rising height. Positioning sensors only at height y1, y2, y3 or y4 would result in a bias of -5%, -4%, $\pm 0\%$ or $+8\%$, respectively, when using the maximum lateral division of $l = 65$. For the lateral division of $l = 3$, the bias would be -3.4%, -2%, $+0.5\%$ or $+12.3\%$, for y1, y2, y3 or y4, respectively.

3.3. Emissions Estimated with Configurations 1, 2 and 3

Figure 10 shows the progression of the error for emissions estimated following Equation (1) when using configuration 1.
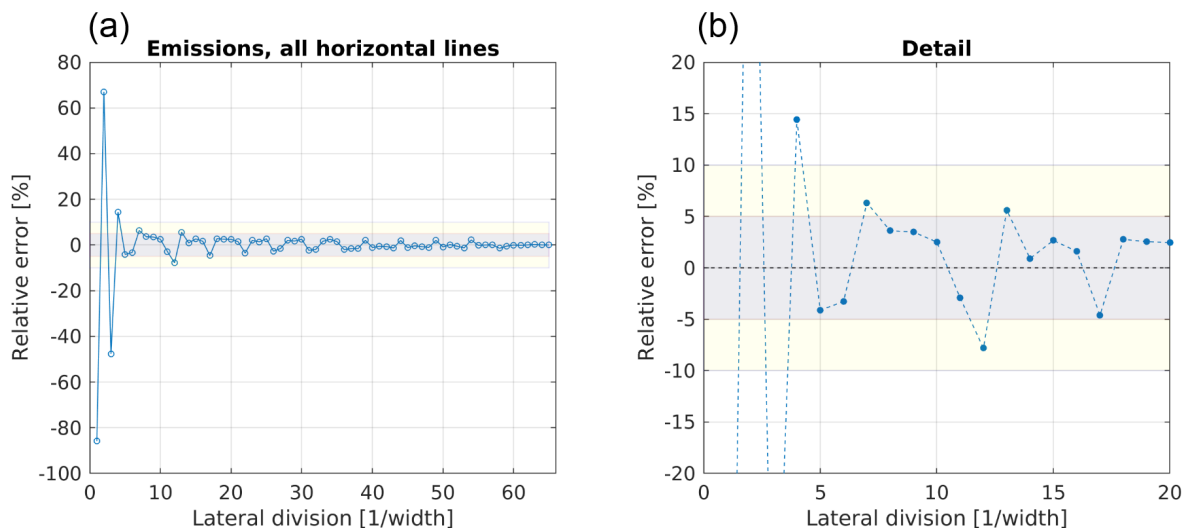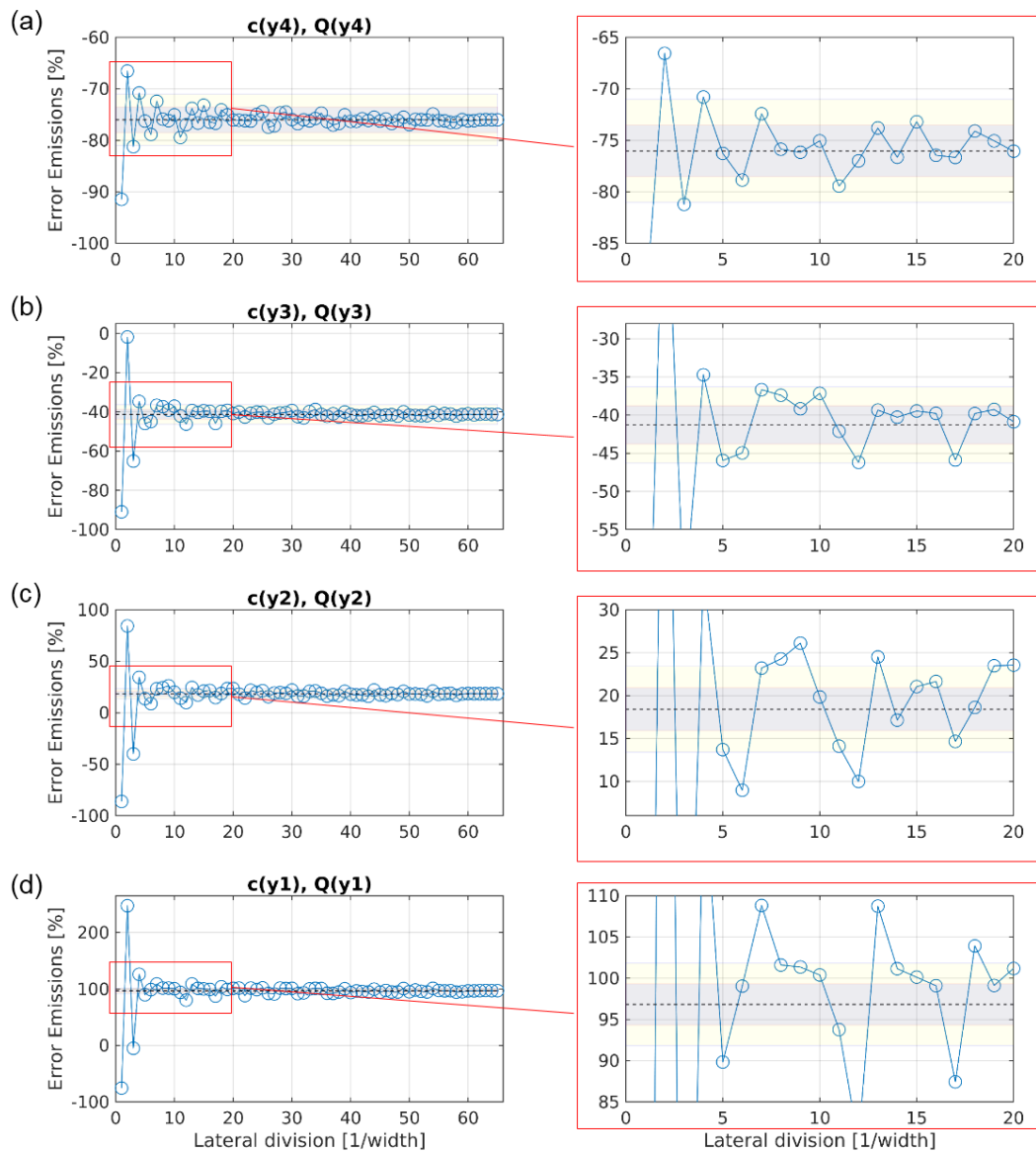

Figure 10. Evolution of the error for estimating the emissions with a growing number of lateral sampling positions, using configuration 1. Subfigure (**a**) shows the error for all 65 lateral divisions, subfigure (**b**) shows a detailed view for the first 20 lateral divisions. The dotted line represents the converged mean value (CMV) of the estimated volume flow rate with the maximum number of lateral divisions. The gray and yellow areas mark the error spans of $\pm 5\%$ and $\pm 10\%$ around the CMV, respectively.

Compared to the results for the volume flow rate, a wider spread of the error around the CMV is visible, especially until the number of divisions reaches $l = 5$. The errors for using a lateral division of $l = 1, 2, 3$ or 4 are -86%, $+67\%$, -48% and $+14\%$, respectively. Beginning with $l = 5$, the error converges within $\pm 5\%$, and for $l > 30$, the error is within $\pm 2.5\%$. Again, for $l = 12$, the negative outlier is seen, resulting from measuring low velocities near the construction beams.

Figure 11 shows the progression of the error for emission estimations when using configuration 2.

The spread around the CMV for y4 is similar as for configuration 1, with a converging error within the $\pm 5\%$ area for lateral divisions of $l \geq 3$. For y3, y2 and y1, the span of the error around their respective CMV got larger, the nearer to the ground the vertical position was. Accordingly, the number of lateral divisions needed for a converging error within $\pm 5\%$ grew, with $l \geq 5$ for y3, $l \geq 13$ for y2 and $l \geq 23$ for y1. This is a direct reflection of the results for the baseline shown in Figure 7: for y4, the lateral distribution of gas concentration is very homogeneous; the distribution gets more and more heterogeneous the lower the height is. The reason for that is the accumulation of concentration in the vicinity of the gas diffusers. Similarly to the estimated volume flow rate with configuration 2, the CMV show a systematic error, but in contrast to the volume flow rate, the trend was towards lower emission estimations with a rising height. Hence, positioning sensors only at height y1, y2, y3 or y4 would result in biases of $+97\%$, $+18\%$, -41% or -76%, respectively, when using the maximum lateral division of $l = 65$.

Figure 12 shows the progression of the error for emission estimations when using configuration 3.

Figure 11. Evolution of the error for estimating the emissions with growing number of lateral sampling positions, using configuration 2. The subfigures (**a**), (**b**), (**c**), and (**d**) show the converging error, when velocities and gas concentrations were only measured at height y_4, y_3, y_2, and y_1, respectively. The dotted line represents the converged mean value (CMV) of the estimated emissions with the maximum number of lateral divisions. The gray and yellow areas mark the error spans of $\pm 2.5\%$ and $\pm 5\%$ around the CMV, respectively.

The spread around the respective CMV, in contrast to configuration 2, is now for all four heights in the same range with a converging error within the $\pm 5\%$ area for lateral divisions of $l \geq 5$. Exceptions to this are recurring outliers for all height at $l = 7$ (around $+6\%$) and $l = 12$ (around -7.5%). Compared to configuration 2, the bias for each height has decreased clearly: measuring with configuration 3 the maximum number of lateral divisions $l = 65$ would result in a bias for the estimated emissions of -2%, -2%, $+3\%$ or $+10\%$ for y1, y2, y3 or y4, respectively. Reducing the number of lateral divisions down to $l = 5$ results in a bias of -6.5%, -6%, $+0.5\%$ or $+7\%$ for y1, y2, y3 or y4, respectively.
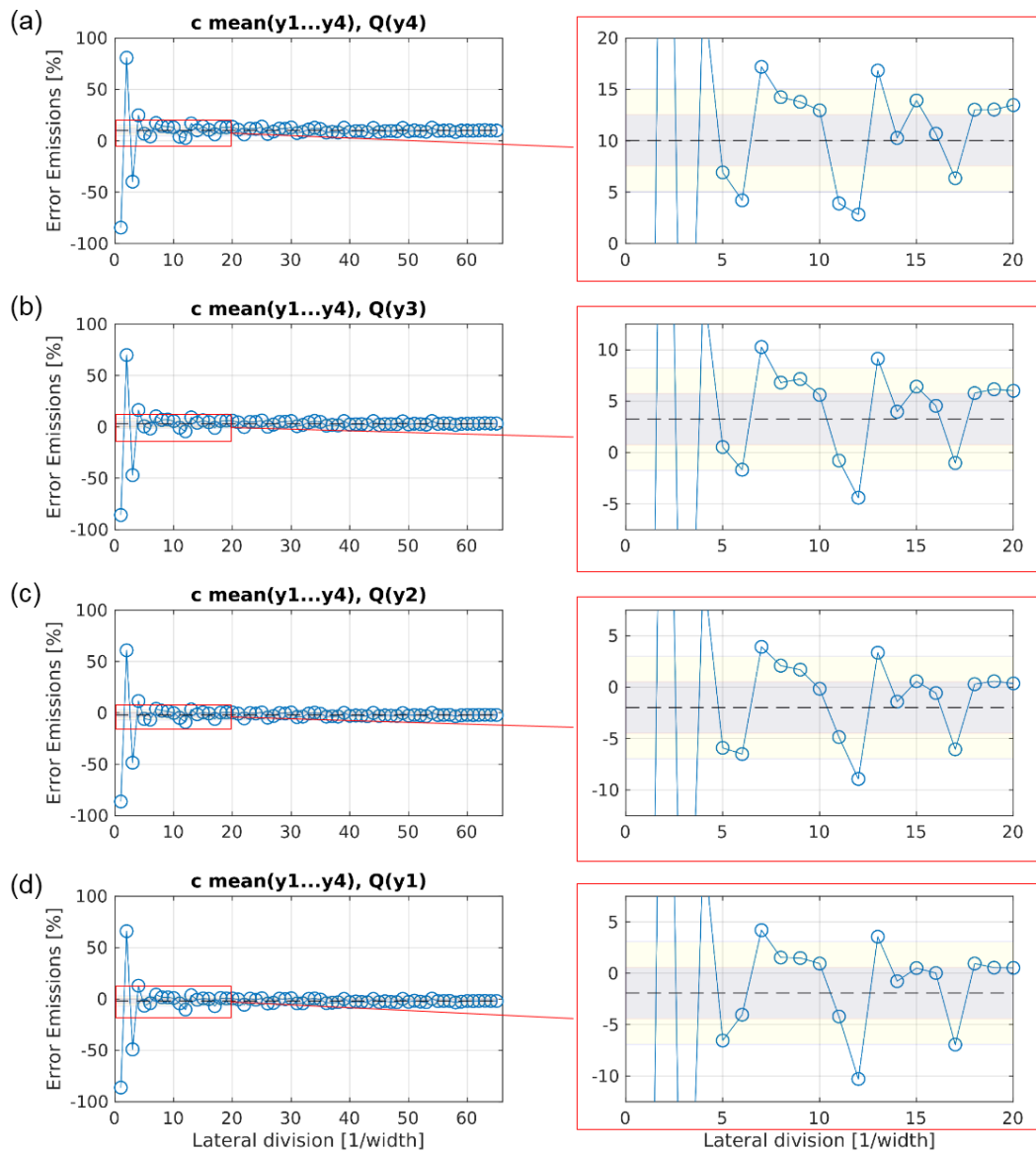
Figure 12. Evolution of the error for estimating the emissions with growing number of lateral sampling positions, using configuration 3. The subfigures (**a**), (**b**), (**c**), and (**d**) show the converging error, when velocities were only measured at height y_4, y_3, y_2, and y_1, respectively, while the concentration was measured as the mean value of the four vertical sampling points.The dotted line represents the converged mean value (CMV) of the estimated emissions with the maximum number of lateral divisions. The gray and yellow areas mark the error spans of $\pm 2.5\%$ and $\pm 5\%$ around the CMV, respectively.

4. Discussion

The results shown for the baseline indicate that hypothesis (1) can be considered true. Both velocities and concentrations vary spatially in vertical and lateral directions. That biases the results for the estimations of volume flow rate and emissions, depending on the number and positions of the sensors.

Vertical gradients in the velocity at the opening were also reported by De Vogeleer et al. [10] and Van Overbeke et al. [25]. They found a velocity maximum at the center of the opening. In contrast, our results show a maximum towards the top of the opening. This difference can be explained by the smaller opening dimensions typical for a pig barn, with stronger influences from the boundaries and the formation of a parabolic velocity profile. Previous wind tunnel studies with the same scaled model but without the gas diffusers installed showed a nearly constant profile at the outlet [23]; hence we assumed the acceleration towards higher positions was due to the presence of flow obstacles inside

the barn. Formations of more or less complex flow patterns due to obstacles inside the barn and their effects on the velocity gradients on the measurement area are hard to predict. Therefore, preliminary tests on the vertical and horizontal velocity gradients can minimize the risk of systematic overestimation or underestimation of the volume flow rate, as was also stated by De Vogeleer et al. [10].

For the volume flow rate, the lateral positioning can introduce negative (-7%) or positive ($+6$%) biases to the estimation of volume flow rate when using configuration 1. The negative bias can easily be prevented by making sure that sensors are not positioned in the direct vicinity of obstacles, e.g., construction elements. The positive bias is related to less obvious flow disturbances originating inside the barn. In this case, the bias can be prevented by increasing the number of lateral divisions. For configuration 1, a number of l = 3 is sufficient to reach results with errors less than 2.5%. When further increasing l, the results do not improve significantly. Scaling up to the real world, this would mean a lateral distance of 32 m between each sensor. Our simplification (a) (see introduction) of a constant cross-flow might have influenced these results. Under real conditions with varying wind directions, the lateral distances needed would probably decrease, which should be the focus of further research. Still, for configuration 1, a number of l = 3 means a total number of velocity sensors of n = 12, which is a lot if we consider that only one opening of the barn was measured.

When reducing the number of sensors by positioning them laterally distributed only at one height, which is the common approach under practical conditions, a systematic error occurred, as assumed in hypothesis (1). For l = 3, the maximum errors occurred when measuring at either the lowest (-3.5%) or highest ($+12.3$%) sampling position. When measuring in the vicinity of the horizontal symmetry line of the opening (either $y2$ or $y3$), the errors for estimating the total volume flow rate were both below 2%. This proves the common practice of positioning anemometers only at one height (e.g., Joo et al. [8], Wang et al. [9]) to be reasonable, provided the height chosen is reasonable. It also implies that the chance of systematically overestimating or underestimating the volume flow rate is more sensitive to the vertical positioning than to the lateral positioning, provided the minimum lateral distribution (l = 3 in this case) is applied. When these findings should be transferred to the real scale, possible effects of simplification (b) (see introduction) should be considered: When barns with adaptive opening sizes (e.g., screens rolling up and down) are measured, it will be hard to find the optimum sampling height for each screen position. Further research regarding simplification (b) is, therefore, needed.

In this study, the most influential factor on the accuracy of emission estimation is the positioning height of the sensors. If sensors for velocity and gas concentrations are all positioned at one constant height, even with the maximum lateral resolution, the best case is an error of 18%; the worst case is an error of 97%. This is one order of magnitude higher than the errors observed for the volume flow rate; hence we can consider hypothesis (2) true. The reason for the high errors in the different vertical sampling positions is the not-well mixed gas at the outlet, leading to high concentration gradients. This in-homogeneous distribution of gas concentrations was also reported by König et al. [7] for CO_2, by Wang et al. [26] for NH_3 and for tracer gas in a wind tunnel study by Nosek et al. [21]. An easy way to smooth these gradients is to apply a sampling system for the concentration measurement device that takes vertical composite samples at each lateral position. By that, the errors could be reduced down to a minimum of -2% and a maximum error of $+10$% with the maximum lateral distribution. When the lateral number of sensors is further decreased, symmetrical divisions of the width with $l \geq 5$ lead to errors between -7 and $+4$% for (height of 3/8 H), which can be interpreted as a good cost–benefit ratio. On a real scale, this would mean a lateral distance of 19 m between each sensor for the measured NVDB. This number is already close to the minimum lateral distance of 10 m for the sampling of gas concentrations recommended in the VERA test protocol [27]. Just like for the volume flow rate estimations, the number of minimum lateral divisions will probably increase under changing inflow directions and will be the focus of further investigations.

Consequently, in order to reduce the number of sensors for direct measurements of gaseous emissions, the focus should be on an elaborate gas sampling system, which can help to reduce the number of velocity sensors. Spatial distribution of gas sampling can easily be enhanced at on-farm

measurements when using, e.g., a tube sampling system with critical orifices. When using open path lasers for the measurement of concentrations at the outlet, one is usually restricted to one constant height. Then, preliminary studies with varying heights could be conducted to quantify the vertical gradients in the gas concentrations and derive height correction factors.

The results shown here were derived for measurements under a stable orthogonal inflow. Although most of NVDBs are aligned towards to a prevalence main wind direction, it can be expected that for real scale conditions, the amount of sensors needed will change for deviating or rapidly changing wind directions. This should be investigated further in future experiments, where the measurements are repeated under varying incident angles.

The investigated dairy barn had the dimensions and a building envelope that are representative for NVDBs in the northern and eastern regions of Germany. The results of this study are expected to be transferable to NVBDs with similar properties, meaning relatively large buildings (>3000 m^2 floor area) with rather high opening ratios of the side walls (up to 90%) and a focus on cross ventilation. However, for other systems (like rather small barns with small opening ratios, extremely open barns typical for parts of southern Europe, or barns with mainly ridge ventilation), additional experiments should be performed to investigate the influences of the respective building variations on the distribution of velocity and gas concentrations at the opening areas.

Gas concentrations and normal velocities were measured consecutively and their respective mean values were used to estimate the mean emission fluxes (simplification (d)). Depending on the flow scenario, turbulent fluxes, which could not be measured in this study, might have a significant impact on the results, as described, e.g., in Nosek et al. [28]. Hence, further experiments should measure concentrations and velocities simultaneously to quantify the turbulent portion of the emissions.

5. Conclusions

Under the simplifications made of a NVDB under constant, isothermal cross-flow with constantly fully-opened sidewalls, the following conclusions can be drawn for the direct measurement of the volume flow rates and emissions:

1. A division of the total opening width into units with a lateral distance of 32 m, each equipped with an anemometer of a height near the horizontal symmetry line, is sufficient to reach results for the volume flow rate with errors less than 5%, compared to the baseline with the highest sensor density.
2. The anemometers should be positioned with greatest possible distance to obstacles like beams, walls, etc., as they can significantly bias the results for volume flow rate. Such behavior was not observed for the gas concentrations.
3. The gas at the outlet area is not well mixed, resulting in high vertical and lateral gradients of gas concentrations. Hence, when deriving emissions with a direct method, the focus should be on the representative sampling of the target gas concentration. When using gas measurement systems that measure at a constant height (e.g., open path laser systems), preliminary studies for each target gas should be carried out in order to quantify the vertical concentration gradients and derive a correction factor for the height.
4. Provided that vertical composite sampling of gas concentrations is possible, a division of the opening width into units with a lateral distance of 19 m, each equipped with an anemometer positioned in the vicinity of the horizontal symmetry line, is sufficient to reach results for the direct estimation of emissions with errors less than 7%, compared to the baseline.

As the concentration gradients of the gas concentrations have a large influence on the emission estimations, the influencing factors on the gas mixing efficiency should be investigated further. Future research should therefore include variations of the gas source characteristics (e.g., uniform area source vs. different hot spots; positioned at floor level vs. positioned at animal height level) and the systematic variation of measures that potentially change the airflow pattern (e.g., different

interior, partly closed opening configurations). Additionally, instead of modeling an isothermal flow, the additional modeling of buoyancy inside the barn could lead to a greater vertical mixing of gas concentrations, resulting in sensor positions less sensitive to the height. This should also be investigated further.

Direct methods have the potential to compensate for the limitations attributed to indirect methods, e.g., when emittents are located both outdoor and indoor the housing system (as in systems with outdoor walking alleys). Theoretically, the mass flow through any given system boundary can be measured with direct methods, but the measured results are highly dependent on the number of sensors. The results of this study will be of help researchers to assess the expected uncertainty associated with the resolution of sensors, when applied on the aforementioned housing systems.

Abbreviations

The following abbreviations are used in this manuscript:

LDA	Laser Doppler Anemometer
FFID	Fast Flame Ionization Detector
AER	Air Exchange Rate
ABLWT	Atmospheric Boundary Layer Wind Tunnel
SP	Sampling Point(s)
CMV	Converged Mean Value
BL	Baseline Configuration
CFG	Configuration

References

1. Tista, M.; Gager, M.; Gaisbauer, S.; Ullrich, B. *European Union Emission Inventory Report 1990–2017 under the UNECE Convention on Long-Range Transboundary Air Pollution (LRTAP)*; Publications Office of the European Union: Luxembourg, 2019.

2. European Statistical Office—Eurostat. Greenhouse Gas Emissions by Source Sector (Source: EEA), 2018. Available online: https://ec.europa.eu/eurostat/de/web/agriculture/data/database (accessed on 6 August 2020).

3. Eren Ozcan, S.; Vranken, E.; Berckmans, D. An overview of ventilation rate measuring and modelling techniques through naturally ventilated buildings. In *Ammonia Emissions in Agriculture*; Wageningen Academic Publishers: Wageningen, The Netherlands, 2007; pp. 351–353.

4. Ogink, N.; Mosquera, J.; Calvet, S.; Zhang, G. Methods for measuring gas emissions from naturally ventilated livestock buildings: Developments over the last decade and perspectives for improvement. *Biosyst. Eng.* **2013**, *116*, 297–308. [CrossRef]

5. Janke, D.; Willink, D.; Ammon, C.; Hempel, S.; Schrade, S.; Demeyer, P.; Hartung, E.; Amon, B.; Ogink, N.; Amon, T. Calculation of ventilation rates and ammonia emissions: Comparison of sampling strategies for a naturally ventilated dairy barn. *Biosyst. Eng.* **2020**, *198*, 15–30. [CrossRef]

6. Calvet, S.; Gates, R.; Zhang, G.; Estellés, F.; Ogink, N.; Pedersen, S.; Berckmans, D. Measuring gas emissions from livestock buildings: A review on uncertainty analysis and error sources. *Biosyst. Eng.* **2013**, *116*, 221–231. [CrossRef]

7. König, M.; Hempel, S.; Janke, D.; Amon, B.; Amon, T. Variabilities in determining air exchange rates in naturally ventilated dairy buildings using the CO_2 production model. *Biosyst. Eng.* **2018**, *174*, 249–259. [CrossRef]

8. Joo, H.; Ndegwa, P.M.; Heber, A.; Bogan, B.; Ni, J.-Q.; Cortus, E.L.; Ramirez-Dorronsoro, J. A direct method of measuring gaseous emissions from naturally ventilated dairy barns. *Atmos. Environ.* **2014**, *86*, 176–186. [CrossRef]

9. Wang, X.; Ndegwa, P.M.; Joo, H.; Neerackal, G.M.; Stöckle, C.O.; Liu, H.; Harrison, J.H. Indirect method versus direct method for measuring ventilation rates in naturally ventilated dairy houses. *Biosyst. Eng.* **2016**, *144*, 13–25. [CrossRef]

10. De Vogeleer, G.; Pieters, J.G.; Van Overbeke, P.; Demeyer, P. Effect of sampling density on the reliability of airflow rate measurements in a naturally ventilated animal mock-up building. *Energy Build.* **2017**, *152*, 313–322. [CrossRef]

11. Ingenier, VDI-Verein Deutcher. Environmental meteorology Physical modelling of flow and dispersion processes in the atmospheric boundary layer In *Application of Wind Tunnels, VDI-Standard: VDI*; Deutsches Institut für Normung: Berlin, Germany, 2000.

12. Zhang, G.; Ikeguchi, A.; Strom, J.; Morsing, S.; Takai, H.; Ravn, P.; Okushima, L. Obstacle Effects on Airflow and Containment Dispersion around a Naturally Ventilated Livestock Building. *Comm. Int. du Genie Rural* **2003**, *5*, 1–9.

13. Aubrun, S.; Leitl, B. Unsteady characteristics of the dispersion process in the vicinity of a pig barn. Wind tunnel experiments and comparison with field data. *Atmos. Environ.* **2004**, *38*, 81–93. [CrossRef]

14. Ikeguchi, A.; Okushima, L.; Zhang, G.; Strom, J. Contaminant Air Propagation between Naturally Ventilated Scale Model Pig Buildings under Steady-state Conditions. *Biosyst. Eng.* **2005**, *90*, 217–226. [CrossRef]

15. Yi, Q.; Zhang, G.; König, M.; Janke, D.; Hempel, S.; Amon, T. Investigation of discharge coefficient for wind-driven naturally ventilated dairy barns. *Energy Build.* **2018**, *165*, 132–140. [CrossRef]

16. Yi, Q.; König, M.; Janke, D.; Hempel, S.; Zhang, G.; Amon, B.; Amon, T. Wind tunnel investigations of sidewall opening effects on indoor airflows of a cross-ventilated dairy building. *Energy Build.* **2018**, *175*, 163–172. [CrossRef]

17. De Paepe, M.; Pieters, J.; Cornelis, W.M.; Gabriels, D.; Merci, B.; Demeyer, P. Airflow measurements in and around scale-model cattle barns in a wind tunnel: Effect of wind incidence angle. *Biosyst. Eng.* **2013**, *115*, 211–219. [CrossRef]

18. De Paepe, M.; Pieters, J.G.; Cornelis, W.M.; Gabriels, D.; Merci, B.; Demeyer, P. Airflow measurements in and around scale model cattle barns in a wind tunnel: Effect of ventilation opening height. *Biosyst. Eng.* **2012**, *113*, 22–32. [CrossRef]

19. Fiedler, M.; Schröter, K.; Reinhardt, A.; Saha, C.; Loebsin, C.; Berg, W.; Amon, T. Wind tunnel investigations on a naturally ventilated barn. *Landtechnik* **2013**, *68*, 265–268.

20. Shen, X.; Su, R.; Ntinas, G.K.; Zhang, G. Influence of sidewall openings on air change rate and airflow conditions inside and outside low-rise naturally ventilated buildings. *Energy Build.* **2016**, *130*, 453–464. [CrossRef]

21. Nosek, Š.; Kluková, Z.; Jakubcová, M.; Yi, Q.; Janke, D.; Demeyer, P.; Jaňour, Z. The impact of atmospheric boundary layer, opening configuration and presence of animals on the ventilation of a cattle barn. *J. Wind. Eng. Ind. Aerodyn.* **2020**, *201*, 104185. [CrossRef]

22. König, M.; Bonkoß, K.; Amon, T. Wind tunnel measurements on reduction of near surface concentrations through naturally barrier on emissions from naturally ventilated barn. In Proceedings of the International Workshop on Physical Modelling of Flow and Dispersion Phenomena (Physmod 2017), Nantes, France, 23–25 August 2017; pp. 89–93.

23. Janke, D.; Caiazzo, A.; Ahmed, N.; Alia, N.; Knoth, O.; Moreau, B.; Wilbrandt, U.; Willink, D.; Amon, T.; John, V. On the feasibility of using open source solvers for the simulation of a turbulent air flow in a dairy barn. *Comput. Electron. Agric.* **2020**, *175*, 105546. [CrossRef]

24. Cermak, J.E.; Poreh, M.; Peterka, J.A.; Ayad, S.S. Wind Tunnel Investigations of Natural Ventilation. *J. Transp. Eng.* **1984**, *110*, 67–79. [CrossRef]

25. Van Overbeke, P.; De Vogeleer, G.; Brusselman, E.; Pieters, J.; Demeyer, P. Development of a reference method for airflow rate measurements through rectangular vents towards application in naturally ventilated animal houses: Part 3: Application in a test facility in the open. *Comput. Electron. Agric.* **2015**, *115*, 97–107. [CrossRef]

26. Wang, X.; Ndegwa, P.M.; Joo, H.; Neerackal, G.M.; Harrison, J.H.; Stöckle, C.O.; Liu, H. Reliable low-cost devices for monitoring ammonia concentrations and emissions in naturally ventilated dairy barns. *Environ. Pollut.* **2016**, *208*, 571–579. [CrossRef] [PubMed]

27. VERA. *VERA TEST PROTOCOL: For Livestock Housing and Management Systems*; International VERA Secretariat: Delft, The Netherlands, 2018.

28. Nosek, Š.; Fuka, V.; Kukačka, L.; Kluková, Z.; Jaňour, Z. Street-canyon pollution with respect to urban-array complexity: The role of lateral and mean pollution fluxes. *Build. Environ.* **2018**, *138*, 221–234. [CrossRef]

Sample Availability: Measurement data of the velocities and gas concentrations are available from the authors.

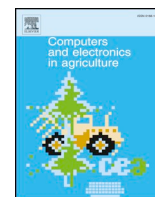**Publisher's Note:** MDPI stays neutral with regard to jurisdictional claims in published maps and institutional affiliations.

4

On the feasibility of using open source solvers for the simulation of a turbulent air flow in a dairy barn

On the feasibility of using open source solvers for the simulation of a turbulent air flow in a dairy barn

David Janke[a,*], Alfonso Caiazzo[b], Naveed Ahmed[c], Najib Alia[b], Oswald Knoth[d], Baptiste Moreau[b], Ulrich Wilbrandt[b], Dilya Willink[a], Thomas Amon[a,f], Volker John[b,e,1]

[a] Leibniz-Institut für Agrartechnik und Bioökonomie e.V. (ATB), Max-Eyth-Allee 100, 14469 Potsdam, Germany
[b] Weierstrass Institute for Applied Analysis and Stochastics (WIAS), Mohrenstr. 39, 10117 Berlin, Germany
[c] Department of Mathematics and Natural Sciences, Gulf University for Science and Technology, Kuwait City, Kuwait
[d] Leibniz-Institut für Troposphärenforschung (TROPOS), Permoserstraße 15, 04318 Leipzig, Germany
[e] Freie Universität Berlin, Department of Mathematics and Computer Science, Arnimallee 6, 14195 Berlin, Germany
[f] Freie Universität Berlin, Institute for Animal Hygiene and Environmental Health, Robert-von-Ostertag-Str. 7-13, 14163 Berlin, Germany

ARTICLE INFO

ABSTRACT

Two transient open source solvers, OpenFOAM and ParMooN, and the commercial solver Ansys Fluent are assessed with respect to the simulation of the turbulent air flow inside and around a dairy barn. For this purpose, data were obtained in an experimental campaign at a 1: 100 scaled wind tunnel model. All solvers used different meshes, discretization schemes, and turbulence models. The experimental data and numerical results agree well for time-averaged stream-wise and vertical-wise velocities. In particular, the air exchange was predicted with high accuracy by both open source solvers with relative differences less than 4% and by the commercial solver with a relative difference of 9% compared to the experimental results. With respect to the turbulent quantities, good agreements at the second (downwind) half of the barn inside and especially outside the barn could be achieved, where all codes accurately predicted the flow separation and, in many cases, the root-mean-square velocities. Deviations between simulations and experimental results regarding turbulent quantities could be observed in the first part of the barn. These deviations can be attributed to the utilization of roughness elements between inlet and barn in the experiment that were not modeled in the numerical simulations. Both open source solvers proved to be promising tools for the accurate prediction of time-dependent phenomena in an agricultural context, e.g., like the transport of particulate matter or pathogen-laden aerosols in and around agricultural buildings.

1. Introduction

In Europe, dairy cows are mainly housed in naturally ventilated barns (NVBs). Also in pigs and poultry farming, the trend is towards naturally ventilated systems or systems with increased spout areas, mainly to increase the animal welfare and the consumers' acceptance. The NVBs act as sources of airborne pollutants, both gaseous and particle-associated. The gaseous pollutants are mainly ammonia (NH_3), methane (CH_4), carbon dioxide (CO_2), or dinitrogen monoxide (N_2O). Pollutants associated with particles are, e.g., particulate matter (PM) or droplets. These particles can act as carriers for pathogens which arise through sick animals inside the barn. Carried out of the barn, the pathogens can spread diseases that are harmful either for other animals or (in case of zoonosis) for human beings. In order to assess and possibly mitigate the risk of airborne pathogen spreading out of NVBs, it is necessary to obtain insights on the flow fields inside and around the barns and to assess the air exchange (AE). The direct coupling of the inside flow regime with the ambient, turbulent weather conditions makes it hard to measure the flow conditions and the AE. The buildings and their openings are very large, velocities and gaseous concentrations are heterogeneously distributed and vary in time and space (König et al., 2018).

Computational fluid dynamics (CFD) is a useful tool for acquiring detailed insight into the complex flow fields encountered in NVBs. In

---

* Corresponding author.

E-mail addresses: djanke@atb-potsdam.de (D. Janke), caiazzo@wias-berlin.de (A. Caiazzo), ahmed.n@gust.edu.kw (N. Ahmed), alia@wias-berlin.de (N. Alia), knoth@tropos.de (O. Knoth), moreau@wias-berlin.de (B. Moreau), wilbrandt@wias-berlin.de (U. Wilbrandt), dwillink@atb-potsdam.de (D. Willink), tamon@atb-potsdam.de (T. Amon), john@wias-berlin.de (V. John).
[1] ORCID 0000-0002-2711-4409.

particular, CFD allows to predict the main features of the flow fields also at locations where measurements are practically infeasible, or to perform virtual assessment studies with the help of computational models. The use of CFD to describe the flow characteristics in NVBs has considerably gained popularity in recent years.

The flow under consideration is time-dependent, and even turbulent, see the beginning of Section 2.8 for a discussion on some features of turbulent flows. Such kinds of flows can be modeled mathematically by the evolutionary incompressible Navier-Stokes equations. In fact, the Reynolds number of the considered flow is so large that the steady-state Navier-Stokes equations do not possess a stable (weak) solution. Since the flow is turbulent, standard numerical discretizations, like central finite differences or the Galerkin finite element method, have to be extended with additional terms that model the impact of turbulence. The concrete numerical solution depends heavily on the kind of turbulence modeling that is used. In particular, there are turbulence modeling techniques that compute time-averaged (steady-state) flow fields, like some RANS (Reynolds averaged Navier-Stokes) approaches. They are highly efficient and have been used in scientific and industrial applications for more than 40 years. In fact, in agricultural applications, the vast majority of numerical flow simulations rely on RANS approaches, where the turbulence is completely parameterized (see e.g. (Lee et al., 2013) or (Bjerg et al., 2013)). In most cases, proprietary software is used for the flow simulations. Commonly applied commercial codes are, e.g., Ansys (containing Fluent and CFX), StarCCM +, or Comsol.

The transport and dispersion of gases and particles in a turbulent flow is by nature a dynamic (time-dependent) process. Therefore, important information might be lost when transport is modeled with a time-averaged flow field such that the use of time-averaged flow fields could lead to inaccurate results. Transient simulations resolve important unsteady scales and so the dynamic characteristics of a flow. In our opinion, the use of transient simulations is expected to provide more accurate results for the simulation of gas and particle transport. However, the gained accuracy comes at the price of greater computational costs. The use of computer clusters, where several processors solve the problem in parallel, is often necessary. Depending on the license policy of the software companies, this can lead to high costs, e.g., when for every additional processor node, an extra license needs to be paid. Also, many of the computer clusters freely accessible to research institutes do not even offer the use of proprietary software. Moreover, commercial tools do not give access to the source code, thus making it difficult to understand the details of numerical methods used within the solver. Open source solvers can represent here an appealing alternative. Besides being free of charge, they provide complete control over the numerical methods and give also the possibility of customizing the code and implementing tailored methods. In the context of research, they favor exchange of data and source codes, and naturally allow for reproducibility of numerical results by different groups. We also refer to the discussion of the benefits of open source software in the introduction of Wilbrandt et al. (2017). Research in the area of CFD brought in recent years the release of several open source packages for flow simulations, such as, to mention some, OpenFOAM (OpenFOAM, 2016), deal.II (Bangerth et al., 2016), FEniCS (Alnæs et al., 2015), DUNE (Blatt et al., 2016; Dedner et al., 2010). Further available options include the in-house research codes ASAM[2] (Jähn et al., 2014) and ParMooN[3] (Ganesan et al., 2016; Wilbrandt et al., 2017), which are currently developed in the research groups of some authors of this paper. To the best of our knowledge, the only studies using non-commercial solvers to investigate the flow inside or around agricultural buildings are the ones

from a research group around Lee and co-workers (see e.g. Lee et al., 2007 or Hong et al., 2017), using OpenFOAM with a steady-state RANS approach, and from a research group around Kateris and co-workers, using Galerkin finite-element-methods with an in-house code written in FORTRAN (Kateris et al., 2012). Studies with transient simulations in the agricultural context are the exception. Only few papers can be found, e.g. Villagran et al. (2019), where 2D transient simulations with Ansys Fluent were carried out with the focus on greenhouses.

This study therefore aims to present a contribution to fill this gap and to investigate the use of transient open source solvers for turbulent flow simulations inside and around agricultural buildings. The main goal of this paper is to demonstrate that open source codes are able to provide accurate simulations of the flow through and around a NVB. Two open source codes with different features are involved in the numerical studies: OpenFOAM and ParMooN. For comparison, a commercial solver (Ansys Fluent) is also included in the study. To this end, a benchmark problem with a typical naturally ventilated barn with cross flow is defined. To achieve the objective of this paper, the benchmark configuration was investigated experimentally in a wind tunnel for obtaining data to compare with. These data sets will be published as well, which we consider to be very useful for the definition of a realistic benchmark problem for turbulent flow simulations. They can be used for assessing turbulent flow solvers in the future. Both codes support different types of grids, discretizations, turbulence models, and solvers. By sharing the experiences made in this study, we hope to reduce eventually existing reservations towards the use of open source codes and promote their application in the agricultural community.

The paper is organized as follows. Section 2 describes the experimental setup to measure the benchmark data set and introduces the corresponding mathematical models, which will be the basis for the numerical studies. Some features of the two considered open source packages as well as the used commercial code will be described in detail in Section 3, while the assessment of the numerical studies is presented in Section 4. Finally, Section 5 contains the conclusions of our investigations.

2. Experimental setup and mathematical model

2.1. The studied dairy barn

The studied building is a naturally ventilated dairy barn with a capacity for 375 cows, located in Northern Germany, near the city of Rostock. The barn has a length of 96 m, a width of , while the roof height varies from 4.2 m at the side walls up to 10.7 m at the gable top. The side walls are completely open, while the gable walls are partially open as sketched in Fig. 1. Further detailed information about the barn can be found in König et al. (2018).

2.2. Wind tunnel setup

Experimental airflow measurements were obtained on a 1:100 scaled model (Fig. 1, right) of the above described barn in the *atmospheric boundary layer wind tunnel* (ABLWT) of ATB Potsdam (Fig. 2). Within the wind tunnel, a fully developed turbulent flow with a logarithmic vertical velocity profile was generated by the presence of roughness elements at the inflow section. The vertical velocity profile and the vertical distribution of turbulence intensity of the generated boundary layer are shown in Fig. 3. The inflow profile fulfilled the criteria for a boundary layer over a moderately rough terrain according to VDI (2000). More detailed information about the ABLWT can be found in Yi et al. (2018). The model was positioned with a 90° angle to the flow direction, so that the barn was under cross-flow.

---

[2] developed at Leibniz Institute for Tropospheric Research (TROPOS) by Dr.Oswald Knoth

[3] developed at Weierstrass Institute for Applied Analysis and Stochastics (WIAS)

Fig. 1. Left: Real scale barn. Right: 1:100 scale model in the wind tunnel.
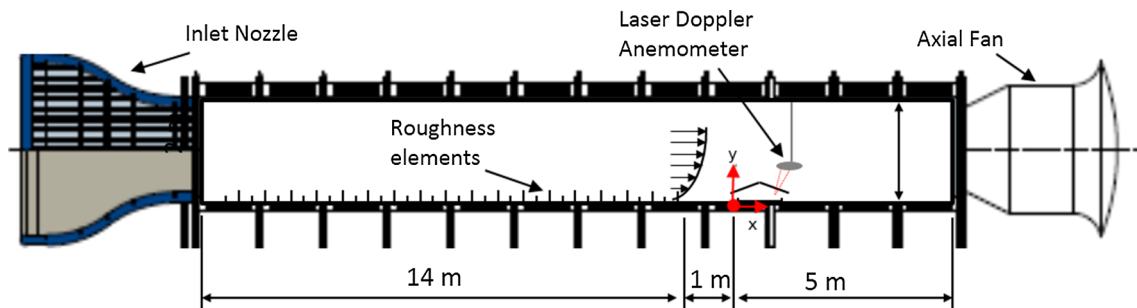
Fig. 2. Sketch of the ABLWT with the scaled model.
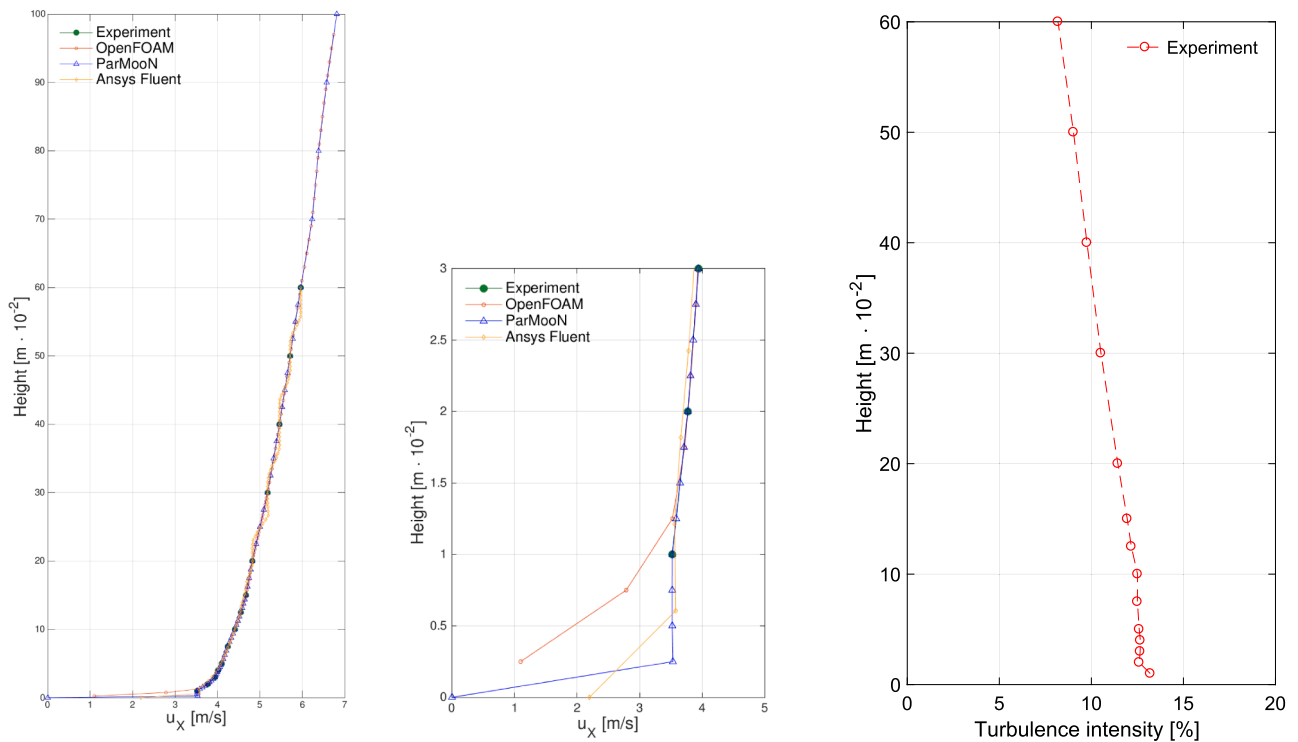
Fig. 3. Left: comparison between the measured inflow profile and the interpolated data. Center: Zoom on the first part (0 to 0.03 meters) of the inlet region. Right: Turbulence intensity at the inflow boundary.

2.3. Velocity measurements

The velocity components along the vertical direction were measured at several vertical sample lines (v1,..,v10) shown in Fig. 4 and their coordinates are given in Table 1. For each point at the sample lines, the

velocity components in x-direction (stream-wise) and y-direction (vertical-wise) were measured with a two-dimensional Laser Doppler Anemometer (LDA) (Dantec Dynamics, Skovlunde, Denmark), mounted on a computer-controlled positioning traverse. The LDA measured the velocity with a sample rate between 20 and 100Hz, depending on the

3
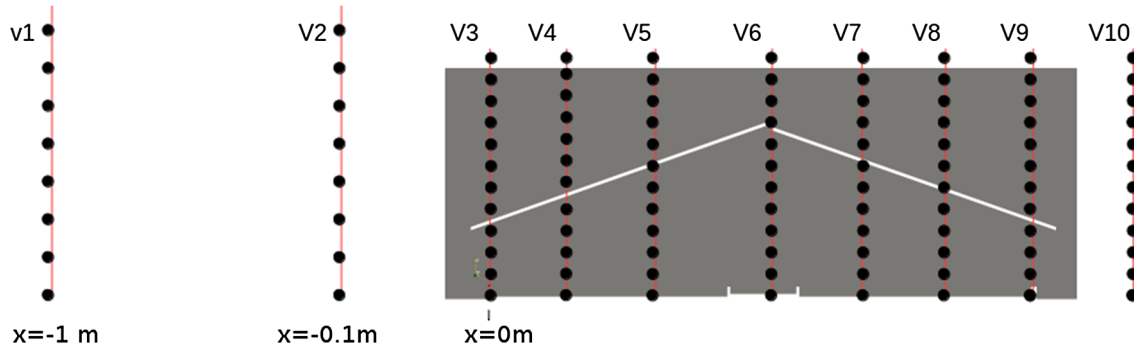
Fig. 4. Visualization of the measured sample lines. All data were acquired in the middle cross-section in the z-direction.

density of measured seeding particles. Each point was measured for a duration of 3min, which was found to be sufficiently long enough to capture the features of the flow with an uncertainty for the mean velocities smaller than 2% and for the root-mean-square velocities smaller than 5%.

2.4. Mathematical model

Air is a compressible fluid. However, since the range of velocities observed in the livestock husbandry is much lower than the speed of sound in air, the flow can be considered as incompressible, expecting only a minor impact on the numerical results.

Let $\Omega \subset \mathbb{R}^3$ be the computational flow domain and let $T > 0$ be the final time, which in the simulations was set to $T = 7$ s. Moreover, let us denote with $\boldsymbol{u}$ [m/s] the air velocity (where u and v stand for the horizontal and vertical components, respectively), and with p [Pa] the air pressure. Without any external force, velocity and pressure obey the incompressible Navier-Stokes equations given by

$$
\begin{aligned}
\partial_t \boldsymbol{u} - \nu \nabla \cdot \mathbb{D}(\boldsymbol{u}) + (\boldsymbol{u} \cdot \nabla)\boldsymbol{u} + \nabla p &= \boldsymbol{0} \quad \text{in}(0, T] \times \Omega, \\
\nabla \cdot \boldsymbol{u} &= 0 \quad \text{in}(0, T] \times \Omega.
\end{aligned}
\tag{1}
$$

The velocity deformation tensor $\mathbb{D}(\boldsymbol{u})$ is the symmetric part of the velocity gradient, i.e., $\mathbb{D}(\boldsymbol{u}) := (\nabla\boldsymbol{u} + \nabla\boldsymbol{u}^T)/2$. In (1), the kinematic viscosity ν [m^2/s] is the ratio of the dynamic viscosity η [kg/ms] over the density ρ [kg/m^3]. For air at 15 °C, these parameters are $\eta = 1.81 \cdot 10^{-5}$ kg/ms and $\rho = 1.225$ kgm^3, and therefore $\nu = 1.48 \cdot 10^{-5}$ m^{2}s.

2.5. Computational domain

The computational domain for the model problem is sketched in Fig. 5, see also Table 2 for additional information. It is a rectangle of 3 m length and 1 m height with the floor and roof geometry of the wind tunnel model. The coordinate system origin is placed on the bottom edge of the windward side of the barn. As already mentioned, the horizontal coordinate is denoted by x and the vertical coordinate by y.

In order to solve the Navier-Stokes Eqs. (1) numerically, the computational domain needs to be discretized by a mesh, i.e., decomposed in a set of polyhedral mesh cells that cover the domain. On the one hand, the size, and consequently the number, of the mesh cells defines the number of degrees of freedom of the discrete problem to be solved. On the other hand, the size of the mesh cells allows for increasing the accuracy of the approximation in regions of interest. Therefore, the computational mesh plays a crucial role in CFD and it has a direct

impact on the results of the numerical solvers. In the study presented in this paper, different meshes were employed, whose structure depended on the particular code. For the sake of clarity, details will be described for each code separately in Section 3.

Remark 1. The geometry used for defining the computational model considered a straight roof (Fig. 5). However, due to the weight of the material, the cross section of the roof in the experiment is a slightly convex curve. For this reason, the coordinates of few measurement points were in the experiment on top of the roof but in the simulations below the roof. These points were not considered for the numerical assessment presented in Section 4.

2.6. Initial condition and boundary conditions

In order to obtain a closed system, the Navier-Stokes Eqs. (1) have to be equipped with an initial condition ($t = 0$) and with boundary conditions on the boundary of Ω.

In practice, the initial condition is not known. For this reason, one has to start with an arbitrary initial flow field, to run a simulation until the flow is fully developed, and then to start with monitoring the flow field. Note that the actual initial condition possesses only an impact on the time interval until a fully developed flow field is reached.

At the inlet boundary ($x = -0.5$ m), the velocity profile was prescribed based on experimental data. Concretely, the velocity was measured in the wind tunnel without the scaled barn model at different heights, see Table 3. For the simulations, some interpolation of this profile was used, compare Fig. 3. Further details on the boundary conditions that were applied in the simulations with the individual codes are given in Section 3.

In order to characterize the flow regime, the Navier-Stokes equations can be non-dimensionalized by introducing characteristic length, velocity, and time scales. Choosing as characteristic length scale $L = 0.11$ m (approximate height of the barn) and as characteristic velocity scale $U = 5$ m/s (approximate maximal velocity in a neighborhood of the barn), the Reynolds number of the flow is given by

$$
\text{Re} = \frac{LU}{\nu} \approx 37200.
$$

This number indicates that the flow is turbulent, requiring therefore suitable numerical methods for its simulation, see Sections 2.8 and 3.

Table 1
Horizontal coordinates and vertical extrema of the measurement sample lines (see also Fig. 4).

	v1	v2	v3	v4	v5	v6	v7	v8	v9	v10
x [m]	-1	-0.1	0	0.05	0.1	0.165	0.242	0.292	0.342	0.39
y_{end} [m]	0.6	0.6	0.15	0.15	0.15	0.15	0.15	0.15	0.15	0.15

4
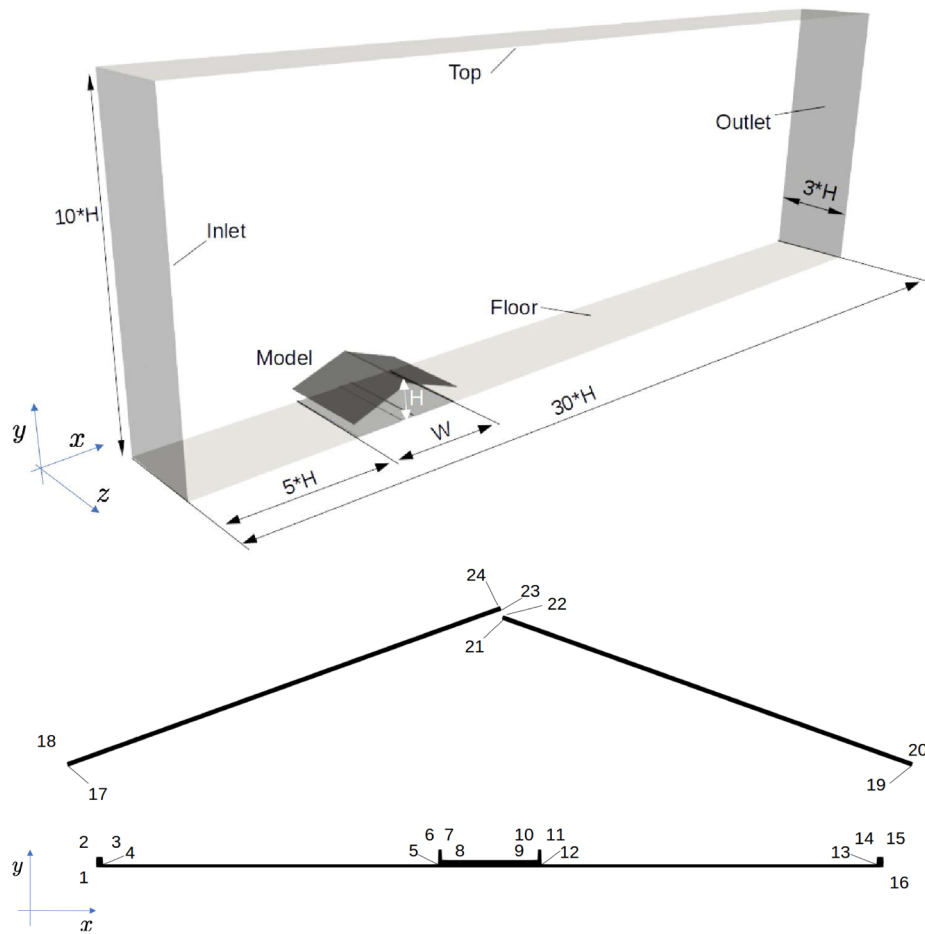
Fig. 5. Top: Sketch of the computational domain. Bottom: Detailed view of the 2D projection of the barn. The numbers 1–24 refer to the edges, whose coordinates are listed in Table 2.

Table 2

Coordinates of the points defining the model geometry (see the sketch in Fig. 5).

Point	x [m]	y [m]
1	0	0
2	0	0.0048
3	0.0032	0.0048
4	0.0032	0.0016
5	0.1485	0.0016
6	0.1485	0.008
7	0.150	0.008
8	0.1503	0.0034
9	0.1917	0.0034
10	0.1917	0.0080
11	0.1935	0.0080
12	0.1935	0.0016
13	0.3388	0.0016
14	0.3388	0.0048
15	0.342	0.0048
16	0.3420	0
17	−0.0120	0.044
18	−0.01253	0.04577
19	0.354	0.044
20	0.35451	0.04562
21	0.1761	0.108
22	0.1767	0.1099
23	0.1761	0.112.0
24	0.1757	0.1138

Table 3

Experimental data from wind tunnel measurements at the inlet.

y [m]	0	0.01	0.02	0.03	0.04	0.05	0.075	0.1	0.125	0.15
u [m/s]	0	3.52	3.77	3.94	4.01	4.10	4.24	4.41	4.55	4.67

y [m]	0.2	0.3	0.4	0.5	0.6	0.7	0.8	0.9	1
u [m/s]	4.82	5.18	5.46	5.71	5.96	6.23	6.38	6.57	6.81

2.7. Time interval

The choice of the final time is briefly motivated in this section. The quantities of interest are time-averaged velocity profiles. Hence, one needs a sufficiently long time interval for obtaining statistically converged results. The area of interest is inside the barn, which has a maximum height of $H \approx 0.11$ m. According to the inflow profile, see Table 3, an air parcel starting at the half of this height has a velocity of about $u = 4$ m/s. Consequently, the parcel passes the whole length of the domain ($30H$) in an interval of time of approximatively 0.8 s. The area of interest inside the barn has a width of $W = 0.34$ m. The given parcel passes this width around three times in one second. Based on these considerations, we assumed that a fully developed full profile can be obtained within a time interval of 1 s. Furthermore, a time interval of 6 s is assumed to be sufficient to achieve statistically converged velocity profiles. These estimates were validated a posteriori by the results of our numerical simulations.

Fig. 6. Domain meshed for OpenFOAM with snappyHexMesh.

2.8. Remarks to turbulence modeling

There is no mathematical definition of what turbulence is. A flow is considered to be turbulent when its dynamics possess a wide spectrum of scales (eddies) – ranging from large scales to very small scales – and with the very small scales being of utmost importance for the physical character of the flow (energy dissipation). The Navier-Stokes Eqs. (1) are a proper mathematical model for describing such flows.

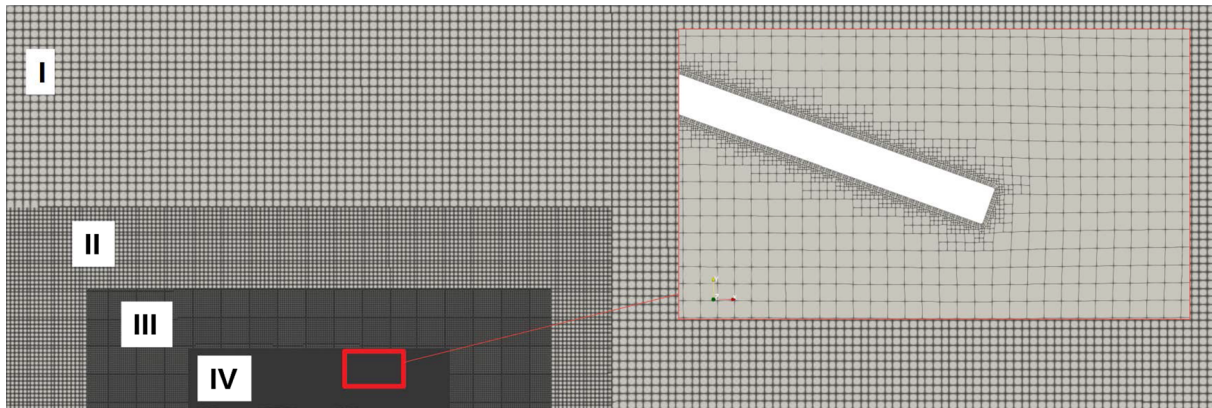Standard discretizations of the Navier-Stokes equations, like the Galerkin finite element method or central finite differences, try to resolve all important scales of the flow. However, the ability of a numerical method to approximate the flow dynamics of small scales depends on the level of resolution of the spatial discretization, i.e., the computational grid. In particular, most of the important scales in turbulent regimes are usually so small that it is not even possible to represent them on computationally affordable grids. These scales are called *unresolved* scales. Of course, scales that cannot be represented cannot be simulated. Because of these unresolved scales, standard discretizations fail for the simulation of turbulent flows, which usually results in a blow-up of the numerical simulations. The remedy consists in augmenting standard discretizations by including so-called turbulence models, which have the purpose to account for the impact of the unresolved scales onto the simulated (resolved) scales. From the numerical point of view, turbulence models introduce additional viscosity into the discrete problem.

Turbulence modeling has been an active field of research for more than forty years. Although numerous turbulence models were proposed, there is neither a standard model nor, in some sense, a best model. There are models, whose derivation is based on physical insight in turbulent flows and there are models, which were derived purely with mathematical arguments. Considering all the different motivations, assumptions, and approximations behind the derivation of turbulence models, it is therefore not surprising that different numerical results can be obtained using different turbulence models.

Commercial codes, e.g., as used for the simulations presented in Saha et al. (2011) and Shen et al. (2013), provide in general classical two-equation turbulence models, like the *k*-ε and *k*-ω model. The properties of these models, in particular their shortcomings, are well described in (Chapters 10 and 11 Pope, 2000). The codes used in the study presented in this paper offer the possibility to use turbulence models of different types, which will be explained briefly in the description of the individual codes.

3. Used CFD software

This section provides some information on the three software packages that were used in our study as well as on specific choices in the setup of the numerical simulations. The open source solver OpenFOAM is widely used by scientists and engineers for flow simulations. The other open source code ParMooN is a more specialized in-house research code. The third solver is the popular commercial package Ansys Fluent.

3.1. Open source package OpenFOAM

OpenFOAM (Open Source Field Operation And Manipulation) is an open source software package containing different applications to model and simulate problems in fluid dynamics, The OpenFOAM Foundation (2016). It is written in C++ and designed in an object-oriented fashion that allows the choice amongst many solvers for both the compressible or incompressible Navier-Stokes equations, including also RANS or Large Eddy Simulation (LES) turbulence models. Since OpenFOAM is a popular open source code and all information are readily available at The OpenFOAM Foundation (2016), we decided to provide here only a brief description of this solver that concentrates on those aspects that are important for our numerical studies.

Meshing can be done in several ways, either by integrated meshing routines or by importing meshes with external (open or closed source) meshing routines like e.g. Gmsh, GAMBIT or SALOME. For this study, the domain was decomposed and meshed with the snappyHexMesh utility, which generates 3-dimensional meshes containing mainly hexahedra and split-hexahedra cells automatically from triangulated geometries in.stl format (e.g. Gisen, 2014). The domain consisted of 4 refinement boxes (I, II, III and IV) as depicted in Fig. 6. The refinement

Table 4
Grid parameters for the coarse, medium and fine grid used in OpenFOAM. 'Size' refers to the edge length in the respective refinement boxes. 'Distance wall' is the distance of the first grid cell's midpoint to the wall in the roof region. y^+ values were chosen as the maximum values from the time-averaged solution at the roof walls. The number of degrees of freedom corresponds to the number of mesh cells.

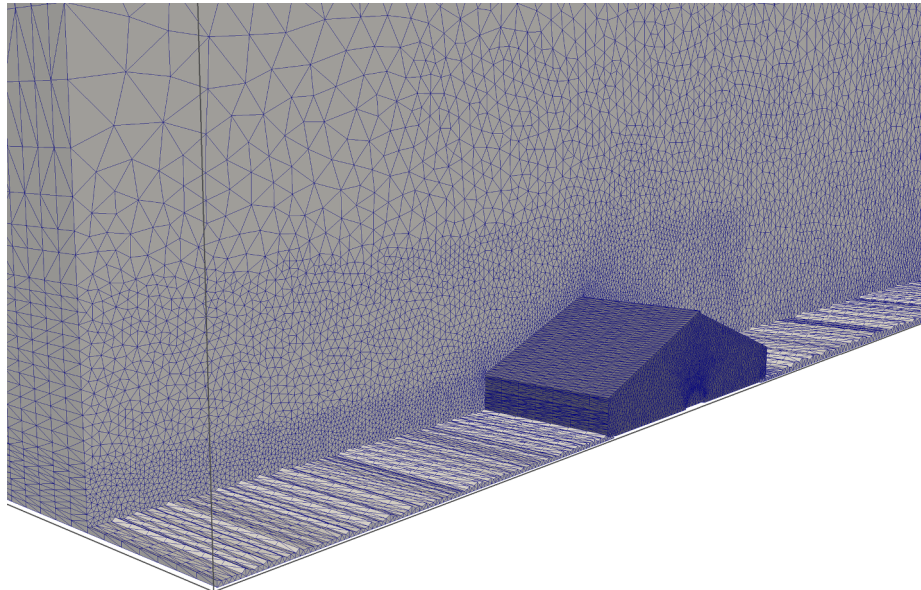| Mesh	N^o cells	Size I [mm]	Size II [mm]	Size III [mm]	Size IV [mm]	Distance wall [mm]	y^+
Coarse	1,434,580	20	10	5	2.5	1	6–14
Medium	4,608,675	10	5	2.5	1.25	0.4	4–8
Fine	14,188,950	5	2.5	1.25	0.625	0.4	4–8

6

Fig. 7. Cut view of Grid 4 used in ParMooN.

was factor 1 for each box, meaning that the edge length of a cell in box IV (inside and nearby the barn) was 8 times smaller than the original edge length in box I. Table 4 provides information on the used grids. (See Fig. 7).

For the simulations presented in this paper, incompressible LES was setup using the pimpleFoam solver, which merges the well-known PISO (Pressure-Implicit with Splitting of Operators, Issa, 1986) algorithm with the SIMPLE (Semi-implicit Method for Pressure Linked Equations) algorithm, Patankar and Spalding (1983), resulting in a fast convergence for transient simulations, described, e.g., by Holzmann (2016). An adaptive time stepping was chosen with the constraint of a Courant number not higher than 3, resulting in time steps in average of $2 \cdot 10^{-4}$ s.

The subgrid scale turbulence was modeled with a one equation eddy viscosity model (simulationType:LES, LESModel:kEqn), where the not resolved scales are solved similarly to common RANS approaches with an additional equation for the turbulent kinetic energy, described in detail by Yoshizawa (1986). The spatial discretization was done using second order linearUpwind schemes, the time variable was discretized with the second order backward scheme, both described in The OpenFOAM Foundation (2016).

The experimentally derived time-averaged velocity profile, shown in Fig. 3, was mapped as boundary condition onto the inlet face for the velocity, while the pressure was defined with a Dirichlet zero-Gradient boundary condition. At the outlet, the boundary condition for velocity was set to zeroGradient and the pressure to fixedValue.

All simulations were performed at the *North-German Supercomputing Alliance* computer cluster (HLRN) on the Cray-MPI system, using Intel Xeon Haswell compute nodes with 2500 MHz CPUs. For the simulation of the medium sized mesh, the domain was decomposed with the scotch algorithm and distributed with openMPI on 120 CPUs. The computation time for reaching 7 s was around 8.6 h.

To make the computation times of the different codes comparable in some way, we introduce the unit of CPU hours [CPUh], which is the computing time calculated down to one single CPU. Consequently, to reach 7 s in flow time, the 8.6 h computing time on 120 CPU have an equivalent of 8.6 h * 120 CPU = 1032 CPUh.

3.2. Open source package ParMooN

The software ParMooN (Parallel Mathematics and object-oriented Numerics) (Ganesan et al., 2016; Wilbrandt et al., 2017) is a C++

finite element library, based on a hybrid MPI/OpenMP parallelization, developed for numerical simulations of partial differential equations from fluid dynamics. This parallel version builds upon the code MooNMD (John and Matthies, 2004), which was used for performing simulations for more than one hundred journal papers. The development of MooNMD paid a special emphasis on implementing turbulence models for incompressible flow simulations, both for academic benchmark problems and applications.

Currently, more than 250 finite elements in two or three dimensions are implemented in ParMooN, including high order polynomials, bubble functions, and discontinuous elements. The software supports both quadrilateral/hexahedral and triangular/tetrahedral meshes. Unstructured simplicial grids in 2D and 3D can be provided using the MEDIT .mesh format, which is supported by several established mesh generation packages such as Gmsh (Geuzaine and Remacle, 2009) or TetGen (Si, 2015).

Concerning the temporal discretization, ParMooN supports methods with different derivations, complexity, and accuracy. A first group of methods, so-called θ-schemes, include the explicit and the implicit Euler methods as well as the Crank-Nicolson scheme. Furthermore, the fractional-step θ-scheme and the backward differentiation formula of second order (BDF2) can be applied. Moreover, higher order variational type time stepping schemes that include the continuous Galerkin-Petrov (k) (cGP(k)), for $k \geqslant 2$, and the discontinuous Galerkin(k) (dG(k)), for $k \geqslant 1$, which are accurate of order $k + 1$, are available and have been successfully applied to several classes of problems.

Linear solvers implemented in ParMooN include iterative approaches (Krylov subspace methods) and several preconditioners, including geometric multigrid methods. Moreover, an extended choice of direct and iterative methods is available via the PETSc library Balay et al. (2016). This library offers, among others, the Boomer AMG method and the parallelized sparse direct solver MUMPS (Amestoy et al., 2006).

ParMooN supports a number of turbulence models, in particular some LES models and variational multiscale (VMS) methods, e.g., see Ahmed et al. (2017) and John (2016).

Altogether, ParMooN is a code whose development is driven by the state-of-the-art research on problems in numerical analysis and scientific computing. It offers many discretizations in time and space as well as many solvers and it is designed such that extensions in many directions are possible. The drawback of this flexibility is that the implementations might not be tailored to be very efficient for specific

7

Table 5
Information on the grids and the degrees of freedom (dof) on these grids used with ParMooN. All grids were especially refined within and around the barn (see also Fig. 7).

	Cells	dof velocity	dof pressure	Description
Grid 1	697 500	2 933 685	128 352	Medium refinement
Grid 2	895 770	3 757 479	163 968	More refinement in front and around the barn
Grid 3	995 985	4 175 142	182 080	Similar to Grid 1, but overall somewhat more refined
Grid 4	1 014 030	4 251 681	185 456	Similar to Grid 2, but even more refined in front and around the barn

problems or discretizations. For instance, all integrals are evaluated via a transform to a reference mesh cell, which is advantageous for the flexibility of using general finite elements, but which introduces some computational overhead. This approach is not necessary if, e.g., only linear finite elements are implemented, since integrals can be evaluated efficiently on the physical mesh cells in this case.

In the following, the setup of the simulations with ParMooN is described. The domain was decomposed with unstructured tetrahedral grids that were generated with Gmsh. The three-dimensional grid was obtained from an unstructured triangular grid in the (x, y)-plane, extruding it via several layers in the z-direction.

Several grids with different resolution were used, see Table 5 for information on the number of mesh cells. In all cases, a rather coarse grid was used in the bulk of the domain. In the neighborhood of the barn, the grids became gradually finer and the highest refinement was within and closely around the barn.

For the spatial discretization, the popular inf-sup stable pair of finite elements P_2/P_1, a so-called Taylor–Hood pair, was utilized. That means that the discrete velocity is a continuous function, piecewise quadratic on each mesh cell, and the discrete pressure is a continuous function, piecewise linear on each mesh cell.

As time stepping scheme, the Crank-Nicolson scheme was utilized. It turned out that the length of the time step $\Delta t = 2.5 \cdot 10^{-4}$s was an appropriate choice in terms of computational time and sensitivity of the results. Hence, the simulation of the whole time interval of 7 s required 28000 time steps. A fully implicit approach was used. The stopping criterion for the solution of the nonlinear problem in each time instant was that the Euclidean norm of the residual vector was below 10^{-5}. This criterion was usually satisfied after one iteration. The arising linear problems were solved with a flexible GMRES (FGMRES) method (Saad, 1993) and the so-called least squares commutator (LSC) preconditioner (Elman et al., 2014) was applied. This preconditioner has been proven to be very efficient for time-dependent incompressible flow problems in the recent study (Ahmed et al., 2018). Its application was similar as described in Ahmed et al. (2018), i.e., the arising pressure Poisson problems were solved directly using MUMPS and the velocity subproblems were solved inexactly with an iterative method (GMRES with SSOR preconditioner, relaxation parameter $\omega = 1$).

A crucial algorithmic component for the simulations of flows through the barn is the turbulence model. For the simulations with ParMooN, a popular LES model, the Smagorinsky model (Smagorinsky, 1963), was used. The motivation for choosing this model consists in demonstrating that with an easy-to-implement extension of an existing solver for laminar flow problems, it is possible to perform simulations also for quite challenging applications. In fact, for the Smagorinsky LES model, the only extension consists in replacing the viscous term of the Navier-Stokes equations (1) by $\nabla \cdot ((\nu + \nu_T) \mathbb{D}(\boldsymbol{u}))$ with the turbulent viscosity ν_T given by

$$\nu_T = C_{\text{Sma}} \delta^2 \| \mathbb{D}(\boldsymbol{u}) \|_F,$$

where C_{Sma} is the user-chosen Smagorinsky constant, δ is the so-called filter width, and $\| \mathbb{A} \|_F$ is the Frobenius norm of a tensor $\mathbb{A} = (a_{ij})_{i=1}^3$ defined by $\| \mathbb{A} \|_F = (\sum_{i,j=1}^3 a_{ij}^2)^{1/2}$. The filter width δ is a measure of the locally smallest resolved scales of the flow. Thus, it is linked to the local mesh width. One can use different measures for the local mesh width. In

our experience, e.g., (John, 2016, Example 8.128), the length of the shortest edge of a mesh cell K is an appropriate unit for the Smagorinsky model and δ should be set on K by two times the length of the shortest edge of K. In fact, we observed that the results obtained with this filter width were much more accurate than using two times the diameter of K. For brevity, studies with respect to the choice of the filter width will not be presented in this paper. Typical values for the Smagorinsky constant C_{Sma} in academic benchmark problems are of order 0.01. Smagorinsky constants of this order were also used in the simulations presented in this paper. Since the considered flow is more complex than in usual academic test problems, we could observe that smaller constants than 0.01, depending on the grid even 0.01, resulted in a blow-up of the simulations. In the considered application, the flow field in front of the barn is much less complex than in and after the barn, since there are no big vortices in front of the barn. To account for this difference and to reduce the viscous effect of the Smagorinsky model in front of the barn, the used Smagorinsky constant was scaled with 10^{-2} for $x \leqslant -0.05$ m.

The inlet boundary condition was constructed on the basis of the experimental data, see Table 3. In particular, inlet velocity values were interpolated between the measured points, except for the points between $y = 0$ m and $y = 0.01$ m, where a constant value, which was equal to the measured velocity at height $y = 0.01$ m, was assigned to all degrees of freedom. As usual in simulations of turbulent flows, boundary layers cannot be resolved, in particular the boundary layer at the bottom. A preliminary numerical study, whose results are omitted for brevity, showed that one gets a quite smeared boundary layer of the computed solution already in front of the barn, at sample line v2, if a linear interpolation is used in this interval. With the described approach, a notable improvement could be obtained. At the top and lateral boundaries, the free-slip condition was imposed. At the outlet boundary ($x = 2.5$ m), a stress-free condition (the so-called do-nothing condition) was applied, i.e., by imposing $(2\nu\mathbb{D}(\boldsymbol{u}) - p\mathbb{I}) \cdot \boldsymbol{n} = 0$, where $\mathbb{I}$ is the unit tensor and $\boldsymbol{n}$ the outward pointing normal vector at the outlet. This condition states that the flow should leave the computational domain in the form it is arriving there. The do-nothing condition is a standard approach at outlets, in particular, in situations where no other information on the downstream domain is available. Concerning the roof boundaries and the bottom boundary, the no-slip condition $\boldsymbol{u} = \boldsymbol{0}$ m/s was utilized.

The inlet condition was extrapolated horizontally in the domain and the resulting function was the initial condition for all simulations with ParMooN. At the time 1 s, a fully developed flow field was reached and the collection of the data was performed in the time range $[1, 7]$ (s). The comparison with different time intervals, e.g., $[1, 6]$ s or $[2, 7]$ s, showed that the obtained results can be considered to be statistically converged.

All simulations with ParMooN were performed on compute servers HP BL460c Gen9 2xXeon, Fourteen-Core 2600 MHz, using 50 processors. The simulation of one time step, including the calculation of the quantities of interest, took around 10 s, such that the computation for the whole time interval took between 80h and 100h, which corresponds to an average duration of 4500CPUh. Although this computing time is significantly longer than for OpenFOAM, it is not straightforward to draw conclusions based on the CPU hours. First of all, the simulations were performed on different hardware architectures (high
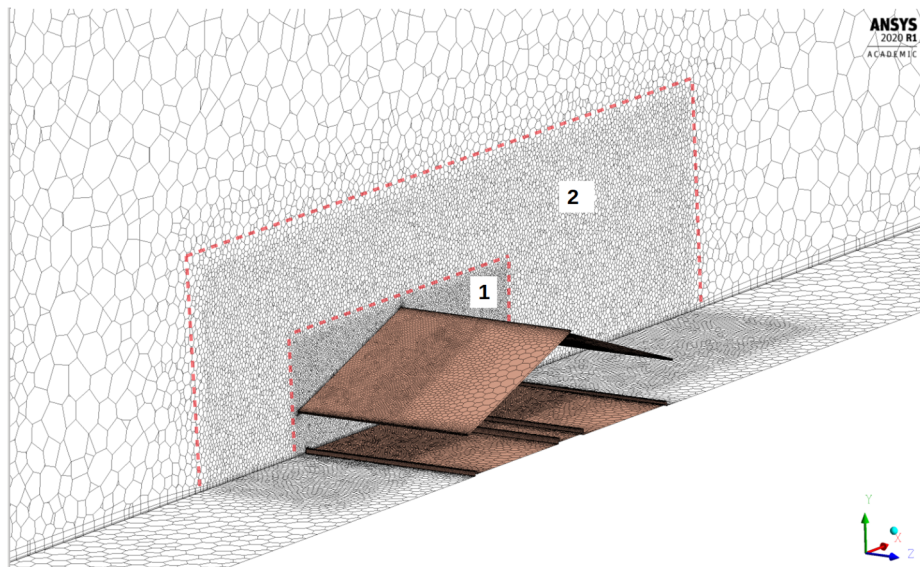
Fig. 8. Cut view of the grid used for the Ansys Fluent simulations. Red marked Sections 1 and 2 show the refinement regions around the barn.
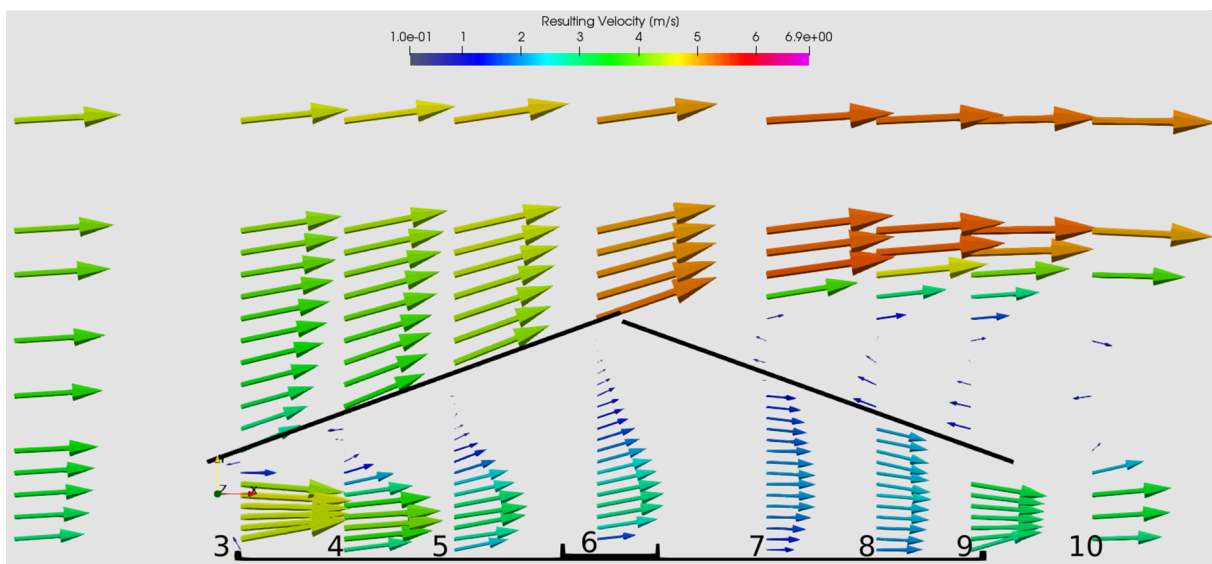

Fig. 9. Experimental results for the time-averaged velocity field. The 2D vectors represent the resulting velocity from the measured vectors in x and y direction. Their origin is at the respective sampling location on the vertical sampling lines, labeled with numbers 3–10.

performance compute cluster with distributed memory vs. workstation with shared memory). Second, since the essential goal of the numerical studies was to compute accurate results, the simulations were not optimized with respect to efficiency, e.g., by using weaker stopping criteria for iterative solvers. Finally, also the feature that ParMooN is a flexible research code and not tailored for the considered class of problems, as explained above, of course contributes to the computing times. For all these reasons, in particular the first one, the CPU hours cannot be considered as an accurate measurement of the codes' efficiency. They are rather used here for providing a rough comparison.

3.3. Ansys Fluent

To have a comparison between open source and commercial software, simulations were also carried out with the well-known Ansys Fluent solver. For the mesh, the dimensions from the OpenFOAM middle mesh were taken for the cell size and near-wall meshing. Due to license limitations, a mesh study was not conducted.

The processes of creating the geometry, meshing, solver setup, calculation, and post-processing were done within the simulation environment Ansys Workbench. The Ansys Meshing software was used to generate an initial unstructured tetrahedral mesh with an inflation layer on the ground and on the model boundaries. The distance of the first inflation layer was set to 0.4 mm, with a number of 5 layer and the *smooth transition* option. Two boxes around the barn were created, where the initial cell size of the domain of 20 mm was gradually refined. In the outer box, the cell size was set to 2.5 mm, in the inner box, the cell size was set to 1.25 mm, see Fig. 8. After the initial meshing, the Ansys Fluent meshing algorithm was used to convert the mesh into a polyhedral mesh, consisting of a total number of 1.950.000 cells.

The experimental values for the velocity in x-direction (Fig. 3) were taken as boundary condition for the velocity at the inlet. At the bottom, the top and the walls of the domain, no-slip conditions were set. On the side walls, symmetry conditions were applied.

LES was performed, with the *Wall-Adapting local Eddy Viscosity* (WALE) model as a subgrid scale turbulence model. Default settings
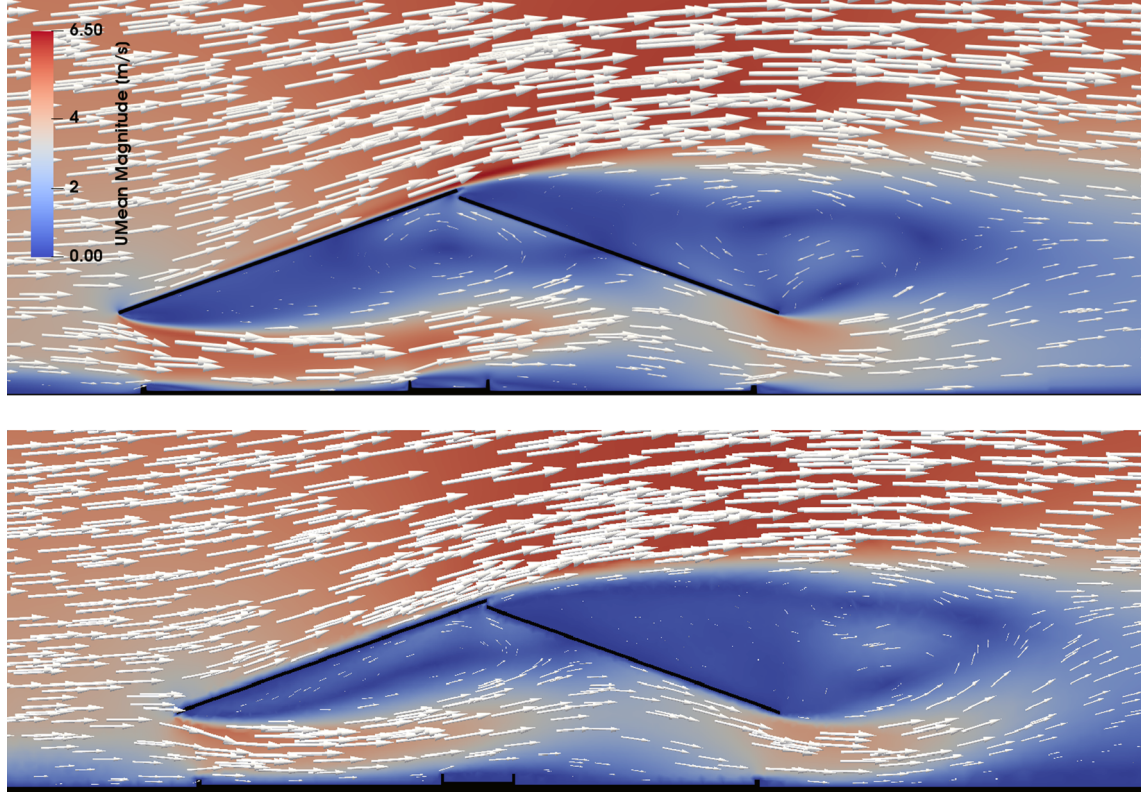
9

Fig. 10. Time-averaged velocity fields for OpenFOAM (top) and ParMooN (bottom). Results were obtained with the finest considered discretization (fine grid for OpenFOAM and Grid 4 for ParMooN).
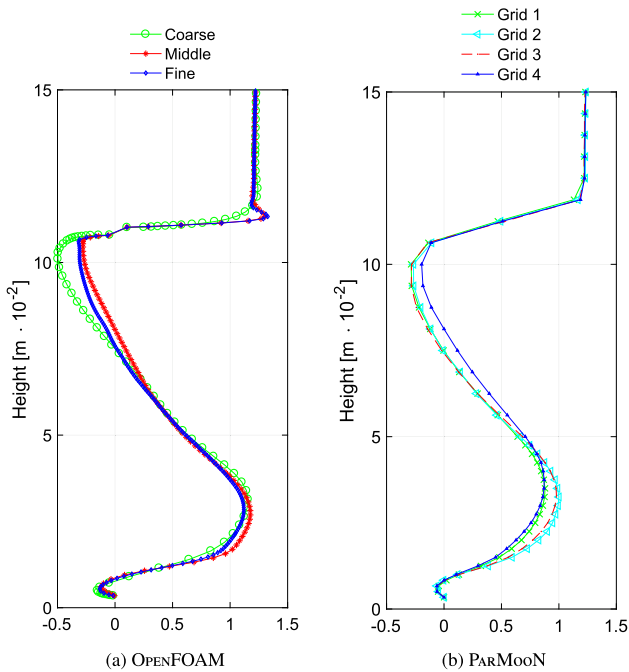

Fig. 11. Grid independence study. Shown are the normalized velocities in x-direction at sample line v6, see Fig. 4. Left: OpenFOAM, right: ParMooN.

were utilized for the near-wall treatment, which is a law-of-the-wall approach dependent on the respective y^+-value. For further descriptions, see the Ansys Fluent theory guide.

As solver scheme, the SIMPLE algorithm was chosen. For the spatial discretization, the *Least Squares Cell Based* scheme for Gradients, the

Second Order scheme for pressure, and the *Bounded Central Differencing* scheme for momentum were used. As temporal discretization, the *Bounded Second Order Implicit* scheme was applied. The above described settings were chosen following the recommendations from the Ansys Fluent interactive guidance software. A time step of $\Delta t = 1.5 \cdot 10^{-4}$ s was taken and the number of iterations per time step was set to be 8. The simulations were carried out at the HLRN computer cluster, described in Section 3.1, using 80 processors, which resulted in an average computation time of around 2.47 s per time step and an overall simulation time of 32h. This corresponds to 2560CPUh, which is approximately twice the duration of OpenFOAM (1032CPUh) and half the duration of ParMooN (~4500CPUh).

4. Results and discussion

This section presents the results of the numerical simulations and compares them with the data obtained in the experimental campaign. The experimental data can be accessed as open source data set (Janke, 2020).

4.1. Experimental results

The measured velocities in the ABLWT experiments are qualitatively shown in Fig. 9. Each sampling point is the origin of the time-averaged 2D velocity vector measured by the LDA, where the length and color of the arrows represent the magnitude of the vector. The following flow pattern attributes can be observed:

(1) when the flow enters the barn at the inlet, it is accelerated and the vectors are directed towards the center line of the opening.
(2) In the first half of the barn under the roof (at sampling lines 3 until 5), a small re-circulation zone in anti-clockwise direction can be seen.

Table 6

Comparison (experimental vs. numerical simulations) of the volume flow through the barn. The flow has been calculated interpolating first the numerical results on the measurement coordinates and then approximating the surface integral with a first order quadrature rule.

	Experimental [m³s⁻¹]	OpenFOAM [m³s⁻¹]	ParMooN[m³s⁻¹]	Ansys Fluent [m³s⁻¹]
Model inlet (v3)	$13.60\cdot10^{-2}$	$13.44\cdot10^{-2}$ (-1.2%)	$13.77\cdot10^{-2}$ ($+1.2\%$)	$14.55\cdot10^{-2}$ ($+7.0\%$)
Model outlet (v9)	$13.40\cdot10^{-2}$	$13.84\cdot10^{-2}$ ($+3.3\%$)	$13.86\cdot10^{-2}$ ($+3.4\%$)	$14.62\cdot10^{-2}$ ($+9.1\%$)
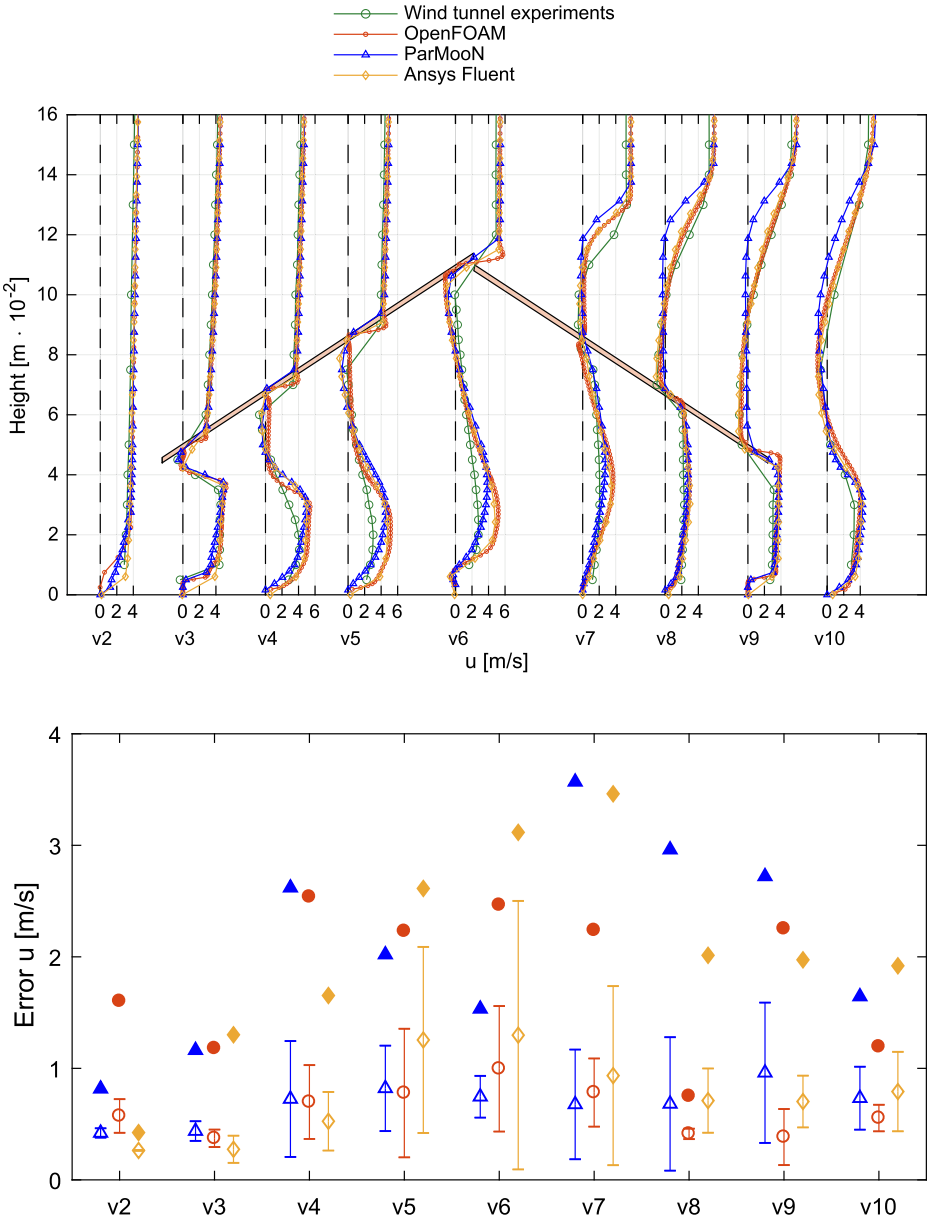
Fig. 12. Comparison between experimental data and numerical results for the horizontal velocity (top) with corresponding error statistics (bottom): bold symbol – maximal error, open symbol – average error, interval – standard deviation. Note the effect of the slightly different form of the roof in the experiment and the simulations explained in Remark 1.

(3) After having passed the inlet towards the middle of the barn (sampling lines 4, 5 and 6), the vertical component of the flow is positive, resulting in a drift towards the roof.

(4) From the middle of the barn towards the outlet (sampling lines 7 and 8), the vertical component is negative, resulting in a drift towards the floor.

(5) Outside the barn over the downwind side half of the roof, a large re-circulation zone in clockwise direction has formed.

Yi et al., 2018 conducted wind tunnel experiments with a setup similar to this study, where the flow inside and around a NVB under cross-wind direction and different opening geometries was studied. For an opening configuration comparable to this study, attributes (1), (3), (4), and (5) could also be observed in their study. However, the re-circulation zone described as attribute (2) could not be observed. This is probably due to the different scale of the model, which was 1:40 in the study of Yi et al. (2018) and resulted in a larger opening.

11
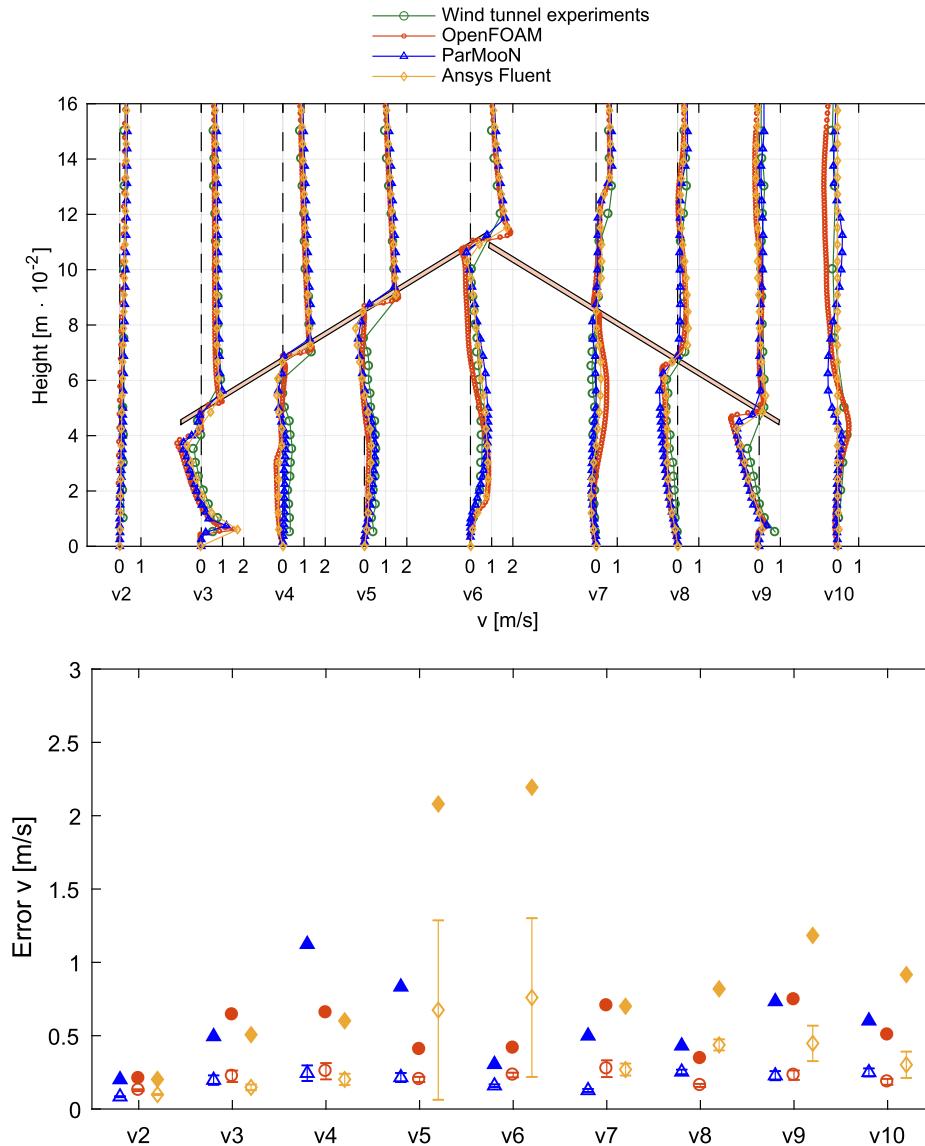
Fig. 13. Comparison between experimental data and numerical results for the vertical velocity (top) with corresponding error statistics (bottom): bold symbol – maximal error, open symbol – average error, interval – standard deviation. Note the effect of the slightly different form of the roof in the experiment and the simulations explained in Remark 1.

Several on-farm measurement campaigns focusing on the inside air flow pattern were conducted in the NVB that served as model for the 1:100 scale model in this study. For wind situations with an orthogonal inflow, attributes (1), (3), and (4) were observed by (Fiedler et al., 2013; Fiedler et al., 2014) at the on-farm measurements. Hempel et al. (2015) conducted additional measurements under the roof and observed also the anti-clockwise re-circulation zone as described in attribute (2).

4.2. Simulation results: air flow pattern

As a first qualitative validation of the open source solvers, Fig. 10 shows the simulated time-averaged 2D air flow patterns inside and around the barn on the symmetry plane of the computational domain. The upper picture shows results for OpenFOAM and the lower picture shows results for ParMooN. Both pictures, which are qualitatively very similar, use the same color scale for the resulting velocity. The white arrows represent the respective velocity vectors with their length scaled by the resulting velocity.

The previously described air flow pattern attributes (1) to (5) from

the wind tunnel experiments are reproduced by both codes. In particular, the re-circulation zone under the roof (attribute (2)) and the large re-circulation zone over the downwind roof side (attribute (5)) are clearly visible. Regarding attribute (5), both codes produce two vortices forming the re-circulation zone, one larger in anti-clockwise direction, and under that, probably originating from the right roof edge, a smaller vortex in clockwise direction. The formation of these two vortices is more pronounced in the OpenFOAM simulations. Since the experimental measurements were not resolved sufficiently fine in this region to detect this feature, this is an example where numerical simulations provide more information of the flow field than experimental data.

4.3. Simulation results: vertical sampling lines

The simulation results were compared to the experimental results at the sampling points on the vertical sampling lines sketched in Fig. 4. In particular, we compared the time-averaged horizontal velocity ($\bar{u}$), the time-averaged vertical velocity ($\bar{v}$) and the corresponding root-mean-square (rms) of their turbulent fluctuations u_{rms} and v_{rms}, defined as:

12
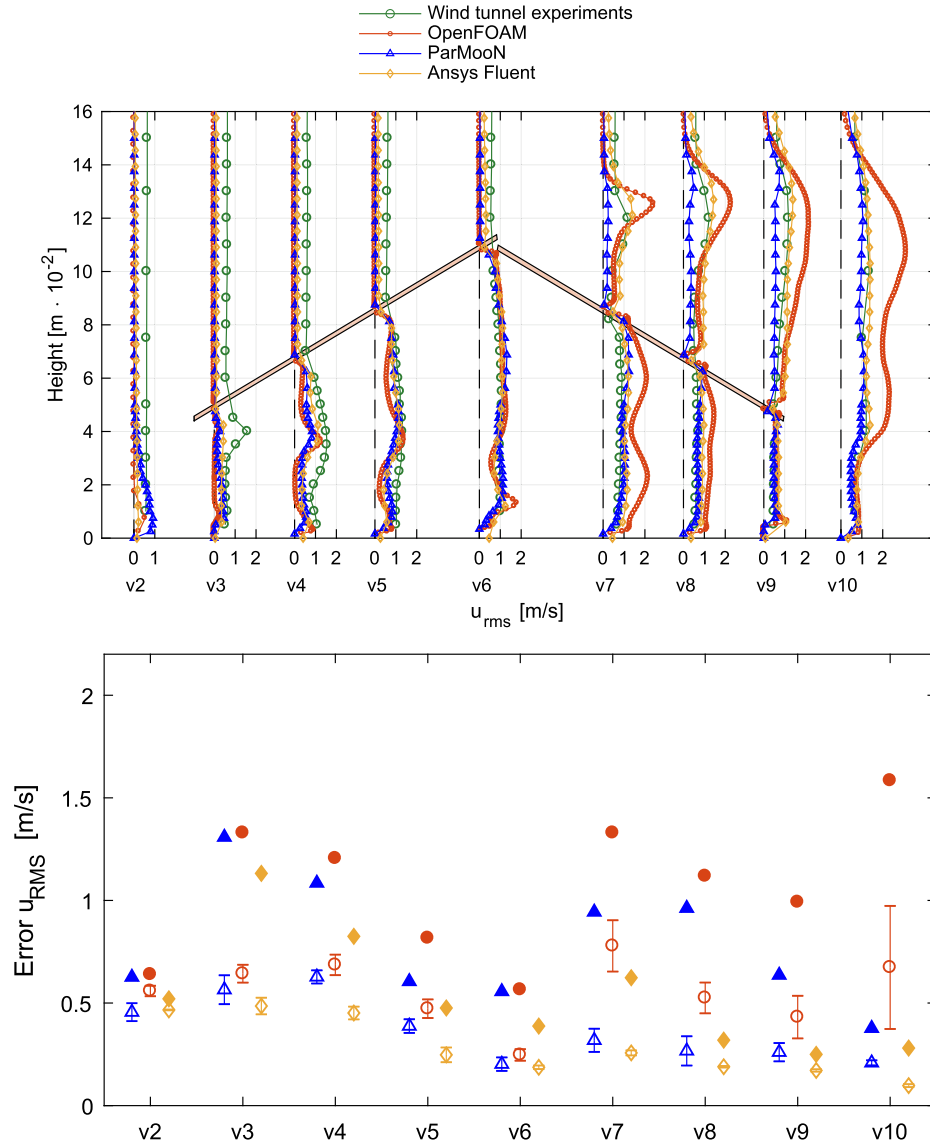
Fig. 14. Comparison between experimental data and numerical results for the root-mean-square of the horizontal velocity (top) with corresponding error statistics (bottom): bold symbol – maximal error, open symbol – average error, interval – standard deviation. Note the effect of the slightly different form of the roof in the experiment and the simulations explained in Remark 1.

$$u_{rms} = \sqrt{\frac{1}{N}\sum_{i=1}^{N} u'u'} \quad \text{and} \quad v_{rms} = \sqrt{\frac{1}{N}\sum_{i=1}^{N} v'v'},$$

with N being the number of time instants for which the velocity was monitored in the simulations. Values superscribed with an apostrophe are the fluctuating parts of the velocities, defined as $u' = u - \bar{u}$ and $v' = v - \bar{v}$.

First of all, the dependency of the numerical results on the grids will be briefly discussed for the open source solvers. Considering sampling line v6, which is in the center of the barn (Fig. 4), one can see that for OpenFOAM, the results on the medium refined and the fine grid are almost identical, see Fig. 11. Also in the case of ParMooN, the results obtained on all grids are quite similar.

In the following, the numerical results at the sample lines are evaluated, including the results obtained with Ansys Fluent. Deviations Δ between the simulated (res_{sim}) and the experimental results (res_{exp}) will be presented as the modulus of the relative differences in percents, with the experimental results as reference, i.e., $\Delta = |(res_{exp} - res_{sim})/res_{exp}| \cdot 100$.

Comparing the volume flow through the barn (Table 6), at the barn's inlet (v3) the differences between simulated and experimental results are less than 2% for both OpenFOAM and ParMooN, and about 7% for Ansys Fluent. Considering the volume flow through the barn with the velocity profile at the barn's outlet (v9), the difference between experimental data and simulations are of the order of 3% for both open source solvers and of the order of 9% for Ansys Fluent.

The horizontal component of the velocity (u) is the most important one, since it represents the main flow direction. Fig. 12 presents the comparison of the experimental data and the numerical results as well as the corresponding error statistics. At sample line v2, the results computed with all codes show a good agreement with the experimental data. Only at the first measurement point at the bottom, OpenFOAM and ParMooN underestimated the horizontal velocity somewhat. This is certainly due to the boundary layer at the wall, where the friction is overestimated compared with the real situation in the turbulent flow. But altogether, one can state that the flow profile given at the inlet, compare Fig. 3, was transported accurately through the domain by all codes. At the inlet of the barn, sample line v3, a very good agreement between the results obtained with OpenFOAM and ParMooN and the

13
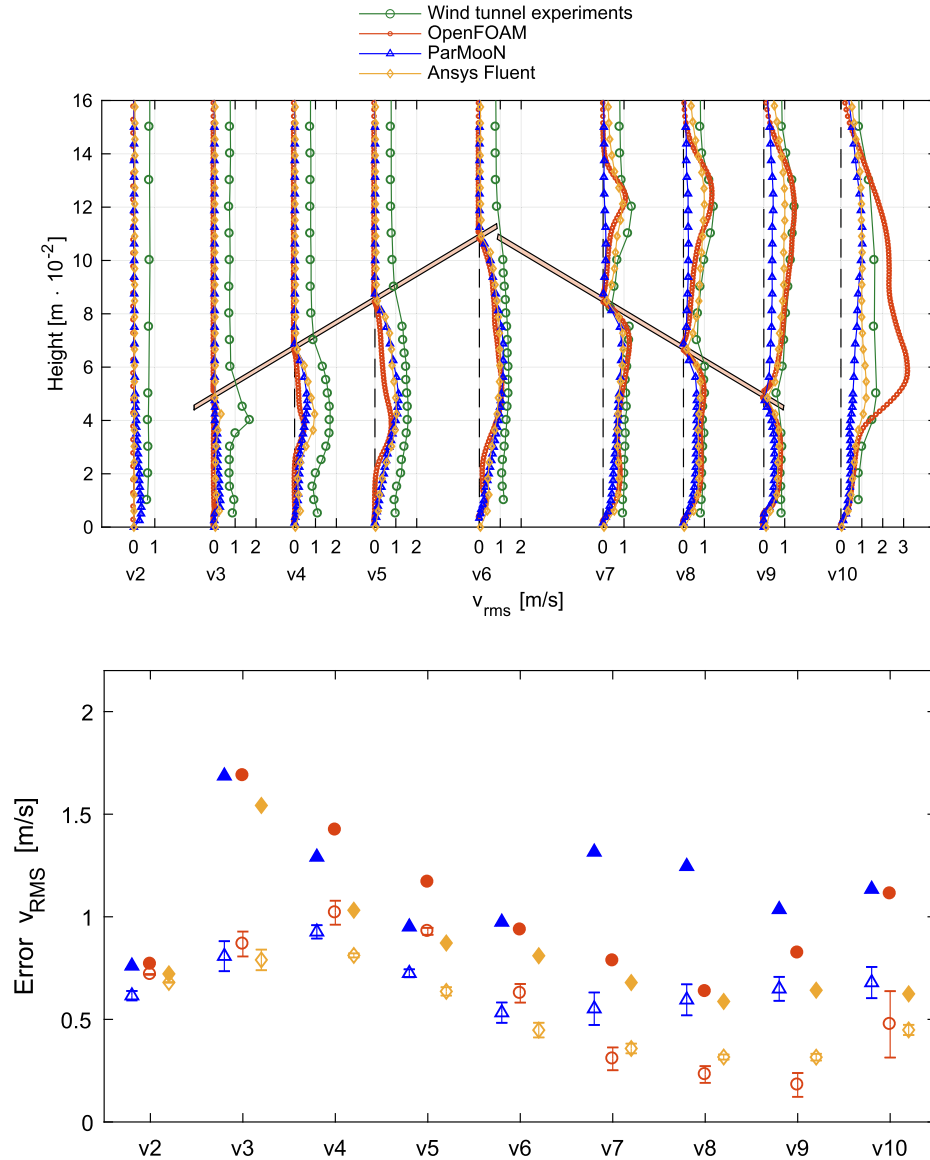
Fig. 15. Comparison between experimental data and numerical results for the root-mean-square of the vertical velocity (top) with corresponding error statistics (bottom): bold symbol – maximal error, open symbol – average error, interval – standard deviation. Note the effect of the slightly different form of the roof in the experiment and the simulations explained in Remark 1.

experimental data is visible. The curve from Ansys Fluent shows some deviations from the experimental data close to the bottom. Inside the barn, sample lines v4–v9, all codes computed qualitatively correct results. There are some deviations from the experimental data and the errors are somewhat larger than at the sample lines v2 and v3. Often, the curves obtained with OpenFOAM and Ansys Fluent are quite close. Based on the mean errors, one can conclude that all codes computed the horizontal velocity with similar accuracy.

The results for the vertical velocity component are presented in Fig. 13. The magnitude of this component is much smaller than for the horizontal component. A generally good agreement between experimental and the numerical results with all used codes was obtained, with slight differences in details and small average errors.

Results for the root-mean-square of the horizontal velocity component are depicted in Fig. 14. One can observe that there are notable differences in some parts between the experimental data and the numerical results. However, it is important to observe that some modeling aspects already introduced differences between the computational and the experimental setup. For example, in the experiments roughness elements were used to induce turbulence of the flow already in front of

the barn (Section 2.2), whereas in the numerical model, turbulent disturbances of the flow in front of the barn are not introduced. We think that this difference is the reason why the experimental root-mean-square velocities are larger in the first part of the barn, i.e., in sample lines v2-v5. For the flow field in the second part of the barn, sample lines v6-v9, not longer the flow in front of the barn but the flow field in its first part possesses the dominating impact. In this region, the numerical results obtained with ParMooN and Ansys Fluent are quite close to the experimental data and one can see that the average errors at sample lines v6-v9 are notably smaller than at sample lines v2-v5 for these CFD solvers. It can be observed generally that in regions where the results computed with the different codes are different, the curves obtained with Ansys Fluent are closer to those from ParMooN than to those predicted with OpenFOAM.

Fig. 15 presents the results for the root-mean-square of the vertical velocity component. Concerning the first half of the barn, the same comments apply as for the root-mean-square of the horizontal velocity. Again, the average errors in the second part of the barn are smaller than in the first part, most notably for OpenFOAM and Ansys Fluent. The results of both codes show in particular a comparatively good

14

agreement with the experimental data at the sample lines v7-v9 above the roof of the barn.

5. Conclusions and outlook

This paper assessed the potential of two open source solvers (OpenFOAM and ParMooN) for simulating the turbulent air flow inside and around a naturally ventilated barn. In particular, results of numerical simulations were compared with experimental data measured in a wind tunnel. The main goal consisted in assessing the solvers in terms of their capability of simulating the transient flow with sufficient accuracy. Additionally, simulations were performed with the widely established commercial code Ansys Fluent and the results were compared with the results from the two open source solvers.

In our opinion, there is a clear result of our studies: both OpenFOAM and ParMooN represent competitive choices for the numerical simulation of the considered application. There was a good agreement of the time-averaged velocities at the sample lines. All three codes computed the velocity with similar accuracy. The differences of the root-mean-square velocities at the first sample lines are due to a difference between the experimental setup and the numerical model. At the other sample lines, there is often a good agreement within the barn, in particular for ParMooN with respect to the horizontal root-mean-square velocity and for OpenFOAM with respect to the vertical root-mean-square velocity. We expect that the agreement of the numerical results and the experimental data, especially for the turbulent characteristics, can be enhanced on the one hand by the introduction of an appropriate turbulent inflow and on the other hand by the application of more sophisticated turbulence models. These topics will be subject of future research.

It is well known that the simulation of turbulent flows, in particular with advanced approaches like LES, is computationally demanding and requires appropriate hardware, which is usually not available in many institutes and companies. The use of multiple processors is indispensable, which requires that the used solver has to support parallel computing. In this respect, external cloud computing services might become a more and more attractive feature in future. They have gained already popularity in recent years, which is connected with declining cost for simulation time.

A limiting factor for the wider spread of open source software might be the more complex handling and work-flow compared with commercial codes, e.g., because of the absence of a graphical user interface (GUI) and, correspondingly, the use of the command line. For OpenFOAM, various efforts have been made to provide GUI-based platforms, where the whole work-flow can be handled via one interface. Less known codes could benefit from providing such GUIs and gain more popularity. Besides that, to promote a wider use of open source solvers, a clear and accessible documentation or handbook of the code is indispensable as well as assembled tutorial cases, from which a non-experienced user can learn most.

CRediT authorship contribution statement

David Janke: Conceptualization, Software, Writing - original draft, Writing - review & editing. **Alfonso Caiazzo:** Conceptualization, Software, Visualization, Writing - original draft, Writing - review & editing. **Naveed Ahmed:** Software, Writing - original draft, Writing - review & editing. **Najib Alia:** Software, Writing - original draft, Writing - review & editing. **Oswald Knoth:** Software, Writing - original draft. **Baptiste Moreau:** Software, Writing - original draft. **Ulrich Wilbrandt:** Software, Writing - original draft, Writing - review & editing. **Dilya Willink:** Software, Data curation. **Thomas Amon:** Supervision, Writing - original draft, Writing - review & editing. **Volker John:** Supervision, Conceptualization, Software, Writing - original draft, Writing - review & editing.

Declaration of Competing Interest

The authors declare that they have no known competing financial interests or personal relationships that could have appeared to influence the work reported in this paper.

Appendix A. Supplementary material

Supplementary data associated with this article can be found, in the online version, at https://doi.org/10.1016/j.compag.2020.105546.

References

Ahmed, N., Bartsch, C., John, V., Wilbrandt, U., 2018. An assessment of some solvers for saddle point problems emerging from the incompressible Navier-Stokes equations. Comput. Methods Appl. Mech. Eng. 331, 492–513. https://doi.org/10.1016/j.cma.2017.12.004.

Ahmed, N., Chacón Rebollo, T., John, V., Rubino, S., 2017. A review of variational multiscale methods for the simulation of turbulent incompressible flows. Arch. Comput. Methods Eng. 24 (1), 115–164. https://doi.org/10.1007/s11831-015-9161-0.

Alnæs, M., Blechta, J., Hake, J., Johansson, A., Kehlet, B., Logg, A., Richardson, C., Ring, J., Rognes, M., Wells, G., 2015. The fenics project version 1.5. Archive of Numerical Software 3 (100). http://journals.ub.uni-heidelberg.de/index.php/ans/article/view/20553.

Amestoy, P.R., Guermouche, A., L'Excellent, J.-Y., Pralet, S., 2006. Hybrid scheduling for the parallel solution of linear systems. Parallel Comput. 32 (2), 136–156.

Balay, S., Abhyankar, S., Adams, M.F., Brown, J., Brune, P., Buschelman, K., Dalcin, L., Eijkhout, V., Gropp, W.D., Kaushik, D., Knepley, M.G., McInnes, L.C., Rupp, K., Smith, B.F., Zampini, S., Zhang, H., Zhang, H., 2016. PETSc Web page. URL http://www.mcs.anl.gov/petsc.

Bangerth, W., Davydov, D., Heister, T., Heltai, L., Kanschat, G., Kronbichler, M., Maier, M., Turcksin, B., Wells, D., 2016. The deal.II library, version 8.4. J. Numer. Math. 24.

Bjerg, B., Cascone, G., Lee, I.-B., Bartzanas, T., Norton, T., Hong, S.-W., Seo, I.-H., Banhazi, T., Liberati, P., Marucci, A., et al., 2013. Modelling of ammonia emissions from naturally ventilated livestock buildings. part 3: Cfd modelling. Biosyst. Eng. 116 (3) 259–275.

Blatt, M., Burchardt, A., Dedner, A., Engwer, C., Fahlke, J., Flemisch, B., Gersbacher, C., Gräser, C., Gruber, F., Grüninger, C., Kempf, D., Klöfkorn, R., Malkmus, T., Müthing, S., Nolte, M., Piatkowski, M., Sander, O., 2016. The distributed and unified numerics environment, version 2.4. Arch. Numer. Software 4 (100), 13–29.

Dedner, A., Klöfkorn, R., Nolte, M., Ohlberger, M., 2010. A generic interface for parallel and adaptive discretization schemes: abstraction principles and the DUNE-FEM module. Computing 90 (3–4), 165–196. https://doi.org/10.1007/s00607-010-0110-3.

Elman, H.C., Silvester, D.J., Wathen, A.J., 2014. Finite elements and fast iterative solvers: with applications in incompressible fluid dynamics. Numerical Mathematics and Scientific Computation, second ed. Oxford University Press, Oxford.

Fiedler, M., Berg, W., Ammon, C., Loebsin, C., Sanftleben, P., Samer, M., von Bobrutzki, K., Kiwan, A., Saha, C.K., 2013. Air velocity measurements using ultrasonic anemometers in the animal zone of a naturally ventilated dairy barn. Biosyst. Eng. 116 (3), 276–285.

Fiedler, M., Fischer, J., Hempel, S., Saha, C., Loebsin, C., Berg, W., Amon, B., Brunsch, R., Amon, T., 2014. Flow fields within a dairy barn-measurements, physical modelling and numerical simulation. In: Proceedings. International Conference of Agricultural Engineering AgEng, pp. 1–5.

Ganesan, S., John, V., Matthies, G., Meesala, R., Abdus, S., Wilbrandt, U., 2016. An object oriented parallel finite element scheme for computing pdes: design and implementation. In: IEEE 23rd International Conference on High Performance Computing Workshops (HiPCW). IEEE, Hyderabad, pp. 106–115.

Geuzaine, C., Remacle, J.-F., 2009. Gmsh: a 3-D finite element mesh generator with built-in pre- and post-processing facilities. Int. J. Numer. Methods Eng. 79 (11), 1309–1331. https://doi.org/10.1002/nme.2579.

Gisen, D., 2014. Generation of a 3d mesh using snappyhexmesh featuring anisotropic refinement and near-wall layers. In: ICHE 2014. Proceedings of the 11th International Conference on Hydroscience & Engineering. pp. 983–990.

Hempel, S., Wiedemann, L., Ammon, C., Fiedler, M., Saha, C., Janke, D., Loebsin, C., Fischer, J., Amon, B., Hoffmann, G., et al., 2015. Determine the through-flow characteristics of naturally ventilated dairy barns to optimise barn climate. In: Bau, Technik und Umwelt in der landwirtschaftlichen Nutztierhaltung 2015. Kuratorium für Technik und Bauwesen in der Landwirtschaft eV, Darmstadt, pp. 346–351.

Holzmann, T., 2016. Mathematics, Numerics, Derivations and OpenFOAM. Holzmann CFD. URL https://www.researchgate.net/publication/307546712?channel=doi&linkId=57cc47b508ae59825185d94f&showFulltext=true.

Hong, S.-W., Exadaktylos, V., Lee, I.-B., Amon, T., Youssef, A., Norton, T., Berckmans, D., 2017. Validation of an open source cfd code to simulate natural ventilation for agricultural buildings. Comput. Electron. Agricul. 138, 80–91.

Issa, R.I., 1986. Solution of the implicitly discretised fluid flow equations by operator-splitting. J. Comput. Phys. 62 (1), 40–65.

Jähn, M., Knoth, O., König, M., Vogelsberg, U., 2014. Asam v2. 7: a compressible atmospheric model with a cartesian cut cell approach. Geoscientific Model Development Discussions 7 4.

15

Janke, D., Yi, Q., Hempel, S., Thormann, L., Amon, B., Amon, T., 2020. Velocity measurements of a 1:100 scaled model of a naturally ventilated dairy barn in an atmospheric boundary layer wind tunnel. PUBLISSO Repository for Life Sciences. URLhttps://doi.org/10.4126/FRL01-006420859.

John, V., 2016. Finite element methods for incompressible flow problems. vol. 51 of Springer Series in Computational Mathematics. Springer, Cham.https://doi.org/10.1007/978-3-319-45750-5.

John, V., Matthies, G., 2004. MooNMD—a program package based on mapped finite element methods. Comput. Vis. Sci. 6 (2–3), 163–169.

Kateris, D., Fragos, V., Kotsopoulos, T., Martzopoulou, A., Moshou, D., 2012. Calculated external pressure coefficients on livestock buildings and comparison with eurocode 1. Wind Struct. 15 (6), 481–494.

König, M., Hempel, S., Janke, D., Amon, B., Amon, T., 2018. Variabilities in determining air exchange rates in naturally ventilated dairy buildings using the co2 production model. Biosyst. Eng. 174, 249–259.

Lee, I.-B., Bitog, J.P.P., Hong, S.-W., Seo, I.-H., Kwon, K.-S., Bartzanas, T., Kacira, M., 2013. The past, present and future of cfd for agro-environmental applications. Comput. Electron. Agricul. 93, 168–183.

Lee, I.-B., Sase, S., Sung, S.-H., 2007. Evaluation of cfd accuracy for the ventilation study of a naturally ventilated broiler house. Japan Agricult. Res. Q.: JARQ 41 (1), 53–64.

OpenFOAM, 2016. OpenFOAM Web page. URLhttp://openfoam.org/.

Patankar, S.V., Spalding, D.B., 1983. A calculation procedure for heat, mass and momentum transfer in three-dimensional parabolic flows. In: Numerical Prediction of Flow, Heat Transfer, Turbulence and Combustion. Elsevier, pp. 54–73.

Pope, S.B., 2000. Turbulent flows. Cambridge University Press, Cambridge.

Saad, Y., 1993. A flexible inner-outer preconditioned GMRES algorithm. SIAM J. Sci. Comput. 14 (2), 461–469.

Saha, C.K., Wu, W., Zhang, G., Bjerg, B., 2011. Assessing effect of wind tunnel sizes on air velocity and concentration boundary layers and on ammonia emission estimation using computational fluid dynamics (cfd). Comput. Electronics Agricul. 78 (1), 49–60 URL http://www.sciencedirect.com/science/article/pii/S0168169911001268.

Shen, X., Zhang, G., Wu, W., Bjerg, B., 2013. Model-based control of natural ventilation in dairy buildings. Comput. Electronics Agricul. 94, 47–57. URLhttp://www.sciencedirect.com/science/article/pii/S016816991300046X.

Si, H., 2015. Tetgen, a delaunay-based quality tetrahedral mesh generator. ACM Trans. Math. Softw. 41 (2) 11:1–11: 36. URL http://doi.acm.org/10.1145/2629697.

Smagorinsky, J., 1963. General circulation experiments with the primitive equations. Mon. Wea. Rev. 91, 99–164.

The OpenFOAM Foundation, 2016. Openfoam user guide version 4.0.http://foam.sourceforge.net/docs/Guides-a4/OpenFOAMUserGuide-A4.pdf.

VDI, 2000. Physical modelling of flow and dispersion processes in the atmospheric boundary layer—application of wind tunnels. VDI Verein Deutcher Ingenieure, Düsseldorf.

Villagran, E.A., Romero, E.J.B., Bojaca, C.R., 2019. Transient cfd analysis of the natural ventilation of three types of greenhouses used for agricultural production in a tropical mountain climate. Biosyst. Eng. 188, 288–304.

Wilbrandt, U., Bartsch, C., Ahmed, N., Alia, N., Anker, F., Blank, L., Caiazzo, A., Ganesan, S., Giere, S., Matthies, G., Meesala, R., Shamim, A., Venkatesan, J., John, V., 2017. ParMooN—a modernized program package based on mapped finite elements. Comput. Math. Appl. 74 (1), 74–88. https://doi.org/10.1016/j.camwa.2016.12.020.

Yi, Q., König, M., Janke, D., Hempel, S., Zhang, G., Amon, B., Amon, T., 2018. Wind tunnel investigations of sidewall opening effects on indoor airflows of a cross-ventilated dairy building. Energy Build. 175, 163–172.

Yoshizawa, A., 1986. Statistical theory for compressible turbulent shear flows, with the application to subgrid modeling. Phys. Fluids 29, 2152–2164.

5

General discussion and conclusion

In this section, the individual main results of each publication are presented and interpreted in the context of the formulated hypotheses and goals of the dissertation and in relation to the the current state of research. The limitations of the single results due to the applied methodology are discussed and the consolidation of the results are shown in the general conclusions, followed by recommendations for future research.

5.1 Summary of the results

5.1.1 Impact of the sampling strategy for indirect methods

Long-term measurements of gas concentrations on a naturally ventilated dairy barn were applied. The barn was equipped with an extensive measuring setup capable of measuring emissions under all wind conditions. This resulted in a gain of data of around 210 %, compared to a setup, where only the main wind direction would have been taken into account. The quasi-continuous measurements of gas concentrations with two Fourier-transform infrared spectrometers (FTIR) over a period of nearly a year along with the before mentioned wind-independent measurement set-up resulted in a database with more than 5600 hourly data sets for gas concentrations of CO_2, NH_3, CH_4, N_2O and accompanying parameters like temperature, wind speed or wind direction. This was the defined specific objective O.1.1, which could be achieved. The dataset for ammonia and methane was published under open access [77, 78]. The generation and publication of a dataset of this magnitude and resolution alone can be considered as a novelty, since no comparable data were available so far. It is not only useful for the investigations that were done in this thesis, but also for future investigations of e.g. the influence of the sampling duration. It could already be used to investigate methane patterns, and the comparison of classical statistical methods with machine learning methods [79, 80].

Inside gas concentrations were measured with six sampling tubes, outside gas concentrations with four. By using the CO_2 mass balance method, five different sampling strategies (combination of outside and inside lines) were investigated and their impact on the estimation of volume flow rates and ammonia emissions was assessed.

71

It could be shown, that the choice of sampling strategy had a significant impact on the estimation of both, volume flow rates and ammonia emissions.

5.1.1.1 Impact on volume flow rates

The sampling strategy, that measured outside and inside CO_2 concentrations depending on the hourly predominant wind direction (strategy 1), estimated the lowest values for volume flow rates. The strategy, that used the mean value of all inside positioned sampling locations for the inside concentration and the mean value of all outside positioned sampling locations as outside value (strategy 3), estimated the highest values for volume flow rates.

When comparing strategy 1 with strategy 3, the differences in volume flow rates were +80%, +94%, and +63% for the winter, transition and summer season, respectively.

5.1.1.2 Impact on emissions

In general, strategy 1 estimated the highest levels of ammonia emissions. The lowest levels of ammonia emissions were estimated by strategy 4, which chose the minimum outside concentration and the average of all inside concentrations every hour. The differences in the estimated emission levels between strategy 1 and 4 were +26%, +19% and +11% for the winter, transition, and summer season, respectively. With the quantification of the influence of the sampling strategy on the estimation of volume flow rates and emissions, the specific objective O.1.2 could be achieved.

This systematic over- or underestimation is most likely due to the distribution of gas concentrations inside the barn. If one assumes, that the gas concentrations get accumulated with the flow direction inside the barn, the highest inside concentrations will be measured at the presumed outlet of the barn, like in strategy 1. If, like in strategy 4, the inside concentration is calculated as the mean value of all sampling locations inside the barn, it is artificially lowered, because sampling lines near the inlet with lower concentrations are taken into account. This is in line with observations made by Van Buggenhout et al. [81], who identified the optimal sampling location at the outlet.

Based on these findings, following recommendations for a sampling strategy could be derived: under clear cross flow, strategy 1 is the preferred one. For unstable and weak wind conditions and ambiguous wind directions, strategy 4 is the preferred one. For the estimation of only ventilation rates, strategy 3 is not recommended. If building and wind combination lead to flow deflection or complex flow patterns (e.g. long barns with mainly lateral flow or large flow obstacles inside the barn), strategy 1 is not recommended. For measurement campaigns with multiple barns with different geometries and wind conditions, strategy 4 is recommended.

When deriving a whole-year emission value from the actual dataset, strictly using strategy 1 would result in a value of 13.74 kg of ammonia per livestock unit and year, while strictly using strategy 4 would result in 11.43 kg of ammonia per livestock unit per year. This is a difference of +2.31 kg or +20 %. This finding is a novelty that was not reported before in the literature.

Consequently, hypotheses H1 and H2 can be considered true for the application of indirect CO_2 mass balance methods: the sampling strategy has a significant influence on the estimation

of volume flow rates and the emission of pollutants, and different sampling strategies lead to a systematic over- or underestimation of volume flow rates and emissions of pollutants.

5.1.2 Impact of the number and position of sensors for direct methods

The naturally ventilated dairy barn, that was already studied for the indirect CO_2 mass balance method, was investigated as a 1:100 scaled model in an atmospheric boundary layer wind tunnel. Important similarity criteria like Reynolds number independency and a correct vertical distribution of the turbulence intensity and mean velocity were fulfilled according to VDI [37], so that the measurement results are scalable to the real world. The barn model was measured under perpendicular inflow, with fully opened sidewalls, with closed gable walls and a closed ridge. Inside the barn, a tracer gas was released with a constant volume flow. On the area of the downwind sided opening, the tracer gas concentrations and the normal velocity vectors were measured, using a flame ionization detector (FID) and a laser Doppler anemometer (LDA), respectively. In total, for a matrix of 65 (lateral) x 4 (vertical) sensor positions, the mean normal velocities $\vec{n}$ and the mean gas concentrations c_P were measured and used to calculate the volume flow and the emissions, according to equation 1.1 and 1.2. This dataset was used as reference to assess the accuracy for the estimation of volume flow rates and emissions, while systematically reducing the number and varying the positions of sensors. The systematic reduction was conducted by incrementally decreasing the number of lateral sampling points, in conjunction with a position variation by either taking all four vertical sensor positions into account or only one respective of the four vertical sensor positions.

5.1.2.1 Normal velocities and volume flow rates

At the measured outlet of the barn model, a variation of the normal velocity vector $\vec{v}$ could be observed, both in lateral and vertical direction. In the vertical direction, a trend was visible, with higher velocities towards the roof. This resulted in a systematic error for the estimation of the volume flow rate Q, dependent on the vertical position of the sensors. If all lateral positions were taken into account and the sensors were positioned only at one of the four measured heights, a systematic error of -5 % for the lowest, -4 %, for the second lowest, $\pm$ 0 % for the second highest, and +12.3 % for the highest sensor position was introduced.

A systematic error dependent on the vertical measurement position was also reported by De Vogeleer et al. [34], who measured deviations of estimations for Q of around 15 %, when the sensors were located only at one height. In contrast to this study, they measured the highest velocities at the center line of the opening, not towards the roof. The reason for that might be the different opening geometry and position of the openings. They investigated a mock-up test building of a pig barn, with side openings a magnitude smaller than those from a dairy barn and positioned at the upper quarter of the side wall. This might lead to a greater influence of the opening boundaries, resulting in a typical parabolic velocity profile, as it was also reported by Van Overbeke et al. [82].

The lateral variations in $\vec{v}$ were less pronounced than the vertical. For the whole width of the model, a lateral division of n=3 was sufficient, to estimate the the volume flow rate with an error less than 5 %. In the real world, this would correspond to a lateral distance of about 24 m. In the literature, higher variabilities in lateral direction are usually reported,

where an opening could even act both, as inlet and outlet [15, 83]. This is probably due to the dynamically changing wind directions, that were not modeled in the wind tunnel.

A big influence could be observed, when measurements were located too near to flow obstacles at the outlet area of the model (construction beams), leading to negative outliers in the volume flow estimation. These negative outliers are not reported in the literature for direct measurements, which indicates, that they can easily be prevented by a careful positioning with a sufficient distance to flow obstacles like frames or beams.

For the investigated barn, an optimal cost-benefit ratio of sensors for the measurement of volume flow rates with a direct method, and under the condition of stable clear cross flow, would be the use of three sensors, all positioned at a height in the vicinity of the middle line.

5.1.2.2 Gas concentrations emission estimations

At the outlet area of the barn model, high variations of gas concentrations could be measured, both in lateral and vertical direction. Generally, the highest concentrations could be observed directly downstream the both gas diffusers, which indicates the insufficient mixing of the tracer gas with the ambient air. The mean concentration at the lowest sampling position was 9 times higher than the mean concentration at the highest sampling position. High vertical gradients were also reported by Nosek et al. [45], who investigated a similar barn model in an ABLWT with the release of a tracer gas on the floor. For the case of fully opened side walls, vertical gradients of a factor of approximately 5 were observed.

Due to the high vertical and lateral gradients of gas concentrations, the results showed systematic errors in the emission estimation up to +97 %, when measurements of concentration and velocity were done on one constant height. This error could be lowered under 5 %, when the concentrations were measured as a vertical composite sample, where at each lateral position, all respective vertical points were taken as one average value.

When applying vertical composite sampling of concentrations is possible, a lateral division of 5 sensors was found to be an optimal cost-benefit ratio, resulting in a sampling distance of 16 meters between the sensors for a naturally ventilated barn of this type under the investigated flow conditions.

For a full-scale NVB, these clear cross flow conditions will be rather the exception than the rule. Further variations of this set up, that will allow some more general conclusions on the direct measurements of NVBs are discussed in section 5.1.4 and 5.2.

5.1.3 Investigation of two open source numerical model

The 1:100 scaled model, that was already studied in the ABLWT for the direct methods, was further investigated for the numerical studies. In the ABLWT, velocity and turbulence profiles were measured using Laser-Doppler anemometry. Ten vertical profiles inside and and around the model were measured with overall 224 sampling positions to capture the flow patterns inside and around the model in highest possible resolution. The experimental data were published under open access [84] for further use by other researchers. By that, specific objective O.3.1 could be achieved.

The airflow was simulated under the same boundary conditions as in the ABLWT, using transient large eddy simulations with two open sources solvers (OPENFOAM and PARMOON), and one commercial solver (ANSYS FLUENT).

The experimental measurements indicated following features of the flow pattern: (1) the flow was accelerated at the inlet and the vectors were directed towards the center line of the model. (2) In the first half of the barn under the roof, a re-circulation zone in anti-clockwise direction had formed. (3) After having passed the inlet towards the middle of the barn, the vertical component of the flow was drifting towards the roof. (4) From the middle of the barn towards the outlet, the flow was drifting towards the floor. (5) Outside the barn over the downwind side half of the roof, a large re-circulation zone in clockwise direction had formed.

All described features of the flow were captured by both of the open source solvers, which led to the first conclusion, that OPENFOAM and PARMOON were feasible to simulate the airflow pattern with good qualitative agreement.

The volume flow rates could be estimated with relative errors less than 4% for both open source solvers, which was interpreted as very good agreement. The relative error of the commercial solver was less than 9%, which led to the conclusion, that in terms of accuracy, open source solvers are as feasible as commercial solvers to predict the volume flow rates.

Based on the above described results, the conclusion was drawn, that transient open source solvers are a feasible tool to simulate the turbulent flow inside and around naturally ventilated barns. Consequently, the specific objective O.3.2 could be achieved.

Despite the advantages of transient LES, the most fundamental barrier to a widespread application is probably the higher computational effort needed. The needed computational times for the simulations with OPENFOAM, PARMOON, and ANSYS FLUENT were 1032, 4500, and 2560 CPU hours, which is the approximate time, the simulations would have needed if only 1 CPU was used. Consequently, on a desktop PC with 8 CPU, the simulation time would have been between 129 and 563 hours, or between 4 and 24 days. In this respect, external cloud computing services might become a more and more attractive feature in future. They have gained already popularity in recent years, which is connected with declining cost for simulation time.

For the accurate prediction of time-dependent phenomena in an agricultural context, e.g., like the transport of particulate matter or pathogen-laden aerosols in and around agricultural buildings, the investigated open source solvers will be an indispensable tool. Especially simulations of the dynamic transport of gas concentrations will help to further develop the direct and indirect methods of the previous studies.

5.1.4 General discussion on the used methodology and their respective limitations

CO_2 mass balance method

The CO_2 mass balance was chosen due to its good cost benefit ratio, as discussed in detail in section 1.3. The methodical induced uncertainties due to the sampling strategy have been extensively discussed in chapter 2 and also in chapter 5.1.1. However, additional remarks and potential limitations that have not been regarded will be discussed here.

One of the most crucial characteristics for the estimation of emissions is the volume flow rate Q [29]. When the metabolic CO_2 is used as a tracer gas to determine Q, several limitations, both in the achievable accuracy and the general applicability arise [29, 85]. Besides the sampling locations, one of the main uncertainties lies within the modeling of the production term for CO_2. Based on experiments in respiration chambers, the CO_2 production is calculated from the heat production of the animals [27, 28]. Due to breeding related changes in the genetics and the metabolism of modern, high performance cows, the derived parameters to model the heat production and the resulting CO_2 production probably have changed over time, which can result in uncertainties of $\pm$ 20 %, as assumed by Zhang, Pedersen, and Kai [85]. The focus of this thesis was the quantification of relative differences between applied sampling strategies, so the absolute values played a subordinate role. However, if the CO_2 mass balancing method is used e.g. for the estimation of emission factors for national inventories, the aspect of a potentially biased CO_2 production term should be taken into account. When using CO_2 as a tracer gas, errors can also occur, when CO_2 sources other than the metabolically produced CO_2 from the animals exist in the barn, e.g. if manure is stored inside the barn. In this case, a correction term can be applied to the production term, as done e.g. in [16]. In the investigated barn of this study, the manure was not stored inside the building, hence this error potential could be considered small.

The drawn conclusions and given recommendations for appropriate sampling strategies under certain wind / building conditions were derived from long term measurements, meaning that certain conditions (like clear cross or lateral flow) could easily be constructed from the dataset with a sufficient amount of data points. Under practical measurement conditions, long term measurements are usually not applied. For example, in the actual version of the VERA Test Protocol for Housing Systems, the minimum requirement for measuring naturally ventilated barns for dairy cows is six independent measurement periods of at least 24 hours, equally distributed over one year [86]. It is obvious, that in such short measurement durations, the dominating flow conditions are rather determined by chance, hence the recommendation of an appropriate sampling strategy can become difficult. Based on the existing dataset, a further investigation of the influence of duration and frequency of the measurements on the sampling-strategy-induced uncertainties could give some clarity on this aspect.

Wind tunnel measurements

The method of wind tunnel experiments in an atmospheric boundary layer wind tunnel was chosen in order to investigate the impact of sensor locations under the most constant possible boundary conditions and with the highest possible spatio-temporal sampling resolution. Under real scale conditions, this would not be possible, due to the varying wind conditions and the immense effort needed for the instrumental setup [83, 23, 22]. However, the applied method is only meaningful, if the gained results can be transferred to the real world. Also, the drawn conclusions should have as much general validity as possible.

The limitations of the carried out experiments can be divided into limitations that are inherent to the method itself and therefore not changeable, and limitations due to the experimental set up, that could be changed. To the former belongs e.g. that the results are only up-scalable for flows exceeding a certain Reynolds number, meaning a similarity in the turbulence regime [37, 38]. This becomes a problem, if the scale model gets very small,

and inside flow patterns need to be measured. Or if, for example, regions with naturally low velocities are to be measured like the manure storage under a slatted floor. Since this was not the case for the experiments in this thesis, this limitation will not further be evaluated.

A limitation that could be overcome, although fraught with difficulty, is the current limitation to isothermal modeling in the atmospheric boundary layer wind tunnel. That means, that buoyancy driven flow and dispersion processes due to temperature gradients inside the barn are not captured in the experiments of this thesis. These effects could have had influence on the results of the experiments in chapter 3, especially on the vertical distribution of gas concentrations at the outlet. In case of a strong, buoyancy driven uplift flow inside the barn (e.g. induced by the warm animals in cold winter days), a better vertical mixing of the tracer gas with the ambient air could have taken part, resulting in smaller vertical gradients of the concentration. The modeling of scalable buoyancy is, however, not trivial due to the necessary similarity of the Richardson number in the real scale and the down scale model [87]. This can require very high surface temperatures inside the scaled down model, that are not easy to implement in the experimental set up.

The investigations for the impact of the sensor locations on the direct measurements of emissions were done under a perpendicular inflow with fully opened side walls, leading to a stable cross flow. The conclusions drawn from this experiment are valid for this flow condition. However, it is expected, that deviating wind incidence angles will lead to more complex flow patterns, where an opening acts both, as inlet and outlet as reported by Van Overbeke et al. [88] or De Vogeleer et al. [34]. In this case, a higher density of sensors would be needed to achieve the same accuracy in the estimation of the volume flow rates. This limitation can easily be overcome by repeating the experiments with variations of the inflow angles and draw more general conclusions from the results.

Computational fluid dynamics

The results from numerically solved flow and dispersion problems using CFD are only meaningful, if the numerical model was properly validated against a reference data set of a similar flow problem [89]. In this thesis, this was done for a fully turbulent flow in and around a naturally ventilated barn, using wind tunnel measurements to validate the prediction of the mean velocities and the turbulent root-mean-square velocities. Consequently, the application of the numerical model by now is limited to the prediction of velocities and turbulent characteristics.

In order to use the numerical model for the prediction of buoyancy driven flow, a similar validation procedure would have to be performed. This could either be done with own experiments under laboratory conditions, or the use of existing datasets, that meet the demands of the actual flow problems, e.g. [90, 91]. The same applies to the use of the model for the prediction of the transport of particles, and the transport and dispersion of gases. For the latter, the measurement results from the wind tunnel experiments for the direct method in chapter 3 can be used.

General limitation of the used methodologies

Estimations of volume flow rates and emissions have been investigated with three different methodologies. However, if the goal is to give the most general conclusions, one limitation must be stated, that is inherit to all three studies that were conducted for this thesis, namely

the limitation on one building geometry. All three applied methodologies used as studied object the experimental barn in which the long term measurements were conducted. Although the building is representative for housing systems of dairy cows in this region, the derived conclusions need not necessarily be true for other regions with other building designs. For example, in smaller buildings, the variation of gas concentrations inside the barn might be smaller, and the velocity gradients at the openings might be higher.

5.2 Proposed future research

Based on the achieved results and regarding the before discussed limitations of the current work, following future research can be proposed:

- The generated dataset from the long term measurements should be further used to investigate the influence of the frequency of sampling, the duration of measurement periods and the number of repetition of measurements on the estimation of volume flow rates and ammonia emissions.

- The long-term measurements should be repeated in other naturally ventilated dairy barns with different geometries, and climatic regions to derive more general conclusions on the influence of the sampling strategy. The variations should include the size of the barn and the opening geometries, and also the ventilation mechanisms (ridge vs. cross ventilation).

- The wind tunnel investigations on the accuracy of the direct method should be continued under a variation of inflow angles. Further, the influence of the tracer gas sources inside the model should be tested by varying their positions and release types, e.g. wide area sources for ammonia from floor surfaces vs. concentrated point sources for methane from unevenly distributed animals.

- Measurements of volume flow rates and emissions on a naturally ventilated dairy barn should be carried out with direct and indirect methods in parallel. The knowledge acquired through wind tunnel experimentation on the accuracy of direct methods should be used to assess the indirect CO_2 mass balance method.

- The feasibility of direct methods for the measurement of emissions of more complex housing systems, like e.g. pig barns with emitting exercise areas, should be tested. This could be done with the release of a tracer gas with a known mass flow and the recovery rate achieved with the direct method.

- The transient open source solver should be further validated for the simulation of buoyancy driven flow and the transport and diffusion of tracer gas. After validation, the transport of gas concentration fields should be investigated under varying wind and temperature boundary conditions. The outcomes of these studies will help to improve both, indirect and direct methods.

5.3 Conclusions

The hypothesis H1 could be proven true: The sampling strategy, respectively the number and position of sensors for velocity and concentrations, has a significant influence on the estimation of volume flow rates and emissions. This could be shown for both, the direct and indirect method.

Hypothesis H2 could be proven true: The results from the investigations on direct and indirect methods clearly show a systematic error, which is induced by the measurement setup. For the indirect methods, the heterogeneous distribution of tracer and polluting gas concentrations inside the barn was the main reason for the systematic error. For the direct methods, large concentration gradients of the pollutant gas, accompanied by gradients in the velocity at the outlet area were the main reasons for the systematic error.

The outcomes of the systematic investigation of different sampling strategies under different influencing factors for indirect CO_2 mass balance methods will help to set up a robust measurement design with an optimised sampling strategy, adjustable to the respective conditions. The findings can be valuable for the further improvement of national or international standards like the DIN 18910 [92], or the VERA Test Protocol for Housing Systems [86]. Furthermore, already published values for volume flow rates and emissions for naturally ventilated barns derived with the CO_2 mass balance method could be re-assessed regarding their used sampling strategy.

The investigation of a basic flow situation in the wind tunnel with a direct method can be regarded as the foundation stone of further investigations of more complex flow situations. Using the gained knowledge on the accuracy of the results, as a function of the number and position of the sensors, the direct method has the potential to be used as reference method for the quantitative assessment of indirect CO_2 mass balance methods.

Further synergy effects of the applied three-column approach can be derived from the outcomes of this thesis:

- The validation of the transient open source solver was carried out with the experimental data generated in the atmospheric boundary layer wind tunnel, which proved to be an ideal tool for the generation of such validation data sets

- The results of chapter 2 and 3 indicate, that the accurate determination of the spatially distribution of gas concentrations is a basic requirement for accurate emission measurements. The transient open source solver will be of great benefit in the fulfilment of this requirement. Once validated, the transport and diffusion of gas inside the barns can be modeled under any desired boundary conditions, and the results can be transferred to improve the on-farm measurements.

- The investigation of the direct method was done in the atmospheric wind tunnel, which again proved to be the tool of choice for these experiments due to the nearly arbitrarily adjustable and constant boundary conditions. The outcomes of the wind tunnel studies can be scaled up and used for direct on-farm measurements of emissions.

With reference to the above listed conclusions, hypothesis H3 could be proven true. The application of different methodologies permits a deeper understanding of the driving mechanisms

of the complex emission system NVB, and the benefits of each method can help to overcome the limitations of the respective other methods. The three column model has proven to be a promising approach for the challenging task of measuring emissions of naturally ventilated dairy barns.

The first main objective of this thesis could be achieved: the induced errors due to the sampling methods could be systematically quantified, both for the direct and indirect method. The second main objective of this thesis could be achieved: recommendations for the measurements of volume flow rates and emissions under the studied conditions could be derived, both for direct and indirect methods. The third main objective could also be achieved: a simulation tool for the investigations of volume flow rates and emissions of arbitrary flow situations and building geometries could be applied and assessed.

Accordingly, this thesis contributed to the further development and improvement of methods to estimate the volume flow rates and gaseous emissions from naturally ventilated barns, and pointed out further gaps in knowledge, that can be filled within the proposed future research.

References

[1] P R Shukla et al. *Climate Change and Land: an IPCC special report on climate change, desertification, land degradation, sustainable land management, food security, and greenhouse gas fluxes in terrestrial ecosystems.* Tech. rep. 906 pp. Last access 20 April 2020. Intergovernmental Panel on Climate Change (IPCC), 2019. URL: `https://www.ipcc.ch/site/assets/uploads/sites/4/2020/02/SRCCL-Complete-BOOK-LRES.pdf`.

[2] Food and Agriculture Organization of the United Nations (FAO). *The state of food and agriculture - climate change, agriculture and food security.* Tech. rep. 194 pp. Last access 29 July 2020. Rome, 2016. URL: `www.fao.org/3/a-i6030e.pdf`.

[3] Pierre J Gerber et al. *Tackling climate change through livestock: a global assessment of emissions and mitigation opportunities.* Food and Agriculture Organization of the United Nations (FAO), 2013.

[4] Natalie Anderson, Ross Strader, and Cliff Davidson. "Airborne reduced nitrogen: ammonia emissions from agriculture and other sources". In: *Environment International* 29.2-3 (2003), pp. 277–286.

[5] Henning Steinfeld et al. *Livestock's long shadow: environmental issues and options.* Food & Agriculture Org., 2006.

[6] European Environment Agency EEA. *European Union emission inventory report 1990-2018 — EEA Report No 5/2020.* Vol. 7. 2020. ISBN: 978-92-9480-237-8. URL: `https://www.eea.europa.eu/publications/european-union-emission-inventory-report-1990-2018`.

[7] UNO. *Paris Agreement.* UN Treaty. Dec. 2015. URL: `https://treaties.un.org/pages/ViewDetails.aspx?src=TREATY&mtdsg_no=XXVII-7-d&chapter=27&clang=_en` (visited on 03/28/2019).

[8] Deutsche Bundesregierung. *Klimaschutzplan 2050 - Klimaschutzpolitische Grundsätze und Ziele der Bundesregierung.* Tech. rep. 92 pp. Last access 20 June 2020-. Berlin, 2016. URL: `https://www.bmu.de/fileadmin/Daten_BMU/Download_PDF/Klimaschutz/klimaschutzplan_2050_bf.pdf`.

[9] UNECE. *Gothenburg protocol to Abate Acidification, Eutrophication anf Ground-level Ozone.* Tech. rep. last access 20 June 2020. Gothenburg, 1999. URL: `https://www.unece.org/environmental-policy/conventions/envlrtapwelcome/guidance-documents/gothenburg-protocol.html`.

REFERENCES

[10] Deutsche Bundesregierung. *Nationales Luftreinehaltung der Bundesrepublik Deutschland*. Tech. rep. last access 20 June 2020. Berlin, 2017. URL: `https://www.bmu.de/fileadmin/Daten_BMU/Download_PDF/Luft/luftreinhalteprogramm_bericht_bf.pdf`.

[11] M Samer et al. "Winter measurements of air exchange rates using tracer gas technique and quantification of gaseous emissions from a naturally ventilated dairy barn". In: *Applied Engineering in Agriculture* 27.6 (2011), pp. 1015–1025.

[12] Sabrina Hempel et al. "Uncertainty in the measurement of indoor temperature and humidity in naturally ventilated dairy buildings as influenced by measurement technique and data variability". In: *Biosystems Engineering* 166 (2018), pp. 58–75.

[13] Sabrina Hempel et al. "Non-linear temperature dependency of ammonia and methane emissions from a naturally ventilated dairy barn". In: *Biosystems Engineering* 145 (2016), pp. 10–21.

[14] Merike Fiedler et al. "Air velocity measurements using ultrasonic anemometers in the animal zone of a naturally ventilated dairy barn". In: *Biosystems Engineering* 116.3 (2013), pp. 276–285.

[15] HS Joo et al. "A direct method of measuring gaseous emissions from naturally ventilated dairy barns". In: *Atmospheric environment* 86 (2014), pp. 176–186.

[16] Xiang Wang et al. "Indirect method versus direct method for measuring ventilation rates in naturally ventilated dairy houses". In: *biosystems engineering* 144 (2016), pp. 13–25.

[17] Qingyan Chen. "Ventilation performance prediction for buildings: A method overview and recent applications". In: *Building and environment* 44.4 (2009), pp. 848–858.

[18] Chayan K Saha et al. "Uncertainty in calculating air exchange rates of a naturally ventilated dairy building based on point concentrations". In: *Environmental Engineering & Management Journal (EEMJ)* 13.9 (2014).

[19] Marcel König et al. "Variabilities in determining air exchange rates in naturally ventilated dairy buildings using the CO2 production model". In: *Biosystems Engineering* 174 (2018), pp. 249–259.

[20] Luciano Mendes et al. "NDIR gas sensor for spatial monitoring of carbon dioxide concentrations in naturally ventilated livestock buildings". In: *Sensors* 15.5 (2015), pp. 11239–11257.

[21] CK Saha et al. "Seasonal and diel variations of ammonia and methane emissions from a naturally ventilated dairy building and the associated factors influencing emissions". In: *Science of the total environment* 468 (2014), pp. 53–62.

[22] Sezin Eren Ozcan, Erik Vranken, and Daniel Berckmans. "An overview of ventilation rate measuring and modelling techniques through naturally ventilated buildings". In: *Ammonia Emissions in Agriculture* (Jan. 2007), pp. 351–353.

[23] Nico WM Ogink et al. "Methods for measuring gas emissions from naturally ventilated livestock buildings: Developments over the last decade and perspectives for improvement". In: *Biosystems engineering* 116.3 (2013), pp. 297–308.

[24] Sabine Schrade. "Ammoniak-und PM10-Emissionen im Laufstall für Milchvieh mit freier Lüftung und Laufhof anhand einer Tracer-Ratio-Methode". PhD thesis. S. Schrade, 2009.

[25] Sabine Schrade et al. "Ammonia emissions and emission factors of naturally ventilated dairy housing with solid floors and an outdoor exercise area in Switzerland". In: *Atmospheric Environment* 47 (2012), pp. 183–194. ISSN: 13522310. DOI: 10.1016/j.atmosenv.2011.11.015.

[26] Joachim Mohn et al. "A dual tracer ratio method for comparative emission measurements in an experimental dairy housing". In: *Atmospheric Environment* 179 (2018), pp. 12–22.

[27] Sälvik K. Pedersen S. "Climatization of animal houses. Heat and moisture production at animal and house levels". In: *Danish Inst of Agric Sci, Horsens, Denmark* (2002), pp. 1–46.

[28] Søren Pedersen et al. "Carbon dioxide production in animal houses: A literature review". In: *Agricultural Engineering International: CIGR Journal* (2008).

[29] Salvador Calvet et al. "Measuring gas emissions from livestock buildings: a review on uncertainty analysis and error sources". In: *Biosystems Engineering* 116.3 (2013), pp. 221–231.

[30] G Zhang et al. "Emission of ammonia and other contaminant gases from naturally ventilated dairy cattle buildings". In: *Biosystems Engineering* 92.3 (2005), pp. 355–364.

[31] NM Ngwabie et al. "Multi-location measurements of greenhouse gases and emission rates of methane and ammonia from a naturally-ventilated barn for dairy cows". In: *Biosystems Engineering* 103.1 (2009), pp. 68–77.

[32] Nadege Edouard et al. "Comparison of CO2-and SF6-based tracer gas methods for the estimation of ventilation rates in a naturally ventilated dairy barn". In: *biosystems engineering* 149 (2016), pp. 11–23.

[33] Philippe Van Overbeke et al. "Development of a reference method for airflow rate measurements through rectangular vents towards application in naturally ventilated animal houses: Part 3: Application in a test facility in the open". In: *Computers and Electronics in Agriculture* 115 (2015), pp. 97–107.

[34] Gerlinde De Vogeleer et al. "Effect of sampling density on the reliability of airflow rate measurements in a naturally ventilated animal mock-up building". In: *Energy and Buildings* 152 (2017), pp. 313–322.

[35] Venkata K Vaddella et al. "Mass transfer coefficients of ammonia for liquid dairy manure". In: *Atmospheric Environment* 66 (2013), pp. 107–113.

[36] T. Hinz, B. Rönnpagel, and S. Linke. *Particulate Matter in and from Agriculture: Proceedings of the Conference Organized by the Institut Für Technologie und Biosystemtechnik, Bundesforschungsanstalt Für Landwirtschaft (FAL) Held at Braunschweig, 3rd and 4th June, 2002.* Landbauforschung Völkenrode / Sonderheft: Sonderheft. FAL, 2002. ISBN: 9783933140586. URL: https://books.google.de/books?id=XZBKAAAAYAAJ.

[37] VDI. *Environmental Meteorology - Physical Modelling Of Flow And Dispersion Processes In The Atmospheric Boundary Layer - Application Of Wind Tunnels.* Guideline. Verein Deutscher Ingenieure, Duesseldorf, Germany, 2000.

REFERENCES

[38]   Jack E Cermak et al. "Wind tunnel investigations of natural ventilation". In: *Journal of transportation engineering* 110.1 (1984), pp. 67–79.

[39]   AAR Townsend. *The structure of turbulent shear flow.* Cambridge university press, 1980.

[40]   Qianying Yi et al. "Wind tunnel investigations of sidewall opening effects on indoor airflows of a cross-ventilated dairy building". In: *Energy and Buildings* 175 (2018), pp. 163–172.

[41]   Xiong Shen et al. "Influence of sidewall openings on air change rate and airflow conditions inside and outside low-rise naturally ventilated buildings". In: *Energy and Buildings* 130 (2016), pp. 453–464.

[42]   Merlijn De Paepe et al. "Airflow measurements in and around scale-model cattle barns in a wind tunnel: Effect of wind incidence angle". In: *biosystems engineering* 115.2 (2013), pp. 211–219.

[43]   Qianying Yi et al. "Investigation of discharge coefficient for wind-driven naturally ventilated dairy barns". In: *Energy and Buildings* 165 (2018), pp. 132–140.

[44]   Qianying Yi et al. "Airflow Characteristics Downwind a Naturally Ventilated Pig Building with a Roofed Outdoor Exercise Yard and Implications on Pollutant Distribution". In: *Applied Sciences* 10.14 (2020), p. 4931.

[45]   Štěpán Nosek et al. "The impact of atmospheric boundary layer, opening configuration and presence of animals on the ventilation of a cattle barn". In: *Journal of Wind Engineering and Industrial Aerodynamics* 201 (2020), p. 104185.

[46]   Giancarlo Alfonsi. "On direct numerical simulation of turbulent flows". In: *Applied Mechanics Reviews* 64.2 (2011).

[47]   Twan van Hooff, Bert Blocken, and Yoshihide Tominaga. "On the accuracy of CFD simulations of cross-ventilation flows for a generic isolated building: comparison of RANS, LES and experiments". In: *Building and Environment* 114 (2017), pp. 148–165.

[48]   Joel H Ferziger, Milovan Perić, and Robert L Street. *Computational methods for fluid dynamics.* Vol. 3. Springer, 2002.

[49]   Bert Blocken. "LES over RANS in building simulation for outdoor and indoor applications: a foregone conclusion?" In: *Building Simulation.* Vol. 11. 5. Springer. 2018, pp. 821–870.

[50]   Marco-Felipe King et al. "Investigating the influence of neighbouring structures on natural ventilation potential of a full-scale cubical building using time-dependent CFD". In: *Journal of Wind Engineering and Industrial Aerodynamics* 169 (2017), pp. 265–279.

[51]   P Gousseau et al. "CFD simulation of near-field pollutant dispersion on a high-resolution grid: a case study by LES and RANS for a building group in downtown Montreal". In: *Atmospheric Environment* 45.2 (2011), pp. 428–438.

[52]   Yi Jiang et al. "Natural ventilation in buildings: measurement in a wind tunnel and numerical simulation with large-eddy simulation". In: *Journal of Wind Engineering and Industrial Aerodynamics* 91.3 (2003), pp. 331–353.

[53] D Lakehal and W Rodi. "Calculation of the flow past a surface-mounted cube with two-layer turbulence models". In: *Journal of Wind Engineering and Industrial Aerodynamics* 67 (1997), pp. 65–78.

[54] Jörg Franke and Alexander Baklanov. *Best practice guideline for the CFD simulation of flows in the urban environment: COST action 732 quality assurance and improvement of microscale meteorological models*. Meteorological Inst., 2007.

[55] In-Bok Lee et al. "The past, present and future of CFD for agro-environmental applications". In: *Computers and electronics in agriculture* 93 (2013), pp. 168–183.

[56] Tomás Norton et al. "Applications of computational fluid dynamics (CFD) in the modelling and design of ventilation systems in the agricultural industry: A review". In: *Bioresource technology* 98.12 (2007), pp. 2386–2414.

[57] Hao Li, Li Rong, and Guoqiang Zhang. "Study on convective heat transfer from pig models by CFD in a virtual wind tunnel". In: *Computers and Electronics in Agriculture* 123 (2016), pp. 203–210.

[58] Kifle G Gebremedhin, Binxin Wu, and K Perano. "Modeling conductive cooling for thermally stressed dairy cows". In: *Journal of thermal biology* 56 (2016), pp. 91–99.

[59] Mario R Mondaca et al. "A conjugate heat and mass transfer model to evaluate the efficiency of conductive cooling for dairy cattle". In: *Transactions of the ASABE* 56.6 (2013), pp. 1471–1482.

[60] Bjarne Bjerg et al. "Modelling of ammonia emissions from naturally ventilated livestock buildings: Part 2, air change modelling". In: *Biosystems engineering* 116.3 (2013), pp. 246–258.

[61] Li Rong et al. "Validation of CFD simulation for ammonia emissions from an aqueous solution". In: *Computers and electronics in agriculture* 75.2 (2011), pp. 261–271.

[62] Raphael Kubeba Tabase et al. "CFD simulation of airflows and ammonia emissions in a pig compartment with underfloor air distribution system: Model validation at different ventilation rates". In: *Computers and Electronics in Agriculture* 171 (2020), p. 105297.

[63] Fernando Rojano et al. "Modelling heat and mass transfer of a broiler house using computational fluid dynamics". In: *Biosystems engineering* 136 (2015), pp. 25–38.

[64] Il-hwan Seo et al. "Modelling of internal environmental conditions in a full-scale commercial pig house containing animals". In: *Biosystems engineering* 111.1 (2012), pp. 91–106.

[65] Eliseo Bustamante et al. "Exploring ventilation efficiency in poultry buildings: the validation of computational fluid dynamics (CFD) in a cross-mechanically ventilated broiler farm". In: *Energies* 6.5 (2013), pp. 2605–2623.

[66] L Mendes et al. "Air motion patterns and air exchange rates of a naturally ventilated dairy barn by means of a CFD model tested against the carbon dioxide mass balance method". In: (2014).

REFERENCES

[67] Jairo Alexander Osorio Saraz et al. "A CFD based approach for determination of ammonia concentration profile and flux from poultry houses with natural ventilation". In: *Revista Facultad Nacional de Agronomia Medellin* 69.1 (2016), pp. 7825–7834.

[68] Tomas Norton et al. "Assessing the ventilation effectiveness of naturally ventilated livestock buildings under wind dominated conditions using computational fluid dynamics". In: *Biosystems engineering* 103.1 (2009), pp. 78–99.

[69] A Mistriotis et al. "Analysis of the efficiency of greenhouse ventilation using computational fluid dynamics". In: *Agricultural and Forest Meteorology* 85.3-4 (1997), pp. 217–228.

[70] Sang-yeon Lee, In-bok Lee, and Rack-woo Kim. "Evaluation of wind-driven natural ventilation of single-span greenhouses built on reclaimed coastal land". In: *Biosystems Engineering* 171 (2018), pp. 120–142.

[71] Guoqiang Zhang et al. "Computational Fluid Dynamics (CFD) research and application in Agricultural and Biological Engineering". In: *Computers and Electronics in Agriculture* 149 (2018), pp. 1–2.

[72] Edwin A Villagran, Esteban J Baeza Romero, and Carlos R Bojaca. "Transient CFD analysis of the natural ventilation of three types of greenhouses used for agricultural production in a tropical mountain climate". In: *Biosystems Engineering* 188 (2019), pp. 288–304.

[73] Se-Woon Hong et al. "Validation of an open source CFD code to simulate natural ventilation for agricultural buildings". In: *Computers and Electronics in Agriculture* 138 (2017), pp. 80–91.

[74] Rack-woo Kim, In-bok Lee, and Kyeong-seok Kwon. "Evaluation of wind pressure acting on multi-span greenhouses using CFD technique, Part 1: Development of the CFD model". In: *Biosystems engineering* 164 (2017), pp. 235–256.

[75] In-bok Lee, Sadanori Sase, and Si-heung Sung. "Evaluation of CFD accuracy for the ventilation study of a naturally ventilated broiler house". In: *Japan Agricultural Research Quarterly: JARQ* 41.1 (2007), pp. 53–64.

[76] DL Kateris et al. "Calculated external pressure coefficients on livestock buildings and comparison with Eurocode 1". In: *Wind & Structures* 15.6 (2012), pp. 481–494.

[77] David Janke et al. *High resolution long-term measurements af carbon dioxide and ammonia concentrations in a naturally ventilated dairy barn.* PUBLISSO Repository for Life Sciences. 2020. URL: https://dx.doi.org/10.4126/FRL01-006420709.

[78] Dilya Willink et al. *High resolution long-term measurements of carbon dioxide, ammonia, and methane concentrations in two naturally ventilated dairy barns.* PUBLISSO Repository for Life Sciences. 2020. eprint: https://doi.org/10.1080/17450399809381921. URL: https://dx.doi.org/10.4126/FRL01-006421675.

[79] Sabrina Hempel et al. "How the selection of training data and modeling approach affects the estimation of ammonia emissions from a naturally ventilated dairy barn - classical statistics versus machine learning". In: *Sustainability* 12 (2020). Special Issue "Environmental Impact of Livestock Production and Mitigation Strategies", p. 1030.

[80] Sabrina Hempel et al. "Methane Emission Characteristics of Naturally Ventilated Cattle Buildings". In: *Sustainability* 12.10 (2020), p. 4314.

[81] S Van Buggenhout et al. "Influence of sampling positions on accuracy of tracer gas measurements in ventilated spaces". In: *Biosystems Engineering* 104.2 (2009), pp. 216–223.

[82] Philippe Van Overbeke et al. "Development of a reference method for airflow rate measurements through rectangular vents towards application in naturally ventilated animal houses: Part 1: Manual 2D approach". In: *Computers and electronics in agriculture* 106 (2014), pp. 31–41.

[83] A. Kiwan et al. "Tracer gas technique, air velocity measurement and natural ventilation method for estimating ventilation rates through naturally ventilated barns". In: *Agricultural Engineering International: CIGR Journal* 14 (Dec. 2012), pp. 22–36.

[84] David Janke et al. *Velocity measurements of a 1:100 scaled model of a naturally ventilated dairy barn in an atmospheric boundary layer wind tunnel.* PUBLISSO Repository for Life Sciences. 2020. URL: `https://dx.doi.org/10.4126/FRL01-006420859`.

[85] GUOQIANG Zhang, Søren Pedersen, and Peter Kai. "Uncertainty analysis of using $CO2$ production models by cows to determine ventilation rate in naturally ventilated buildings". In: *XVII World Congress on Agric CIGR. Eng.* 2010, p. 1.

[86] International VERA Secretariat. *VERA TEST PROTOCOL for Livestock Housing and Management Systems.* 3rd ed. last access 20 April 2020. 2018. URL: `https://www.vera-verification.eu/app/uploads/sites/9/2019/05/VERA_Testprotocol_Housing_v3_2018.pdf`.

[87] Jonas Allegrini, Viktor Dorer, and Jan Carmeliet. "Wind tunnel measurements of buoyant flows in street canyons". In: *Building and Environment* 59 (2013), pp. 315–326.

[88] Philippe Van Overbeke et al. "Methodology for airflow rate measurements in a naturally ventilated mock-up animal building with side and ridge vents". In: *Building and Environment* 105 (2016), pp. 153–163.

[89] William L Oberkampf and Timothy G Trucano. "Verification and validation in computational fluid dynamics". In: *Progress in aerospace sciences* 38.3 (2002), pp. 209–272.

[90] Blake W Lance. "Experimental validation data for CFD of steady and transient mixed convection on a vertical flat plate". PhD thesis. Utah State University, 2015.

[91] Jeff R. Harris, Blake W. Lance, and Barton L. Smith. "Experimental Validation Data for Computational Fluid Dynamics of Forced Convection on a Vertical Flat Plate". In: *Journal of Fluids Engineering* 138.1 (Aug. 2015). 011401. ISSN: 0098-2202. DOI: `https://doi.org/10.1115/1.4031007`. eprint: `https://asmedigitalcollection.asme.org/fluidsengineering/article-pdf/138/1/011401/6196330/fe_138_01_011401.pdf`.

[92] VDI. *DIN 18910:2017-08. Thermal insulation for closed livestock buildings - Thermal insulation and ventilation - Principles for planning and design for closed ventilated livestock buildings.* Guideline. Verein Deutscher Ingenieure, Duesseldorf, Germany, 2017.